Mathematical Models of the Developing *C. elegans* Hermaphrodite Gonad

Thesis by

David M. Goulet

In Partial Fulfillment of the Requirements

for the Degree of

Doctor of Philosophy

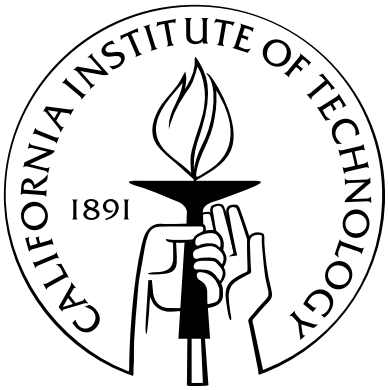

California Institute of Technology

Pasadena, California

2006

(Defended May 5, 2006)

I would like to dedicate this thesis to my friends, collegues, and mentors. Their patience, knowledge, insight, inspiration, and humor have made my years at Caltech the most memorable, nurturing, and formative of my life.

Acknowledgements

I wish to thank Professor Paul Sternberg and his *C. elegans* research group. I approached Paul knowing nothing of his research or of *C. elegans* yet he enthusiastically welcomed me, not just as an observer of his group, but as a member. His patience and openness gave me insight into the workings of an amazing group of biologists. He helped me to have the ideal cross-disciplinary research experience.

I wish to thank Dr. Danny Petrasec whose tremendous enthusiasm for quantitative biology was an inspiration. Danny's uncommon talents as a medical doctor and an applied mathematician were of essential help to me in navigating my way through unfamiliar research terrain. Danny was a Rosetta stone, a mentor, and a friend.

I wish to thank Professor Donald Cohen for so many things. While I was an undergrad, he excited me to do research in applied math and inspired me to pursue graduate school. When I became a grad student, he helped me to improve my work without ever being critical and he celebrated my successes, no matter how small. Don's patience and sympathy far exceed anything that should be expected of a professor. He treated me to enumerable lunches and dinners, offered to help when I was ill, and was always supportive through my personal and academic struggles. Don has been an unforgettable friend. Without him, this thesis would have been impossible.

Abstract

The study of growing and developing organisms is a fascinating branch of experimental biology. Once created, cells must exchange chemical and physical cues with neighboring cells in order to grow, divide, and differentiate properly. In this thesis we study portions of development of the *C. elegans* hermaphrodite gonad, building mathematical models of the development process. Using our models, we show that vulval precursor cells make fate decisions under a flexible program that takes advantage of inherent chemical oscillations. This flexibility allows the cells to react more sensitively to weak signaling gradients and to the actions of neighboring cells. With our mathematical models, we also show that the development of the anchor cell cannot proceed properly using the currently known decision mechanisms. We draw upon knowledge of homologous proteins in *D. melanogaster* to propose a modification to the current theory on anchor cell development. Our models suggest that this modified mechanism, though not yet identified in *C. elegans*, is sufficient to specify anchor cell fates in accordance with experimental observations. In studying our mathematical models, novel analytical techniques were developed to understand the asymptotic behavior of systems of delay differential equations.

Contents

List of Figures

List of Tables

Part I

Biology

Chapter 1

Introduction to *C. elegans*

The aim of this chapter is to discuss general features of *C. elegans* and the development of its vulva. Genes, proteins, receptors, etc. are referred to by their corresponding human analogs, making this introduction more accessible to a general audience. Details and nomenclature more specific to *C. elegans* are mainly reserved for Chapter 2.

Caenorhabditis elegans is an invertebrate parasitic worm that, when fully developed, measures roughly 1 mm from head to tail. There are no females of the species, only males and hermaphrodites [33]. Along with others such as the human (*Homo sapiens*), the mouse (*Mus musculus*), and the fruitfly (*Drosophila melanogaster*), it is one of the most well-understood animals physiologically, genetically, and behaviorally. *C. elegans* has many nice properties that make it a useful object of study (see Table (1.1)). Its genome is relatively small. It's composed of a small number of cells. It has a relatively small collection of neurons. It's transparency, size, and low motility also make it ideal for observation of behavior, development, and genetic expression markers.

Starting from fertilization, the embryonic *C. elegans* undergoes four larval stages

Table 1.1: Complexity of *C. elegans*and *H. sapiens*

	C. elegans hermaphrodite/male	*H.sapiens*
Base Pairs	$\sim 10^8$	$\sim 3 \times 10^9$
Cells	810/970	$\sim 10^{14}$
Neurons	302/381	$\sim 10^{11}$
Size (mm)	~ 1	$\sim 10^3$

of growth and development to reach adulthood. These stages, each followed by a molt, are denoted as stage L1 through L4.

The mature adult wild-type *C. elegans* vulva is composed of 22 cells arranged in a compact dimpled structure located on the ventral portion of the worm slightly posterior to the midpoint between head and tail. See Figure (1.1). Together with the uterus it forms the egg-bearing reproductive organ in the *C. elegans* hermaphrodite. The vulva also functions as the opening through which sperm enter during copulation [35], but isn't necessary for hermaphrodites to self-fertilize [33]. Vulval development begins in L1 when the six vulval precursor cells, or VPCs, are born. The development of the vulva is initiated during L3 stage and completed during late L4. During L3 cell-cell signaling specifies the fates of these cells. The VPCs then undergo a sequence of divisions, ultimately yielding 22 vulval cells, and six non-vulval cells. The vulval cells then move, arrange and fuse to form the mature vulva [35].

The apical portion of the vulva is composed of eight cells known as the VulE and VulF fate. These cells are flanked by 14 cells of VulA,B,C,D fates that form the periphery of the vulva. Those flanking VulA-D fuse to the hypordermis. These play no role in the mature vulval function and are thus said to be non-vulval while those

Figure 1.1: Location of *C. elegans* vulva. Triangle points to head. Short arrow points to tail. Long arrow points to vulva. Image courtesy of Wormatlas.org.

of VulA-F fates are said to be of vulval fate or Vul.

Prior to the cell divisions leading to the 22 vulval cells, the pre-vulval structure consists of six VPCs arranged in a linear fashion between the basement membrane and the epidermal syncytium, *i.e.*, Hyp7. Hyp7 is a long polynucleate cell (133–139 nuclei) forming much of the structure of the midbody. These VPC are denoted by P3.p through P8.p.

For proper development of the vulva, the activation of the VPC surface receptor EGFR by the ligand EGF is required. In the absence of this signaling, these cells divide once and then their daughters fuse to the syncytium [33]. Those VPCs whose progeny are of VulE,F fate are said to have adopted primary fate, 1°. Those whose progeny are VulA-D fate are said to have adopted the secondary fate, 2°. The remaining VPCs whose progeny don't divide and simply fuse to the hypodermis are termed

the tertiary fate, 3°. Primary, secondary, and tertiary fated VPCs differ not just in their roles of forming different parts of the mature vulva, but also in their pattern of divisions. Tertiary cells produce two non-dividing daughters. Secondary cells produce six great-grand-daughters and one non-dividing grand-daughter. Primary cells produce eight great-grand-daughters.

VPCs appear to have similar numbers of EGFR receptors initially and in accordance with this are equally competent to respond to signaling by EGF. The primary source of EGF is a cell located dorsal to P6.p on the opposite side of the basement membrane. During L3 stage, this cell, known as the anchor cell or AC begins to secrete EGF. EGF secreted by the anchor cell then diffuses in the extracellular space between surrounding cells, crosses the basement membrane, and binds to EGFR receptors on the VPCs. Once bound, the receptor releases its intracellular domain, which initiates a series of biochemical reactions inside the cell. At the end of this signaling cascade the nucleus of the cell is encouraged to begin translating particular genes from DNA into RNA, which are later used as the templates to build proteins. One such class of proteins, DELTA, is used by VPCs as ligands to trigger NOTCH receptors on neighboring VPCs or possibly their own NOTCH receptors. The EGF signal from the anchor cell is termed the inductive signal, as it induces VPCs to become primary fated. The DELTA/NOTCH signaling between VPCs is part of what's known as the lateral signal. This lateral signal is thought to be responsible for producing cells of secondary fate. The inductive and lateral signaling events are illustrated in Figure (1.2).

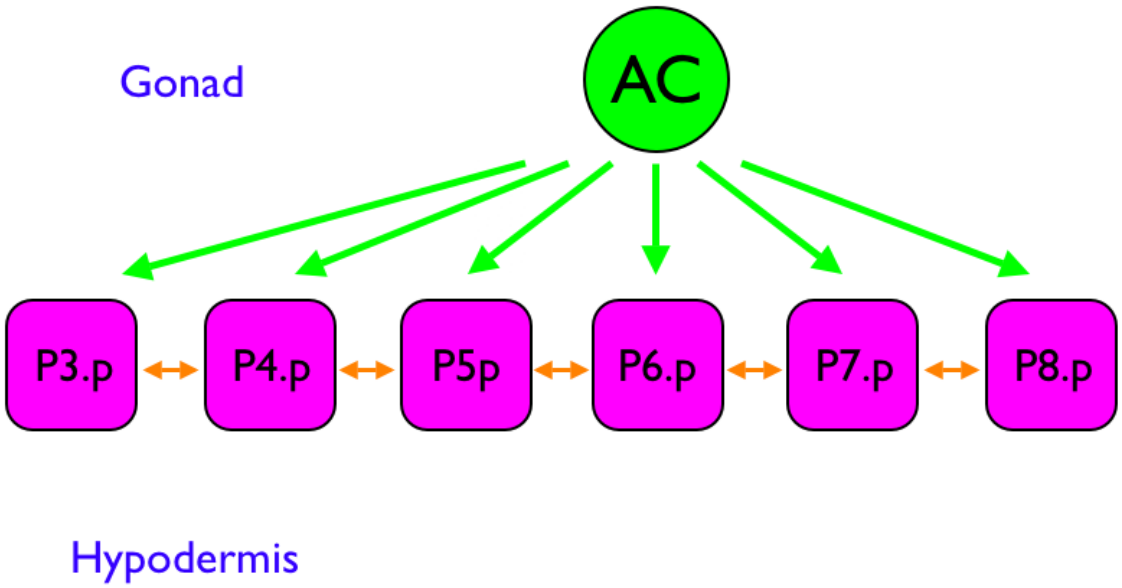

Figure 1.2: Signaling Events Coordinating Vulval Induction. Inductive signal from the anchor cell promotes lateral signaling between the vulval precursor cells.

As seen in experiments, the dynamics of these interacting signaling cascades produce patterning in the VPC fates. Through various modes of feedback, small differences between the VPCs can be amplified to bring about distinct cell fates and characteristics. Experiments with genetic mutants and laser ablations of VPCs show how the dynamics of this intercellular circuit allow compensation when less than ideal developmental conditions are present. Although much is known about the development of the C. elegans vulva, there are many important questions left to be answered.

In Chapter 2, the details of these signaling pathways and their interactions will be elaborated on. In Chapter 5 mathematical models for this signaling process are constructed and analyzed. In Chapter 3 a related developmental process, the determination of the anchor cell, is discussed with models and analysis following in Chapter 6. In Chapter 4 mathematical techniques are developed that aid in later modeling and analysis. Mathematical proofs and details from all chapters are mainly left to the Appendix.

Chapter 2

Biological Background: Vulval Induction

2.1 Introduction

In this chapter *C. elegans* vulval development is discussed in more detail and with specialized nomenclature. A familiarity with *C. elegans* is presumed.

2.2 Inductive Signaling

During L3 the anchor cell, part of the somatic gonad, produces LIN-3, a homolog to human Epithelial Growth Factor, EGF [20]. The VPCs have receptors for LIN-3 on their surfaces. This receptor, LET-23, is a receptor tyrosine kinase of the EGFR family. The binding of LIN-3 to LET-23 is known as the inductive signal .

Signaling by the AC is necessary for VPCs to adopt normal fates because if the AC is ablated prior to induction all of the VPCs adopt non-vulval fates. Signaling by the AC is also sufficient for VPCs to develop properly because if all of the other cells in the somatic gonad, except the AC, are ablated, the VPCs still acquire normal

fates [28].

Once secreted, LIN-3 diffuses throughout the somatic gonad, crosses the basement membrane, diffuses around the VPCs and binds to LET-23 receptors. As a result of this diffusive process, there is evidence of a gradient of LIN-3 in the proximity of the VPCs [23, 25]. If all but one of the VPCs are ablated, the remaining isolated VPC adopts either a primary or secondary fate depending on its distance from the AC [25]. See examples in Table (5.1). This observation also supports the direct induction hypothesis, *i.e.*, the gradient of LIN-3 determines VPC cell fates [43]. All evidence for a gradient of LIN-3 is indirect, as levels of LIN-3 have never been quantified. As mentioned in the introduction, other signaling events contribute to cell fate specification and these signals seem capable of enhancing small physiological differences brought about by even a weak gradient.

In addition to spatial gradients of LIN-3 being formed, the VPCs themselves may act to enhance the signaling event in a spatially graded fashion. There is evidence that around the time of initial LIN-3 signaling the level of LET-23 receptors on P6.p increases while the level on P5.p and P7.p decreases [39]. Additionally, it is known that on P6.p the LET-23 receptors aren't distributed uniformly, but rather are localized to be closer to the AC. In mutants where localization is impeded while total receptor level is not, a vulvaless phenotype results [39]. If localization is impeded while total level of receptor is increased, normal vulval development is rescued. Hence the localized distribution of LET-23 on P6.p appears to exploit geometry to achieve a maximal effect from a limited level of receptor and weak gradient. Likewise, up-

regulation of LET-23 on P6.p with simultaneous down-regulation on P5.p and P7.p promotes the proper pattern of cell fates.

In a wild-type animal, this and other signaling pathways lead the six VPCs to adopt the fates 3°-3°-2°-1°-2°-3°.

2.3 The Map Kinase Pathway

LET-23 receptors activated by bound LIN-3 convey the inductive signal into the cell by activating a cascade of biochemical reactions related to the MAP kinase pathway in humans. See Table (2.1). Activated LIN-3/LET-23 complex affects SEM-5, which is believed to be an adaptor between the receptor tyrosine kinase and LET-60, starting a cascade of interactions, ending with the activation of the MAP kinase, MPK-1. The sequence of interactions is given schematically by Equation (2.1).

$$\text{LIN-3/LET-23} \rightarrow \text{SEM-5} \rightarrow \text{SOS-1} \rightarrow \text{LET-60} \rightarrow \text{LIN-45} \rightarrow \text{MEK-2} \rightarrow \text{MPK-1} \tag{2.1}$$

Although details are still not known, the targets of this pathway appear to be transcription factors. For example, MPK-1 (a MAPK homolog) disrupts a complex formed by LIN-1 and LIN-31 by phosphorylating it [33]. These are both transcription factors whose targets are currently unknown.

Transcription promoted and inhibited as a result of MAPK activity leads cells to proceed through a characteristic pattern of divisions typical of the primary fate.

Table 2.1: Human and *C. elegans* Orthologs in the MAPK Pathway

Human	*C. elegans*
EGF	LIN-3
EGFR	LET-23
GRB-2	SEM-5
SOS	SOS-1
RAS	LET-60
RAF	LIN-45
MEK	MEK-2
MAPK	MPK-1 (SUR-1)

Aside from inducing primary fated VPCs, activation of the MAPK pathway also leads to the transcription of three genes believed to produce the lateral signal, lag-2, apx-1, and dsl-1 [5].

In addition to the core components there are many positive and negative regulators of the MAPK pathway that play small roles in wild-type primary and secondary VPCs. Examples of these types of regulators include LIN-15 which activates the MAPK pathway independent of LIN-3, and DPY-22 which inhibits the MAPK pathway and may be important in preventing signaling in non-vulval cells [33]. Effects of these regulators are typically not observed in wild-type VPCs. Mutations in these alleles can lead to dramatically different pattern formation. An example of this was shown in a LIN-15 mutant [40] where a 2°-1°-2°-1°-2°-1° phenotype was strongly penetrant.

2.4 Lateral Signaling

As mentioned in § (2.3), activation of the MAPK pathway promotes the transcription of three genes thought to be responsible for production of the lateral signal, apx-1, lag-2, and dsl-1. See Figures 2.1 and 2.2. It has been shown through use of a transcriptional reporter [5] that apx-1 and dsl-1 aren't transcribed in any of the VPCs prior to inductive signaling, but are subsequently transcribed in P6.p to produce APX-1 and DSL-1, respectively. In contrast, the reporter for lag-2 is evident in all six VPCs in early L3 but later becomes more apparent in P6.p while diminishing in the other VPCs. These results show that activation of the MAPK pathway up-regulates the transcription of genes responsible for the lateral signal. Also suggested by these results is that lateral signal produced by P6.p affects neighboring VPCs in such a way that transcription of lag-2 is down-regulated in them, making them less able to laterally signal their neighbors.

The lateral signal, be it the transmembrane ligands LAG-2 and APX-1 or the secreted ligand DSL-1, is detected by VPCs through binding of these ligands to LIN-12 receptors. Activation of these receptors is thought to induce the secondary fate [40]. As mentioned above, lateral signal production can be up-regulated in some cells while being down-regulated in others. Additionally it has been shown that the LIN-12 receptor is down-regulated by the MAPK pathway [38]. This would appear to contradict the observation that lin-12 expression is continuous and uniform [44]. There is no contradiction, however. LIN-12 is expressed continuously and uniformly [44] but is post-transcriptionally down-regulated possibly via targeting to lysosomes, impair-

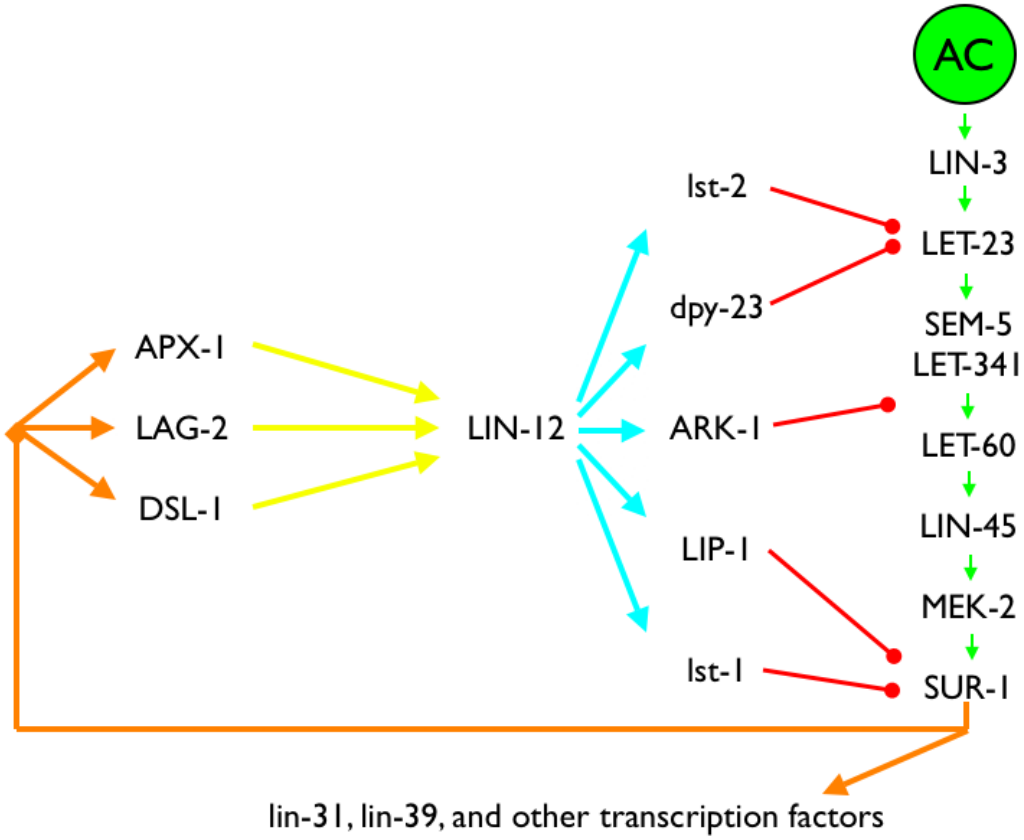

Figure 2.1: Signaling Events Coordinating Vulval Induction 2

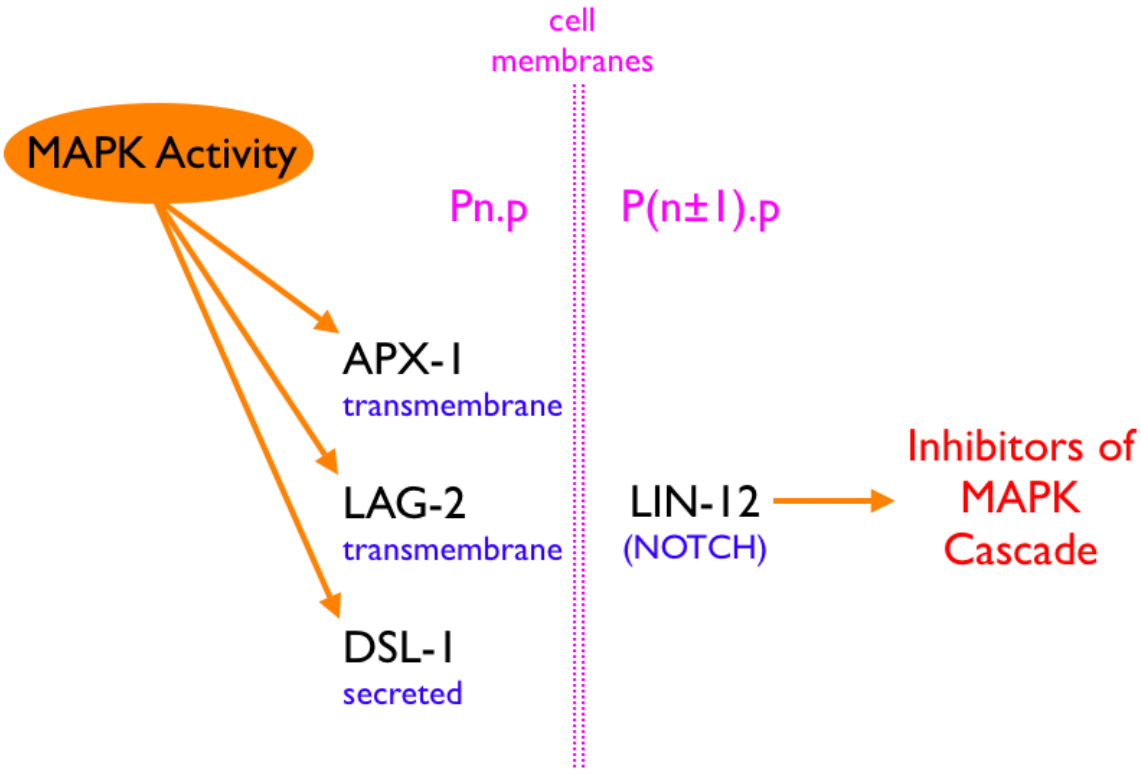

Figure 2.2: Lateral Signal

ment of receptor recycling or enhancement of receptor internalization [38].

These results indicate that activation of the MAPK pathway causes VPCs to begin laterally signaling their neighbors while they themselves become less susceptible to such signaling. It has been shown that if P6.p is prevented from down-regulating LIN-12 then it can't laterally signal P5.p and P7.p effectively; indeed, a 3-3-3-1-3-3 pattern of fates is observed [38].

If LIN-12 persists on P6.p then ligand produced by P5.p, P6.p, or P7.p in either transmembrane or secreted forms might initiate a lateral signaling event in P6.p. One explanation is that this lateral signaling can impede the ability of P6.p to laterally signal its neighbors by down-regulating the amount of lateral signaling ligand. This is in agreement with the conclusion drawn from the results of [5], discussed above. Although the exact mechanism of this feedback loop for VPCs is unknown, there are detailed results from a similar type of post-transcriptional down-regulation in the AC/VU decision. It has been observed in [24] that LIN-12 lateral signaling events between the cells Z1.ppp and Z4.aaa lead one of these two initially equipotent cells to stop producing lateral signal and become the VU while the other cell stops producing LIN-12 and becomes the AC. The authors provide evidence of positive and negative feedback loops involving HLH-2, a positive regulator of LAG-2 ligand transcription, which explains how LIN-12 receptor signaling can cause these cells to cease transcription of LAG-2, a lateral signal ligand.

Based on these three different sources of evidence, it seems highly probable that, through some as yet unidentified mechanism, lateral signaling of a VPC reduces its

ability to laterally signal its neighbor. Activation of LIN-12 receptors by lateral signal also appears to affect the transcription of genes involved in the MAPK pathway. LAG-1 is a DNA binding protein that forms a complex with the LIN-12 intracellular binding domain to activate transcription of target genes. Based on computational screens, several good targets for the LAG-1/LIN-12(intra) complex have been identified in VPCs [47]. These targets are ark-1, dpy-23, lst-1, lst-2, lst-3, lst-4, lip-1, vha-7, T22A3.2, F35D11.3, and Y40H4A.2. Of these, six were found to act as negative regulators of EGFR-MAPK activity (ark-1, dpy-23, lst-1, lst-2, lst-3, lst-4). See Table (2.2).

Two genes (dpy-23 and lst-3) are expressed at low levels in the VPCs during mid-L3 stage but then are expressed more strongly in P5.p and P7.p. Thus it appears that these negative regulators of the EGFR-MAPK pathway are up-regulated by the lateral signal. Three other genes (lst-1, lst-2, lst-4) have a more complicated pattern of expression. A high level of expression is seen in all VPCs but at time of inductive signaling expression is slightly diminished in P5.p and P7.p and greatly diminished in P6.p. Later, strong expression returns to P5.p and P7.p but remains low in P6.p. This pattern suggests that these genes are initially down-regulated by inductive signal and later up-regulated by lateral signal. Thus the EGFR-MAPK pathway seems capable of down-regulating the transcription of its own negative regulators while the activation of LIN-12 by lateral signal up-regulates them. This raises the question of whether the MAPK pathway has targets in common with the LAG-1/LIN-12 pathway. We do not pursue this question here.

Mentioned in [47] are two other targets of LIN-12 that also act as negative regulators of the EGFR-MAPK pathway, ark-1 and lip-1. ARK-1 is thought to inhibit EGFR-MAPK signaling upstream of LET-60 [22] while LIP-1 is a MAP kinase phosphatase [33]. See Table (2.2) for all target genes discussed by those authors and Figure (2.3) for a depiction of these inhibitory events.

Table 2.2: Known Lateral Signal Target Genes

Gene or Gene Product	Known or Probable Role
ARK-1	Inhibits upstream of Let-60.
LIP-1	A known MAPK phosphatase.
dpy-23 lst-4	Play a role in the degradation of EGFR.
lst-1	May act directly on MAPK.
lst-2	May influence endocytotic trafficking of LET-23 or the sub-cellular localization of other components of the EGFR-MAPK pathway.
lst-3	No obvious direct role.

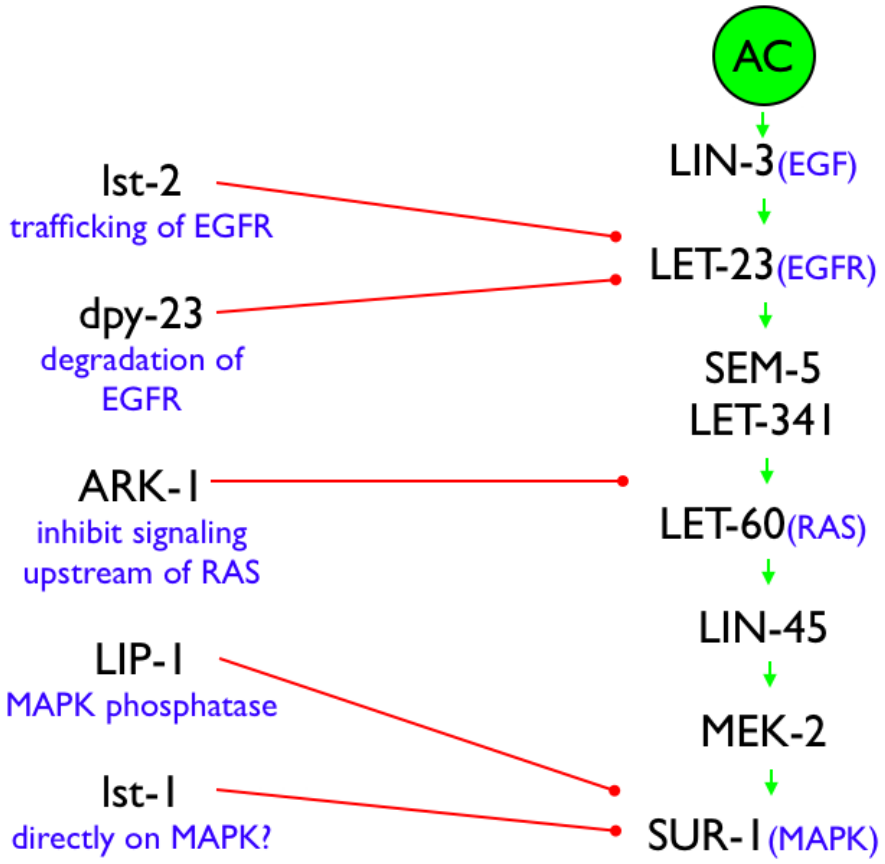

Figure 2.3: Signaling Events Coordinating Vulval Induction 3

Chapter 3

Biological Background: The AC/VU Decision

3.1 Introduction

As discussed in § (2.2) the anchor cell (AC) plays a critical role in the development of the mature *C. elegans* hermaphrodite vulva. During L2, prior to vulval induction in L3, the AC must emerge from a pair of equipotent gonadal cells known as Z1.ppp and Z4.aaa. These two cells, though proximal in space, are born of distinct mother cells and differ in birth time.

In wild-type hermaphrodite *C. elegans* one of these two cells becomes the AC while the other becomes a Ventral Uterine Precursor Cell (VU). The specification of these distinct fates is made decisively but not consistently. Indeed, both Z1.ppp and Z4.aaa are equally likely to become the AC. This duality was illuminated by the authors of [24]. They showed that while the AC fate is adopted by Z1.ppp or Z4.aaa with equal frequency, the decision is strongly correlated with birth order. The main evidence for this was a set of 13 observations in which the first born of Z1.ppp and Z4.aaa adopted the VU fate 12 times. See Table (3.1).

From the fruit of further observations, the authors gained insight allowing them to propose a signaling mechanism likely to be the lynchpin of the AC/VU Decision. In § (3.2) we provide a detailed exposition of this proposed mechanism. In Chapter 6, we construct a mathematical model representing this mechanism. In that chapter we also present quantitative results showing that the mechanism exhibits some expected features but has clear shortcomings. We close Chapter 6 with a modified proposed mechanism, with added features homologous to those observed in *Drosophila*, and show how this new proposal provides for a mathematical model with more qualitatively accurate features.

3.2 The Karp and Greenwald Model

In [24] Xantha Karp and Iva Greenwald provide convincing evidence of several features of the AC/VU decision. This section summarizes those results, making references to other sources when necessary.

A series of experiments has demonstrated that both Z1.ppp and Z4.aaa are equipotent, *i.e.*, they are equally capable of adopting either the AC or VU fate. In a wild-type worm one of these precursors becomes the AC and the other the VU. As decisive as this may seem, that cell which becomes the AC and that which becomes the VU are not consistent across a sample of wild-type worms. Though this outcome may seem indicative of a noisy or randomly behaving system, in fact it is telling of more subtle and intricate dynamics.

When Z1.ppp and Z4.aaa were tracked from birth in a population of 13 worms, it

was seen that, though both are equally likely to become AC, the latter-born of the two became AC 12 times. In this set of observations birth time separations varied from two minutes to two hours (see Table (3.1) adapted from [24]). This strong correlation suggests three possible causal relationships:

(i) A cell becomes VU as a result of being born first.

(ii) A cell is born first as a result of or as part of a predetermination to become VU.

(iii) Birth order and fate specification, though correlated, are not causes or effects of one another but merely coincident or perhaps the effects of a common cause.

Table 3.1: Birth time separations in the AC/VU decision. Data adapted from [24].

First Born	Fate of First Born	Birth Separation (minutes)
Z1.ppp	VU	7
Z1.ppp	VU	15
Z1.ppp	VU	27
Z1.ppp	VU	60
Z1.ppp	VU	75
Z1.ppp	VU	115
Z4.aaa	VU	2
Z4.aaa	VU	12
Z4.aaa	VU	15
Z4.aaa	VU	25
Z4.aaa	VU	25
Z4.aaa	AC	40
Z4.aaa	VU	75

Hypotheses (ii) and (iii) each presume that interaction between Z1.ppp and Z4.aaa is of no consequence in the fate decision. Indeed, if (ii) or (iii) were true, then preventing interaction between cells would lead to a wild-type outcome. The only known

means of interaction between these cells is via a DELTA/NOTCH-type signaling event mediated by LAG-2/LIN-12. Experiments described in [16] show that LIN-12 activity is both necessary and sufficient to specify the VU fate. In the absence of signaling, a two AC phenotype is observed making relationship (i) the only consistent choice.

Identifying this causal relationship is a large piece of the fate specification puzzle, but now questions arise as to why the first born should be VU. Firstly, how do birth order differences as small as two minutes provide for decisive and consistent cell fate specification? Secondly, what is the full nature of the lateral signaling event leading to this specification?

In [24] progress is made towards addressing the latter of these inquiries. Specifically, levels of the protein HLH-2 were observed to diminish in response to LIN-12 activity. HLH-2 is a known activator of lag-2 transcription. Further investigations have shown that the nature of the removal of HLH-2 protein is post-transcriptional, since reporters of hlh-2 transcription were apparently unchanged while HLH-2 protein vanished from presumptive AC cells. These features lead those authors to propose the lateral signaling mechanism depicted in Figure (3.1). In Chapter 6 we build a mathematical representation of this proposed mechanism and address the question of how it (or a slight modification of it) might be capable of producing the observed rapid and definitive fate specifications.

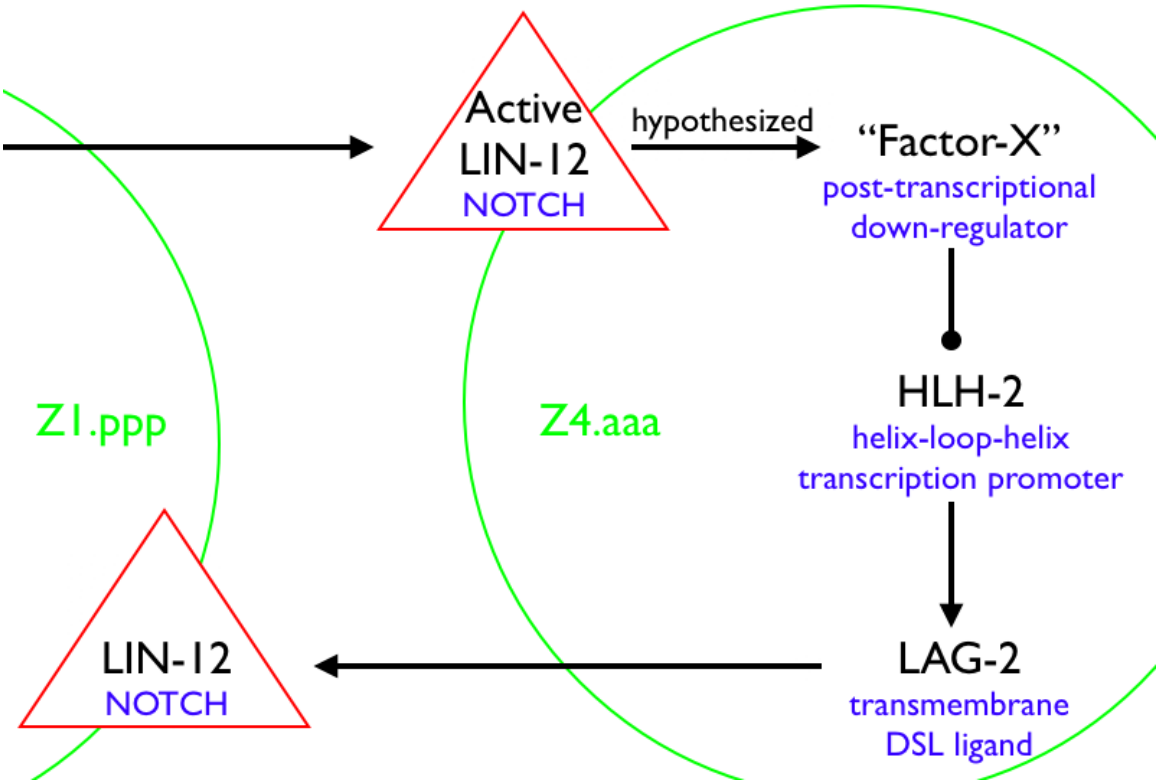

Figure 3.1: Sequence of Activations/Inhibitions Leading to AC/VU Fate Specification

Part II

Mathematics

Chapter 4

Mathematical Modeling: Continuous Reaction Models

4.1 Philosophy

When applying mathematics, it is important to let the object of study dictate which mathematical ideas will be employed. Familiar mathematics should not be haphazardly forced upon unfamiliar systems. Mathematics is the language of nature, so in studying natural systems we should listen carefully to this language before making decisions about how to model a system.

All mathematicians are familiar with this idea. We've all seen the advantages of using carefully chosen coordinate systems, eigenvectors, and function spaces as the foundation of our models and analysis. This idea is succinctly expressed by a phrase that Professor Donald Cohen relates to his students, "If you want to model an elephant, use elephant functions."

Masters of other disciplines are also well-versed in this idea. To paraphrase martial artist and philosopher Bruce Lee, one should "utilize all ways and be bound by none" [30]. It is unfortunate that not all applied mathematicians adhere to this

principle. While the mastery of a specific set of techniques is admirable and valuable, artificially imposing those skills on ill-suited systems is foolhardy and dishonors the discipline of applied mathematics.

It is my intention in this thesis to "listen" to the biological systems under study and to develop models and methods that I think are most appropriate, rather than insist that phenomena be entirely governed by known equations extracted from the established dogma. For these reasons, this chapter and the appendix are devoted entirely towards developing mathematical techniques which are well-suited to studying the biological systems of interest. Essentially I aim to find "*C. elegans* functions," although I make no claim of having achieved this goal.

4.2 Introduction

The canonical EGFR/RAS/MAPK pathway in *C. elegans* VPCs is an example of a linear sequence of biochemical interaction/reactions. Such a pathway might be modeled by a system of ODE; however, for a long chain of reactions analytic extraction of qualitative information about the behavior of the system would be difficult or impossible.

In large systems of interacting objects, continuum models are probably more useful for studying large scale qualitative behavior than are object tracking models. For example, the diffusion equation describes the average motion of a practically infinite sea of particles undergoing independent random walks. The diffusion equation can be derived from a mass balance and Ficke's law, a macro-scale constitutive rela-

tion, or from first principles using Brownian motion as the description of individual particle behavior ([32],[11]). As another example, the equations of one-dimensional linear elasticity can be derived from mass/momentum/energy balances and Hooke's law, a constitutive relation, or from the approximation of the elastic object by an infinite ensemble of infinitesimally small linear springs connected in series [6]. In well-studied examples such as these, mechanistic particle tracking models and large scale phenomenological models agree, allowing mechanical reasoning to buttress empirical observations.

When one moves from an object tracking model to a continuum model, the number of governing equations drops dramatically, *e.g.*, from 10^{23} to 1, while the complexity of the equations themselves increases, *e.g.*, from ODE to PDE. This trade-off in complexity does not afford any computational advantage– solving 100 first order ODE initial value problems is no simpler than solving 1 first order in time parabolic PDE on a grid of 100 points. The main advantage afforded by a continuum model is in the mathematical analysis. Asymptotic methods, scaling arguments, model reduction, and other approximation methods are undoubtedly more simple for 1 PDE than they would be for 1,000,000 ODE.

Furthermore, we are often not concerned with the motion of individual atoms and molecules but with the collective behavior of many such entities coupled through a network of interactions. Continuum models are superior in this regard as well, because they resolve not to tell us of fine details but of broad global results.

For these reasons, we now pursue continuum approximation models of long chains

of similar chemical reactions. Our goal will be to formulate continuum models that preserve the essential qualitative global features of their discrete progenitors.

4.2.1 Example Reactions

A Linear Chain Consider the following type of repeated reaction:

$$u_0 \longleftrightarrow \cdots \longleftrightarrow u_{n-1} \longleftrightarrow u_n \longleftrightarrow u_{n+1} \longleftrightarrow \cdots \longleftrightarrow u_N \ . \tag{4.1}$$

This describes, for example, the spontaneous isomerization of a protein. Each u_i is an isomer of a given protein, and by temperature changes, ph modifications, or otherwise, the chemical is being induced to change into "neighboring" states, with the rates of transition described by forward and backward rate constants. Such a reaction might be thought of as a "chain" with repeated "links" of the form

$$u_n \longleftrightarrow u_{n+1} \ . \tag{4.2}$$

This chain could also represent a series of enzyme-aided reactions where the enzymes are plentiful enough to assume that their concentrations are fixed throughout the process. The rate constants for each state transition would then depend on this abundant but steady enzyme level.

Catalysts In more complex chains of reactions, the links could be more intricate. For example, if the isomerization of a protein to different states won't proceed spon-

taneously but instead requires an enzyme catalyst, we might write the link as

$$u_n + E_n \longleftrightarrow C_n \longrightarrow u_{n+1} + E_n \ . \tag{4.3}$$

Here u_n is the substrate in state n, E_n is the n-type enzyme, and C_n is an intermediate enzyme/substrate complex. When enzyme is so abundant relative to substrate as to essentially remain fixed throughout their interaction, we recover the previous linear chain representation.

Polymerization A description of polymerization is given by the following link:

$$u_n + M_n \longleftrightarrow u_{n+1} \ . \tag{4.4}$$

Here M_n is a monomer of type n and u_n is an n-mer.

Ligand Binding By a small modification, the link for polymerization can also be formed into a description of a cell-surface receptor with N total independent ligand binding sites for a single ligand type.

$$u_n + L \longleftrightarrow u_{n+1} \tag{4.5}$$

Here, u_n represents the receptor with n ligands bound and L is the unbound ligand. u_0 is the empty state and u_N is the completely saturated receptor.

4.2.2 Combining Multiple Chains

Separate chains could be interconnected through "cross-links." For example, consider the example above of a receptor with N binding sites. If this receptor internalizes, then the ligands could possibly be released one at a time inside the cell:

$$v_{n+1} \longleftrightarrow v_n + L \; . \tag{4.6}$$

If we suppose that the receptor is able to internalize in any state, then we could cross-link the linear chains to get a planar arrangement that we might call a "mail."

$$\begin{array}{ccc} L + u_n & \longleftrightarrow & u_{n+1} \\ & \searrow \quad \nearrow & \\ & v_n + L \longleftrightarrow v_{n+1} & \end{array} \tag{4.7}$$

4.3 Finite State ODE Models

We now examine in detail how a linked reaction chain can be described by a system of ODE and subsequently, through a careful limiting process, leads to a continuum model approximation.

Consider reaction (4.1). If we label each of the chemical species with an index $n \in \{0, 1, \ldots, N\}$ we can apply the law of mass action [26] to write a system of

ordinary differential equations describing the concentration of each species:

$$\begin{aligned} \frac{du_0}{dt} &= -k_0^+ u_0 + k_1^- u_1 \\ \frac{du_n}{dt} &= k_{n-1}^+ u_{n-1} - (k_n^- + k_n^+) u_n + k_{n+1}^- u_{n+1} \\ \frac{du_N}{dt} &= k_{N-1}^+ u_{N-1} - k_N^- u_N \quad . \end{aligned} \tag{4.8}$$

Here k_n^+ are the forward reaction rate constants and k_n^- their backward counterparts. The quantities $u_n(t)$ are the concentrations of the corresponding chemical species. We now have a large linear system of ODE to solve and analyze. Computing a numerical solution is trivial, but qualitative analysis for a general set of rate constants could be quite taxing. It would be advantageous to find a system capturing the behavior of (4.8) but that is more analytically tractable. To this end, other investigators have proposed approximating models to replace System (4.8) by fewer equations. Examples include ([12],[13]) where restrictive assumptions are made to enable the reduction of (4.8) to a smaller set of ODE together with a delay differential equation (DDE). In § (4.6) we'll compare their approach to the approach we develop here. We believe our approach to be less restrictive and more generally applicable to systems other than (4.8).

4.4 PDE Continuum Models

4.4.1 Introduction

From a numerical analyst's perspective, System (4.8) bears some similarity to the application of the Method of Lines [46] to the numerical solution of a parabolic partial differential equation. From this vantage we might ask what PDE is being solved and with what order of accuracy. Should we discover an underlying PDE, no computational advantage will be afforded, but qualitative analysis may be facilitated.

4.4.2 From ODE to PDE

As the number of chemicals in the chain becomes large ($N \to \infty$) a bar chart plot of the $u_i(t)$ at a fixed time would look more like the shaded area under a smooth curve. This conjures the concepts behind the Fundamental Theorem of Integral Calculus [3] and its proof based on the convergence of Riemann sums to areas under smooth curves. For this reason, we choose to supplant the concentration of n discrete states of chemical at time t, $u_n(t)$, with a continuous function, $u(x,t)$, where x is a continuous variable we call the "state."

It is worth noting that biological phenomena disparate from that considered here have independently inspired the use of a continuous "state" approach. For example, Segel and Perelson [37] use shape-state space to describe the broad variety of antibodies in an immune response model. Interestingly, the continuous state models derived in this thesis were conceived independently and are essentially different in both char-

acter and utility. The independent conception of this idea in different biological modeling environments is reminiscent of convergent biological evolution in different phylogenetic paths, *e.g.*, the evolution of the mammalian and squid eyes ([15],[34]). In the case of vision, the common solution to the problem of seeing by unrelated species speaks to the advantages of the eyed over the eyeless. In the present case, the common solution to the modeling of complex but unrelated biological problems speaks to the advantages of continuous over discrete models.

As $N \to \infty$ the discrete variable n/N becomes a better approximation to a continuous one.

$$\frac{n}{N} \in \left\{ \frac{1}{N}, \frac{2}{N}, \ldots, \frac{N}{N} \right\} \quad \to \quad x \in [0,1] \quad , \tag{4.9}$$

$$\frac{1}{N} \quad \to \quad \Delta x \quad . \tag{4.10}$$

This allows us to consider the change from a discrete dependent variable to a continuous one by introducing a density function $u(x,t)$.

$$u_n(t) = \int_{(n-\frac{1}{2})\frac{1}{N}}^{(n+\frac{1}{2})\frac{1}{N}} u(s,t)\, ds \quad \to \quad \int_{x-\frac{1}{2}\Delta x}^{x+\frac{1}{2}\Delta x} u(s,t)\, ds \quad , \tag{4.11}$$

$$k_n^{\pm} = k^{\pm}\left(\frac{n}{N}\right) \quad \to \quad k^{\pm}(x) \quad . \tag{4.12}$$

Here $u_n(t)$ is the concentration of the n^{th} chemical at time t, see Equation (4.8). Here also $u(x,t)dx$ is approximately the concentration of chemical in states $[x, x+dx)$ at time t. With this formalism $u(x,t)$ now describes the density of chemicals in each of infinitely many states at a particular time. What we have developed here is a finite

volume approach [31] to solving a PDE for $u(x,t)$. We could have also included a normalized kernel function in our integrand, but in the case of smooth symmetric kernels, the end result is identical. For this reason, we preserve the lucidity of our exposition and omit the kernel function.

With the density function defined as above, we rewrite the large ODE System (4.8) as a single integral balance:

$$\begin{aligned}\frac{\partial}{\partial t}\int_{x-\frac{1}{2}\Delta x}^{x+\frac{1}{2}\Delta x} u(s,t)\,ds &= \int_{x-\frac{3}{2}\Delta x}^{x-\frac{1}{2}\Delta x} k^{+}(s)u(s,t)\,ds \\ &- \int_{x-\frac{1}{2}\Delta x}^{x+\frac{1}{2}\Delta x} (k^{-}(s)+k^{+}(s))u(s,t)\,ds \\ &+ \int_{x+\frac{1}{2}\Delta x}^{x+\frac{3}{2}\Delta x} k^{-}(s)u(s,t)\,ds \quad . \end{aligned} \tag{4.13}$$

As it is written, this equation is somewhat deceptive, because as $\Delta x \to 0$ the rates of transfer of chemical in state x to states $x \pm \Delta x$ will also increase. Indeed, as the "distance" between states, Δx, approaches 0 the rate of transfer between states should become infinite. To expand the integral balance in a Taylor series in Δx would depend on the relative orders of magnitude of the rate constants as $\Delta x \to 0$. In order for such a Taylor series to lead to an expression whose leading order terms capture both state and time dependence we must assume that for $\Delta x = o(1)$ the rate constants are given as follows:

$$k^{\pm}(x,\Delta x) = \frac{q^{\pm}(x)}{\Delta x} + o(1/\Delta x) \quad . \tag{4.14}$$

Additional justification of this assumption on physical chemistry grounds is elusive.

In problems of asymptotic analysis *a priori* assumptions about the relative order of variables are often made with the goal of obtaining a "distinguished limit" [27]. In the present case, assumption (4.14) is the simplest one which yields a PDE with both state and time dependance and that allows for state changes up and down the reaction chain. In this sense our PDE and our assumption are "distinguished." Further *a posteriori* support is given below in this section and in § (4.6) where we compare the approximate model to exact solutions of the full ODE system.

Consider the limit $\Delta x \to 0$. Assume that $q^{\pm}(x)$, and $u(x,t)$ are continuously differentiable in (x,t), and expand the integral balance, Equation (4.13), in a Taylor series in the small parameter Δx:

$$\frac{\partial u}{\partial t} + \frac{\partial}{\partial x}\left(q^{+} - q^{-}\right) u = \frac{\Delta x}{2}\frac{\partial^2}{\partial x^2}\left(\left(q^{+} + q^{-}\right) u\right) + O(\Delta x)^2 \quad . \tag{4.15}$$

This equation might be truncated at a certain order so as to produce a PDE that retains essential properties of the original ODE system. Define the quantities $D(x)$ and $c(x)$ as follows:

$$D \equiv \frac{q^{+} + q^{-}}{2} \quad , \tag{4.16}$$

$$c \equiv q^{+} - q^{-} - \Delta x \frac{dD}{dx} \quad . \tag{4.17}$$

Truncating Equation (4.15) at $O(\Delta x)$ and rearranging terms gives a linear convection diffusion equation:

$$\frac{\partial u}{\partial t} + \frac{\partial}{\partial x}\left(cu\right) = \Delta x \frac{\partial}{\partial x}\left(D\frac{\partial u}{\partial x}\right) \quad . \tag{4.18}$$

With the assumption on the limiting behavior of rate constants, ODE System (4.8) is a finite-volume method of lines approximation to the PDE (4.18) with accuracy $O(\Delta x)^2$.

Interpretation In thinking about the progess of a molecular state down the interaction chain it becomes clear that the forward and backward reaction rates can interoperate in only two distinct ways. Either the rates balance, resulting in a state u_n that is equally likely to transition to state u_{n-1} or u_{n+1}, or they are dissimilar so that the state is more likely to transition in one direction than the other. The case where a state is equally likely to proceed in either direction up or down the chain is reminiscent of diffusion processes and Brownian motion, while the situation of directionally biased movement is reminiscent of convective diffusion. It seems plausible then that these are the two processes that dominate the transitions of the state so that a linear chain of reactions like Equation (4.1) is modeled sufficiently by the reaction diffusion Equation (4.18) with $c(x)$ and $D(x)$ derived from the rate constants, k. In § (4.6) we provide evidence that this model accurately describes a linear chain of reactions even when the total number of rections, N, is not large. We will also demonstrate that removing the diffusion term results in a good model in some circumstances but a poor model in others.

4.4.2.1 A More Complex Example

To demonstrate the generality of our approach we examine another type of chemical reaction chain. Consider again the enzyme-aided chain of reactions. The link is given

by Equation (4.3). The law of mass action allows us to describe these reactions by an ODE system:

$$\begin{aligned} \frac{du_n}{dt} &= -k_n^+ u_n E_n + k_n^- C_n + q_{n-1} C_{n-1} \quad , \\ \frac{dE_n}{dt} &= -k_n^+ u_n E_n + k_n^- C_n + q_n C_n \quad , \\ \frac{dC_n}{dt} &= k_n^+ u_n E_n - k_n^- C_n - q_n C_n \quad . \end{aligned} \tag{4.19}$$

These equations admit a simple conservation law because enzyme is never lost in the process; it simply transitions between the free and bound states.

$$\frac{d}{dt}\left(E_n + C_n\right) = 0 \quad . \tag{4.20}$$

This may be rewritten as $E_n + C_n = e_n + c_n$. Here lower-case script denotes the initial amount of the corresponding quantity, *i.e.*, $e_n = E_n(0)$. It is typically assumed in mathematical investigations of catalysis that either Michaelis-Menten kinetics dominate, or that the fast equilibrium hypothesis is valid [26]. These each yield a conceptually similar reduction of the ODE system. The Michaelis-Menten model follows from the often valid assumption that the amount of enzyme bound in complex is approximately constant.

$$\frac{\partial C_n}{\partial t} = 0 \quad . \tag{4.21}$$

Together with the conservation law, this affords a substantial reduction of System (4.19).

$$\frac{du_n}{dt} = \frac{q^*_{n-1}u_{n-1}}{m_{n-1}+u_{n-1}} - \frac{q^*_n u_n}{m_n+u_n} \quad . \tag{4.22}$$

The coefficients m_n and q^*_n and the concentrations of enzyme and complex are as follows:

$$E_n = \frac{(e_n+c_n)\,m_n}{m_n+u_n} \quad , \tag{4.23}$$

$$C_n = \frac{(e_n+c_n)\,u_n}{m_n+u_n} \quad , \tag{4.24}$$

$$m_n = \frac{q_n+k^-_n}{k^+_n} \quad , \tag{4.25}$$

$$q^*_n = q_{n-1}\,(e_{n-1}+c_{n-1}) \quad . \tag{4.26}$$

If the dependent variable is scaled, $u_n = m_n v_n$, then the dimensionless variable v_n satisfies a dimensionless system of ODE.

$$\frac{du_n}{dt} = \frac{k_{n-1}v_{n-1}}{1+v_{n-1}} - \frac{k_n v_n}{1+v_n} \quad , \tag{4.27}$$

$$k_n = q^*_n/m_n \quad . \tag{4.28}$$

As in the last derivation, as $\Delta x \to 0$, $q_n = O(1/\Delta x)$. Note however that $k = O(1)$ because $e_n = O(\Delta x)$ and $c_n = O(\Delta x)$. This leads to a study of systems of the form

$$\frac{dv_n}{dt} = k_{n-1} f\,(v_{n-1}) - k_n f\,(v_n) \quad , \tag{4.29}$$

with $k_n = O(1)$. Proceeding as in § (4.4) we arrive at the following approximation:

$$\frac{\partial v}{\partial t} + \Delta x f'(0) \frac{\partial}{\partial x}(kv) = O(\Delta x)^2 \quad . \tag{4.30}$$

Setting the lower order terms on the right side of Equation (4.30) gives a convection diffusion equation describing slow moving waves. In the case of the enzyme reactions currently under treatment, $f'(0) = 1$ and the solution to Equation (4.30) is

$$v(x,t) = v_0 \left(f^{-1} \left(f(x) - t\Delta x \right) \right) \frac{k \left(f^{-1} \left(f(x) - t\Delta x \right) \right)}{k(x)}. \tag{4.31}$$

Here $f(x) = \int \frac{1}{k(x)} dx$ is an invertible function because $k > 0$. The function $u_0(x)$ is the initial data. This example serves only to illustrate the general applicability of the continuous reaction technique. No claim is made regarding the accuracy of this approximation and the PDE solution above is not compared to that of the general ODE system (4.27) in this thesis.

Note that if $k(x)$ is identically constant, then this solution reduces to $u = u_0(x - t\ k\Delta x)$, a constant velocity traveling wave.

4.5 Boundary Conditions

4.5.1 Introduction

In § (4.4) we developed a method for distilling certain systems of ordinary differential equations into a single partial differential equation. Our focus nows turns toward developing accompanying boundary conditions.

4.5.2 Derivation

Consider again System (4.8) whose collection of ODE we distilled into the PDE (4.18). For purposes of our later modeling we modify these equations to include a source flux term into state $x = 0$.

$$\frac{du_0}{dt} = s(t) - k_0^+ u_0 + k_1^- u_1 \quad , \tag{4.32}$$

$$\frac{du_n}{dt} = k_{n-1}^+ u_{n-1} - (k_n^- + k_n^+) u_n + k_{n+1}^- u_{n+1} \quad , \tag{4.33}$$

$$\frac{du_N}{dt} = k_{N-1}^+ u_{N-1} - k_N^- u_N \quad . \tag{4.34}$$

As in § (4.4) we introduce the continuous variable x and dependent variable $u(x,t)$. We assume that PDE (4.18) is satisfied on $x \in (0, x_e)$ and repeat the limiting procedure on the equations describing states $n = 0, N$ to find the boundary conditions to $O(\Delta x)$.

$$\left(c\,u - \Delta x\, D \frac{\partial u}{\partial x} - \frac{\Delta x}{2} \frac{\partial}{\partial x}(c\,u) \right)_{x=0} = s \quad , \tag{4.35}$$

$$\left(c\,u - \Delta x\, D \frac{\partial u}{\partial x} + \frac{\Delta x}{2} \frac{\partial}{\partial x}(c\,u) \right)_{x=0} = 0 \quad . \tag{4.36}$$

As shown in § (4.6), when the reaction chains are composed of essentially irreversible reactions, setting $D = 0$ in Equation (4.18) results in a model with negligible loss of qualitative accuracy. However, setting $D = 0$ in the boundary conditions (4.35, 4.36) results in two conditions on u, which obeys a PDE with only a single derivative in x. We know that the linear advection equation obtained with $D = 0$ is generally well-posed only when a single boundary condition is given together with initial data.

The presence of two boundary conditions yields an over-specified problem. Setting $D = 0$ in the boundary conditions is singular in this sense.

This conundrum may be resolved for the systems of interest to us. In our sysems, $c(x)$ will be positive so that a signal, $s(t)$, entering into state $x = 0$ transitions unidirectionally to state $x = x_e$. State x_e is the end of the reaction chain and, because backward reactions have been neglected by setting $D = 0$, is also the ultimate destination of the signal. In contrast, a pulse in $u(x, t)$ traveling down the chain of states will, according the the PDE alone, continue onward, past state x_e. We reconcile these two observations by defining a new variable $v(t)$, which is a "bin" that collects all of the signal arriving in state x_e:

$$\frac{dv}{dt} \;=\; (c\,u)_{x=x_e} \quad . \tag{4.37}$$

It is $v(t)$ not $u(x_e, t)$ that quantifies the signal level at the end of the reaction chain when backward reactions are negligible, $D = 0$. In later modeling we'll allow the end-state, x_e, to participate in other reactions, leading to additional terms being inserted into Equation (4.37).

4.6 Validity of the Continuous Reaction Approximation

4.6.1 Introduction

In this section we discuss the goodness of the approximation method developed in § 4.4. In particular we show which sets of assumptions on the reaction coefficients lead to approximations that compare favorably to exact and numerical solutions. We also contrast our approach to techniques developed by other authors for treating such systems.

4.6.2 Exact Solutions

4.6.2.1 Irreversible Reactions

Consider system (4.8) with the addition of a source term. In the special case of negligible backward reactions and identical forward reactions, this system reduces to

$$\begin{aligned} \frac{du_0}{dt} &= s - k^+ u_0 \quad , \\ \frac{du_n}{dt} &= k^+ u_{n-1} - k_n^+ u_n \quad , \\ \frac{du_N}{dt} &= k_{N-1}^+ u_{N-1} \quad . \end{aligned} \tag{4.38}$$

Here s describes a constant source of signal input into the zero state. This system is sufficiently simple so as to admit an easily derived analytical solution. For $0 \leq n < N$

the solution is

$$u_n(t) = \frac{s}{k}\left(1 - e^{-kt}\sum_{i=0}^{n}\frac{(k\ t)^i}{i!}\right) \quad . \tag{4.39}$$

An alternative representation is

$$u_n(t) = \frac{s}{k\ n!}\int_0^{kt} s^n e^{-s}\ ds \quad . \tag{4.40}$$

The series representation makes it clear that $\lim_{n\to\infty} u_n(t) = 0$ while the integral representation makes it clear that $\lim_{t\to\infty} u_n(t) = s/k$. Thus, for fixed t and $N \to \infty$, the u's transition from $u_0 = (s/k)(1 - e^{-kt})$ to $u_\infty = 0$ while for fixed n, $u_n(t)$ transitions from $u_n(0) = 0$ to $u_n(\infty) = s/k$. This analysis indicates that the sequence of u's is behaving much like a traveling wave. When we use the continuous reaction approximation, neglect the backward reaction, and assume that all of the k's are identical, we arrive at $v_t + cv_x = 0$, the equation of one-dimensional linear advection (*c.f.* Equation 4.18). Its solutions are traveling waves as well. In the present case, with $(cu)_{x=0} = s$ for $t > 0$ and $u(x, 0) = 0$, its solution is $u = 0$ for $x < ct$ and $u = s/c$ for $x > ct$.

To make this comparison more precise, recall assumption (4.14) and definitions (4.17) and (4.11). With $k = c/\Delta x$ and $x = n\Delta x$ in solution (4.40) the asymptotic expansion of $u(x, t)$ is computed for $\Delta x \ll 1$ using the method of Laplace [1]:

$$u(x,t) \sim \begin{cases} s/c + O(\Delta x) & \text{for} \quad x < ct - \alpha \\ \\ O(\Delta x) & \text{for} \quad x > ct + \alpha \end{cases} \quad . \tag{4.41}$$

This holds for $\frac{x}{\Delta x} \gg 1$ and for all α with $\frac{\alpha}{\Delta x} \gg 1$. The expansion shows that the continuous reaction approach gives the leading order term in the asymptotic expansion of the exact solution. Alternatively, for $N = 1/\Delta x \gg 1$ and $k = O(1/\Delta x)$ the exact solution, Equation (4.40), is equal to the PDE solution, to leading order in Δx. This justifies the removal of lower order terms in Equation (4.15) for this special case.

4.6.2.2 Symmetric Reversible Reactions

There are other special cases where exact solutions can be computed. If each reaction is identical and symmetrically reversible ($k^+ = k^-$, independent of n), then the ODE system (4.8) with the addition of a source term takes the following form:

$$\begin{aligned} \frac{du_0}{dt} &= s - ku_0 + ku_1 \quad , \\ \frac{du_n}{dt} &= ku_{n-1} - 2ku_n + ku_{n+1} \quad , \\ \frac{du_N}{dt} &= ku_{N-1} - ku_N \quad . \end{aligned} \tag{4.42}$$

The exact solution of this is difficult to calculate. It is composed of linear time growth terms as well as exponentially vanishing in time terms (henceforth referred to as EVT). If t is large enough, *i.e.*, $kt \gg 1$, then the EVT can be neglected to find an approximate solution:

$$u_n(t) = \frac{s}{k}\left(\frac{k\,t}{N+1} + \frac{n(n+1)}{2(N+1)} - n + \alpha\right) + EVT \quad .$$

Here α is a constant independent of n and t. Setting $N = 1/\Delta x$, $x = n/N$ and $k = D/\Delta x$ gives a function of x and t that satisfies the diffusion equation $\frac{\partial u}{\partial t} = \Delta x\, D \frac{\partial^2 u}{\partial x^2}$.

So, up to terms that vanish exponentially in time, solutions to the full set of ODE are, after a change of variables, solutions to the diffusion equation developed in § (4.4).

4.6.3 Other Methods

Methods for treating large systems of ODE describing chemical reactions have been developed by others [12], [13]. Each of those methods relies on the reactions being irreversible, or on identifying a rate limiting step in the reaction chain. The example discussed in § (4.6.2.2) shows that the method developed in § (4.4) doesn't make these requirements, and the example of § (4.6.2.1) shows that our method is also valid in the case of irreversible reactions. Whether our method is suitable for reaction chains with rate limiting steps is not discussed here. Our method can also be applied to more complicated reaction sequences, as in § (4.4.2.1). In contrast, the main drawback of our method is that it requires a conceptual abstraction of the reaction chain and the willingness to view it as a infinite sequence of infinitesimal reactions. The strength of this approach will be evident in the modeling we do in later chapters.

Chapter 5

Autocrine Signaling of Vulval Precursor Cells

5.1 Introduction

In Chapter 2 we described a means by which a solitary Vulval Precursor Cell (VPC) may, through autocrine signaling, influence its own development. Specifically, the MAP kinase pathway, stimulated by LIN-3 from the anchor cell (AC), yields products leading to secreted DELTA ligands that then trigger LIN-12 receptors on the cell itself. See Figure (2.1). The activation of the lateral signaling pathway can inhibit the MAPK pathway at several points. As we discussed in § (2.4), there is evidence for inhibition of MAPK itself, on the trafficking and degradation of LET-23 receptors, and of the initiation of the MAPK pathway by activated receptors.

There are many motivations for studying an isolated VPC. By removing the influence of its neighbors we gain a better understanding of the default behavior of a VPC. Firstly, if a VPC is isolated it is possible that it could signal itself in an autocrine fashion via the secreted DELTA-type ligand DSL-1. This could potentially play a strong role in the specification of the fate of an isolated VPC and perhaps even in specifying

VPC fates in a wild-type gonad. Additionally, if autocrine signaling is present, then, as we have described in § (2.4), the MAPK pathway will be inhibited in several ways. Multiple inhibitors may play redundant roles, or possibly have varied influences on fate outcomes. Finally, experiments have shown that a VPC in isolation may adopt different fates depending on its distance from the AC. See Table (5.1). This may seem to be an obvious consequence of a graded inductive signal, however it is possible that this outcome may arise from more subtle influences. We focus, in particular, on cases when cell fates of isolated VPC are not clearly determined. Experiments in [25] show that the P3.p cell does not adopt a single fate consistently when in isolation, while P4.p does. See Table (5.1). In this section we pursue a model of an isolated VPC to address the following questions:

- Does the fate of an isolated VPC depend strictly on a dose dependent response to a graded inductive signal?
- What role does an autocrine lateral signal play in fate determination?
- What role does the presence of multiple inhibitors play in cell fate determination?
- Why aren't isolated P3.p cell fates specified consistently?

5.2 Models for Autocrine Signaling

In the language of Chapter 4 we think of both the MAPK and lateral signal pathways as being segments of a linear chain of reactions. This leads to a continuous model,

Table 5.1: Fates Adopted by Isolated Vulval Precursor Cells. Laser ablations were performed on 34 worms by [25] to study isolated VPC. Data adapted from Table 1 in [25]. Rows 1–3 show the fates adopted by an isolated P4.p VPC in otherwise wild-type worms. The primary fate is specified in 10 of 14 worms. Rows 4–6 show the fates adopted by an isolated P3.p VPC in otherwise wild-type worms. Secondary, tertiary, and hybrid type fates are specified in apparently uniform multiplicities. The primary fate is never specified. Row 7 shows the fate adopted by an isolated P3.p VPC in worms with multiple copies of lin-3, the gene encoding the inductive signal in the AC. The primary fate is always adopted in this case.

Row	Cell Type	Fate	#
1	P4.p	2°	2
2	P4.p	1°/2° hybrid	2
3	P4.p	1°	10
4	P3.p	3°	4
5	P3.p	2°/3° hybrid	2
6	P3.p	2°	3
7	P3.p*	1°	11

which in the simplest case takes the form of Equation (4.18). If we suspect that the reaction chain is nearly irreversible, then arguments in § (4.6) allow the reduction to the form of a simple linear advection equation:

$$\frac{\partial u}{\partial t} + \frac{\partial}{\partial x}(cu) \;=\; 0 \quad . \tag{5.1}$$

Because the species at the end state of the chain, $u(x_e, t)$, *i.e.*, the secreted ligand, leads to the inhibition of the MAPK pathway, we think of it as inhibiting some intermediate state in the chain $u(x_i, t)$. To formulate boundary conditions for this problem we refer to § (4.5). In terms of the fluxes in our continuous models, the

boundary and initial conditions are as follows:

$$
\begin{aligned}
c(0)u(0,t) &= s(t) \quad , && (5.2)\\
c(x_i^+)u(x_i^+,t) &= c(x_i^-)u(x_i^-,t) - q_i u(x_i^+,t)v(t) \quad , && (5.3)\\
\frac{dv}{dt} &= c(x_e)u(x_e,t) - q_e u(x_i^+,t)v(t) \quad , && (5.4)\\
v(0) &= v_0 \quad . && (5.5)
\end{aligned}
$$

Here, superscripts + and – denote right and left hand limits, respectively, x_i is the state in the MAPK pathway being inhibited, x_e is the end state of the chain, and $v\,(t)$ is the level of inhibitor, which is assumed initially to be v_0. In formulating these conditions, we assume that the inhibition is a destructive process, annihilating both states according to the constants q_i and q_e. If we assume that both species are removed irreversibly in a bimolecular reaction, then $q_i = q_e$. If we suspect that the inhibitor is acting in an enzymatic fashion, then it would not be consumed in the inhibition process, so $q_e = 0$. The function $s(t)$ is the source flux of inductive signal from the anchor cell, which we will prescribe. In this model we have accounted for the presence of a single inhibitor acting on state x_i. By adjusting the value of x_i we intend to study the action of each inhibitor individually to determine whether different inhibitors have different effects.

The non-linear PDE/ODE system (5.1–5.5) could be quite difficult to solve; however, when there are no rate limiting steps in the reaction chain it is reasonable to posit that c(x) is a constant, *c.f.*, § (4.6). This leads to a problem that appears only

slightly less complex:

$$\begin{aligned}
\frac{\partial u}{\partial t} + c\,\frac{\partial u}{\partial x} &= 0 \quad , && (5.6)\\
c\,u(0,t) &= s(t) \quad , && (5.7)\\
c\,u(x_i^+,t) &= c\,u(x_i^-,t) - q_i\,u(x_i^+,t)\,v(t) \quad , && (5.8)\\
\frac{dv}{dt} &= c\,u(x_e,t) - q_e\,u(x_i^+,t)\,v(t) \quad , && (5.9)\\
v(0) &= v_0 \quad . && (5.10)
\end{aligned}$$

Equation (5.6) has a solution in the form $u = f(t - \frac{x}{c})$ for all $x < x_i$. Inserting this into the boundary condition in 5.7 gives $f(t) = \frac{1}{c}s(t)$. Equation (5.6) has a solution in the form $u = g(t - \frac{x}{c})$ for all $x > x_i$. Inserting this and the expression for $f(t)$ into Equation (5.8) then gives $g(t) = \frac{s(t)}{c+q_i v(t+\frac{x_i}{c})}$. Finally, using this expression for g(t) in 5.9 gives a non-linear initial value delay differential equation problem for v(t).

$$\begin{aligned}
\frac{dv(t)}{dt} &= c\frac{s(t-\frac{x_e}{c})}{c+q_i\,v(t-\frac{x_e-x_i}{c})} - q_e\frac{s(t-\frac{x_i}{c})\,v(t)}{c+q_i\,v(t)} && (5.11)\\
v(0) &= v_0
\end{aligned}$$

See Appendix (A.1) for a discussion of existence and uniqueness of solutions to initial value problems for delay differential equations.

5.2.1 Dimensionless Groups and Scaling

Our variables have the following scales:

$$[v] = \text{concentration} \tag{5.12}$$

$$[u] = \text{concentration per state} \tag{5.13}$$

$$[s] = \text{concentration per time} \tag{5.14}$$

$$[t] = \text{time} \tag{5.15}$$

$$[x] = \text{states} \tag{5.16}$$

$$[c] = \text{states per time} \tag{5.17}$$

$$[q] = \text{states per time per concentration} \tag{5.18}$$

Let v^*, u^*, and s^* be some characteristic values of v, u, and s, respectively. By examining Equation (5.6) we find a physically relevant ratio, $\frac{x_e}{c} \equiv T$. This is the time required for source effects to propagate through the chain. This quantity motivates a choice of dimensionless variables.

$$\tau = \frac{t}{T} \tag{5.19}$$

$$y = \frac{x}{x_e} \tag{5.20}$$

$$S(\tau) = \frac{1}{s^*} s(T\tau) \tag{5.21}$$

$$V(\tau) = \frac{1}{v^*} v(T\tau) \tag{5.22}$$

$$G(\tau) = \frac{1}{v^*} g(T\tau) \tag{5.23}$$

$$U(\tau - y) = \frac{1}{u^*} u(T(\tau - y) \tag{5.24}$$

Our problem is now dimensionless.

$$\begin{aligned} \alpha \frac{dV(\tau)}{d\tau} &= \frac{S(\tau-1)}{1+\beta_i\, V(\tau-(1-\phi))} - \beta_e \frac{V(\tau)\, S(\tau-\phi)}{1+\beta_i\, V(\tau)} && (5.25) \\ V(\tau) &= G(\tau) \quad \text{for } \tau \in [-1,0] \\ U(\tau-y) &= \frac{\delta}{1+\beta_i V(\tau-y+\phi)} \quad \text{for} \quad y > \phi && (5.26) \end{aligned}$$

with

$$\begin{aligned} \alpha &= \frac{v^*}{T\, s^*} && (5.27) \\ \beta_i &= \frac{v^*\, q_i}{c} && (5.28) \\ \beta_e &= \frac{v^*\, q_e}{c} && (5.29) \\ \delta &= \frac{s^*}{u^* c} && (5.30) \\ \phi &= \frac{x_i}{x_e} < 1 && (5.31) \end{aligned}$$

5.2.2 The Biological Problem

We suppose that initially the levels of inhibitor are constant, v_0, and that the external signal begins at time $t = 0$ and from then on is the constant s^*. Because the signal input rate s^* is fixed, we scale u and v according to this level.

$$\begin{aligned} v^* &= s^*\, T && (5.32) \\ u^* &= \frac{s^*}{c} && (5.33) \end{aligned}$$

One consequence of this is $\alpha = 1$ and $\delta = 1$. This leads to the following problem:

$$\begin{aligned} \frac{dV(\tau)}{d\tau} &= \frac{H(\tau-1)}{1+\beta_i V(\tau-(1-\phi))} - \beta_e \frac{V(\tau)\,H(\tau-\phi)}{1+\beta_i V(\tau)} \quad , \qquad (5.34) \\ V(\tau) &= \gamma \left(= \frac{v_0}{s^* T}\right) \quad \text{for } \tau \in [-1,0] \quad , \\ U(\tau-y) &= \frac{1}{1+\beta_i V(\tau-y+\phi)} \quad \text{for } y > \phi \quad . \qquad (5.35) \end{aligned}$$

Here $H(\tau)$ is the Heaviside unit step function [1]. In the remainder of this chapter we'll pursue the qualitative behavior of (5.34) over the parameter space $\{\gamma,\, \phi,\, \beta_i,\, \beta_e\}$ and discuss the implication to inhibitory autocrine signaling in *C. elegans* vulval precursor cells.

5.2.2.1 No Inhibition

If autocrine signaling doesn't occur, then MAPK activity is directly proportional to LIN-3 signal level. Under this hypothesis fate specification is decided entirely by the proximity of the VPC to the AC or the level of LIN-3 signal from the AC. This is consistent with VPCs adopting either 1° or 3° fates but is inadequate to explain 2° fate outcomes, which are thought to arise as a result of lateral signaling [21, 23, 40, 41]. The necessity of the lateral signal in specifying 2° fates requires us to include autocrine signaling if we hope to explain the experimental results of Table (5.1).

5.2.2.2 Non-Destructive Inhibition

If the inhibitor is not degraded in the process of inhibiting the MAPK pathway then $q_e = 0$, which gives $\beta_e = 0$. Putting this into Equation (5.34) and dropping the

subscript gives (5.36).

$$\begin{aligned} \frac{dV(\tau)}{d\tau} &= \frac{H(\tau-1)}{1+\beta\, V(\tau-(1-\phi))} \\ V(\tau) &= \gamma \quad \text{for } \tau \in [-1,0] \end{aligned} \tag{5.36}$$

Notice that the right hand side of Equation (5.36) is zero for $\tau < 1$. As a consequence $V(\tau) = \gamma$ up to time $\tau = 1$. This allows us to restate the problem as an "initial" value problem starting at $\tau = 1$ by defining $\delta = 1 - \phi$, $W(z) = V(\delta z + 1)$, and $z = \frac{\tau-1}{\delta}$. Our problem now has only one delay.

$$\begin{aligned} \frac{dW(z)}{dz} &= \frac{\delta}{1+\beta\, W(z-1)} \\ W(z) &= \gamma \quad \text{for } z \in [-1,0] \end{aligned} \tag{5.37}$$

Result 1 *If $\gamma > 0$ and $\beta > 0$ then the solution of the DDE initial value problem (5.37) is monotonic increasing, bounded for all finite $z > 0$ and unbounded as $z \to \infty$.*

Proof of Result 1: $1 + \beta\, W(z-1) = 1 + \beta\,\gamma > 0$ initally, so W is initially increasing. Let z_0 be the first value of z for which $W'(z) = 0$. At this point $\frac{1}{1+\beta\, W(z_0-1)} = 0$. This is not possible for finite W. Hence W is monotonically increasing whenever it is finite. Because W is monotonic increasing, $W > \gamma$ for all $0 < z < z^*$, where z^* is a point where W becomes infinite. If no such point exists, then $z^* = \infty$. This shows that $W' \leq \frac{\delta}{1+\beta\gamma}$ so that $W \leq \frac{\delta}{1+\beta\gamma} z + \gamma$, which is finite for all finite z. Hence, W is bounded and monotonically increasing for all $0 < z < \infty$. To prove unboundedness,

suppose that, as $z \to \infty$, $W(z)$ remains bounded by some value, M. So, $W' > \frac{\delta}{1+\beta M}$, which implies that W isn't bounded as $z \to \infty$, a contradiction. □

It is simple to show that, for large z, $W(z)$ behaves asymptotically as $W \sim \sqrt{\frac{2\delta z}{\beta}}$. We elaborate on this in Appendix (A.2.3.1). See Figure (5.1) for a plot of the numerical approximation and Figure (A.1) for asymptotic estimates and bounds.

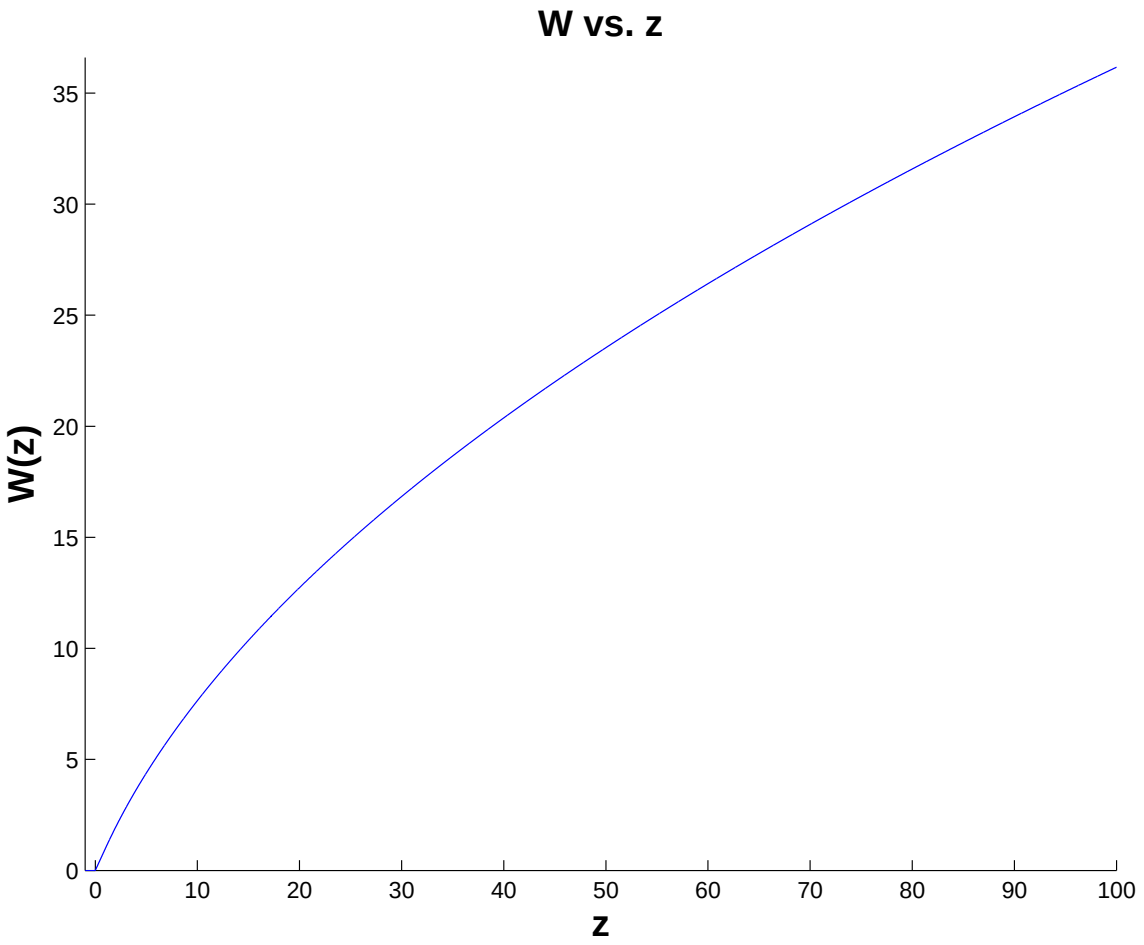

Figure 5.1: Non-Destructive Inhibition during Autocrine Signaling. $\gamma = 0 \quad \delta = 1 \quad \beta = 0.1$. $W(z)$ is monotonically increasing for all parameter values and grows like $\sqrt{\frac{2\delta z}{\beta}}$, as we prove in Appendix (A.2.3.1).

In terms of dimensional variables this shows that $v(t) \sim \sqrt{\frac{2\,s^*\,c\,t}{q_i}}$ so that both MAPK activity and LIN-12 activity vanish monotonically, $u \sim \sqrt{\frac{s^*}{2\,c\,q_i\,t}}$. The decisive shutdown of both signaling pathways would seem indicative of the 3° fate. This shutdown is delayed if s^* is increased, *i.e.*, lin-3 exists in multiple copies or the VPC is closer to the AC. Observations in Table (5.1) suggest that increasing s^* should not simply delay the shutdown of the pathways but rather prevent it altogether. For this reason we deduce that our non-destructive inhibition model is probably not an accurate description of the fate specification mechanism.

5.2.2.3 Destructive Inhibition

If inhibitor is removed by its action on the substrate, then $q_i = q_e \neq 0$ so that $\beta_i = \beta e \equiv \beta \neq 0$.

$$\frac{dV(\tau)}{d\tau} = \frac{H(\tau-1)}{1+\beta\,V(\tau-(1-\phi))} - \beta\frac{V(\tau)\,H(\tau-\phi)}{1+\beta\,V(\tau)} \tag{5.38}$$

$$V(\tau) = \gamma \quad \text{for } \tau \in [-1,0]$$

$$U = \frac{1}{1+\beta\,V(\tau-(1-\phi))} \tag{5.39}$$

In Appendix (A.2.3.2) we show that for $\phi = 1$ this system has monotonic solutions that converge to $1/\beta$. Also, in that appendix, we show that for the other extreme value, $\phi = 0$, the solutions, to leading order in β for $\beta \ll 1$, are monotonic and converge to $1/\beta$. For $\beta > 0$ and $\phi \neq 1$ the system can exhibit oscillations. These oscillations become more pronounced for $(1-\phi)\,\beta \gtrsim 1.113$ and approach a period-2 solution as $(1-\phi)\,\beta \to \infty$. See the analysis in Appendix (A.3.1.1) for the proof of

this. This transition, in dimensional variables is given by

$$\left(1 - \frac{x_i}{x_e}\right) \frac{q\, s^*\, x_e}{c^2} > 1.113\ldots \quad . \tag{5.40}$$

The equilibrium value of the dimensional concentration of inhibitor is given by c/q corresponding to dimensional MAPK and LIN-12 activity on the order of s^*/c. See Figure (5.2). It is remarkable that these equilibrium activity levels don't depend on the inhibitor strength q or on the type of inhibitor, described by x_i. On these grounds we might infer that fate specification in isolated VPC is dependent solely on proximity to the AC. However, we observe that increased LIN-3 signal strength, s^*, also encourages oscillatory MAPK and LIN-12 activity. The same can be said for strong inhibitors (increased q), inhibitors acting farther upstream of MAPK ($x_i \ll x_e$), and cells with a slower transduction of the inductive and lateral signals (c smaller).

Many of these parameters should be identical in each cell. The MAPK and LIN-12 pathways are thought to be invariant from cell to cell and so q, x_i, x_e, and c should be fixed quantities in any VPC. We expect only the signal strength to vary from cell to cell. Our analysis has shown that increasing signal strength, s^*, leads to an increase in MAPK and LIN-12 activity while also encouraging oscillations in these activities.

How can this explain the data in Table (5.1)? This data indicates the established dogma, *i.e.*, insufficient levels of inductive signal leads VPC to the 3° fate. It also indicates (see rows 4–6) that intermediate levels of inductive signal apparently lead to stochastic cell fate determination. From this we observe the correlation between cell fates and inductive signal equilibrium levels. More interestingly, our model shows

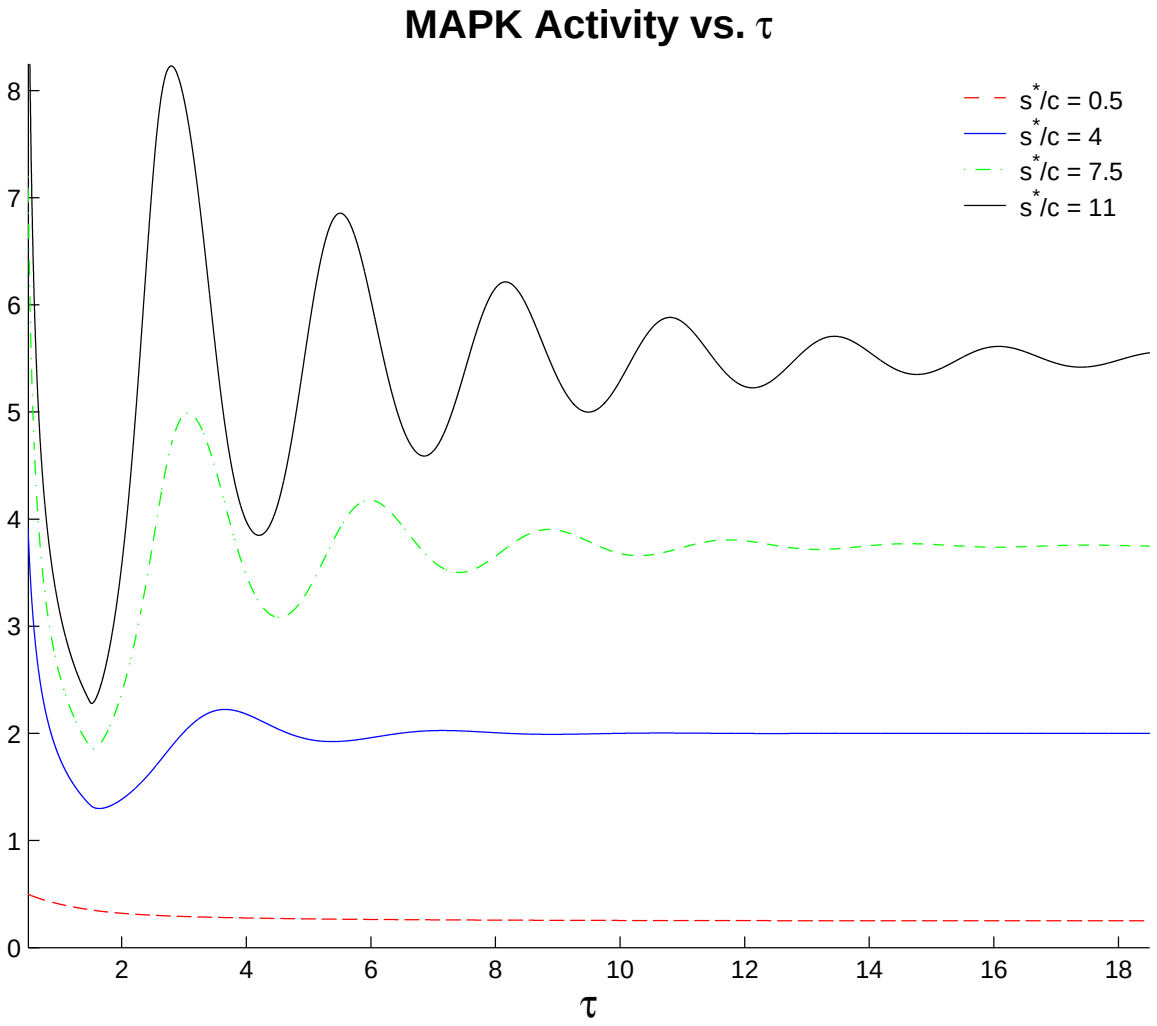

Figure 5.2: Destructive Inhibition during Autocrine Signaling. $\gamma = \phi = 0$. Activity of MAPK (and hence LIN-12) exhibits damped oscillations in time decaying toward equilibrium, $U^* = s^*/2c$. Lower levels of signal (bottom red dashed curve) cause consistently low levels of MAPK activity while higher levels (top black solid curve) exhibit higher yet oscillatory levels of MAPK activity.

that the same correlation exists between cell fates and oscillations in MAPK/LIN-12 activity. The time resolution needed to experimentally observe such oscillations may not currently be attainable, and we find no such observations in the literature. Given the correlation between cell fate outcome, inductive signal strength, and MAPK/LIN-12 pathway activity, it is possible that our model is the first "observation" of a truly oscillatory cell fate behavior.

Intermediate inductive signal levels may be sufficient to specify the primary fate. But if these levels oscillate, as our model suggests, then definitive fate specification should not be expected. The apparently stochastic cell fate specifications seen in Table (5.1) are then easily explained. At higher signal levels, 1° fates appear to be specified definitively despite oscillations. This suggests that two types of information are processed by the VPC– the absolute level of signal and the fluctuations in that signal.

Oscillatory genetic and protein activity is ubiquitous in cells. From periodic fluctuations in glycolytic processes [2], to cyclin activities throughout the cell cycle [42], to oscillatory intracellular Ca^{2+} levels [26], time varying chemical oscillations function in many capacities *in vivo*. *C. elegans* vulval precursor cells perhaps join this list as a cell type that exhibits what one author calls "flexible control" [29] over its cell fate decisions. Indeed, a cell fate decision not made in an instant or based on an absolute level, but integrated over a series of time points allows the cell to make a decision based on a greater amount of information about itself and its surroundings.

At low signal levels, 3° fates are specified by constant low MAPK activity. At

high levels, 1° fates are specified by an oscillating level of high MAPK activity. The flexibility comes at intermediate levels of signal, where an oscillating level of MAPK activity gives the cells the flexibility of choosing 1°, 2°, or 3° fates. If the VPC were not isolated but instead had one or two neighbors, being in such a transient state would make a VPC highly sensitive to signal from these neighbors. Oscillating between high and low levels of MAPK activity would allow influence from a neighbor to "lockin" a high or low level and precisely specify a fate.

This suggests that while P4.p cells seem destined to become mainly 1° when isolated, P3.p, because of the reduced signal level that they experience, remain flexible in their decision making, waiting for cues from neighbors before committing to a fate.

Chapter 6

The AC/VU Decision

6.1 Introduction

As described in § (3.2), an intercellular signaling event involving NOTCH (LIN-12) and DELTA (LAG-2) is the likely mechanism by which the Ventral Uterine (VU) fate is specified during an interaction between Z1.ppp and Z4.aaa. See Figure (3.1). The goal of this section is to develop a mathematical model of this interaction. In subsequent sections we analyze and interpret the model in a biological context and propose modifications to the model that bring it into better agreement with laboratory observations. This refinement process points to a novel mechanism, which has not yet been observed biologically. Upon first inspection, the model depicted in Figure (6.1) appears not to have the linear structure essential for the application of the model-reducing technique developed in § (4.4) and successfully employed previously in the study of autocrine signaling of vulval precursor cells in § (5.2). However, as Figure (6.2) elucidates, the mechanism can be decomposed into two distinct yet interactive linear chains.

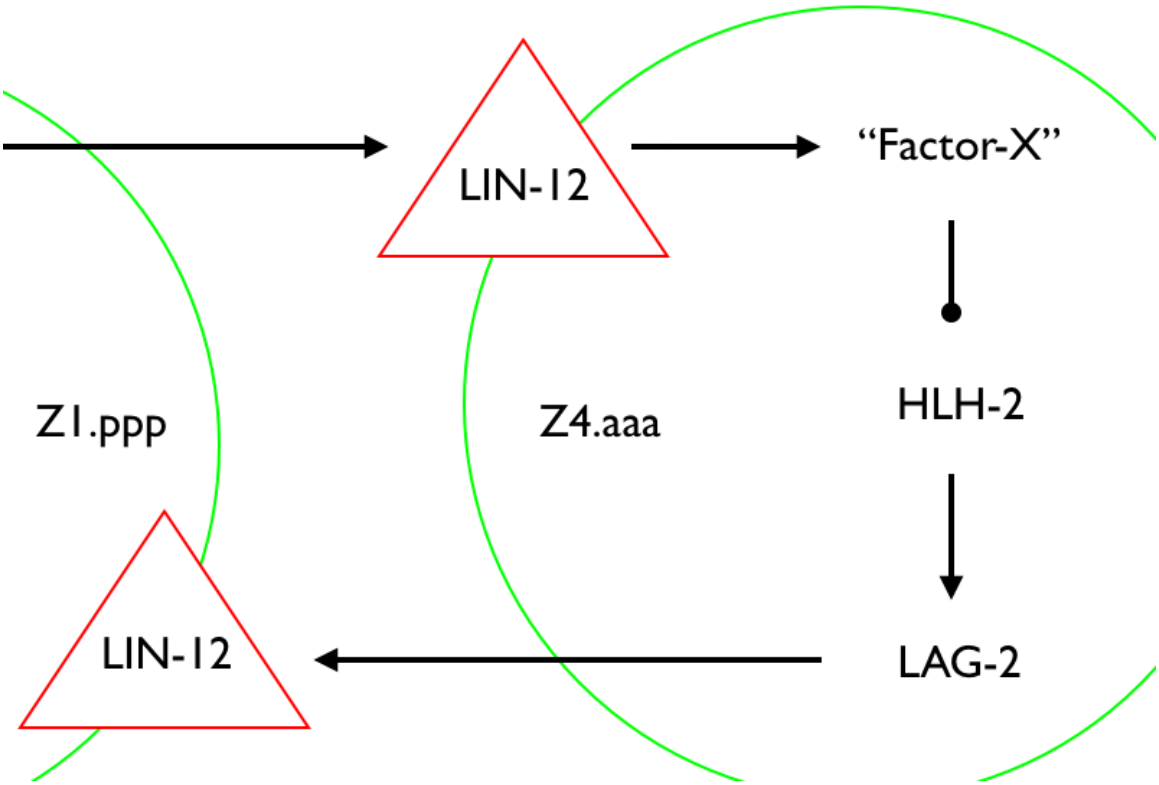

Figure 6.1: The Karp and Greenwald Model. HLH-2 protein activates the transcription of the DELTA-type trans-membrane ligand LAG-2 leading to activated NOTCH-type receptor LIN-12 on the neighboring cell. Activated LIN-12 is thought to activate Factor-X, a hereto unidentified post-transcriptional down-regulator of HLH-2.

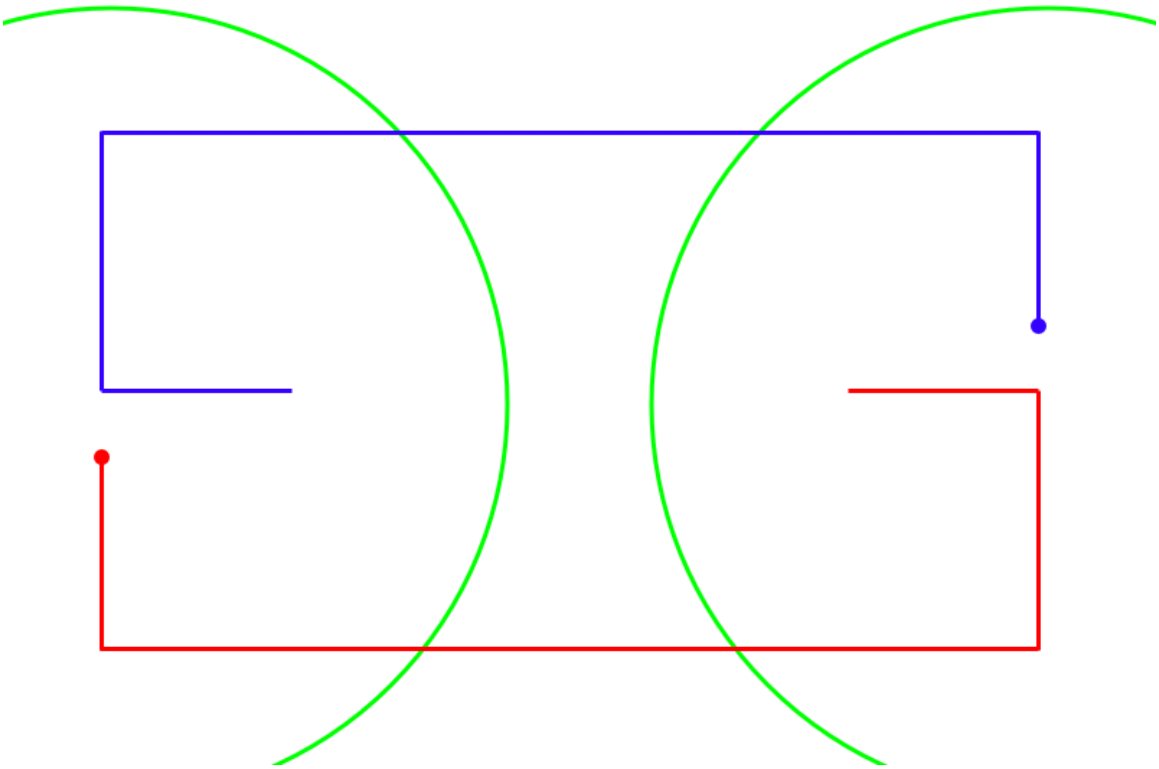

Figure 6.2: The Karp and Greenwald Model: Decompostion Into Linear Chains. Abstracting the Karp and Greenwald model reveals the linear chains of interactions involved in the signaling event. The terminal ends (filled disks) show the point at which a given chain inhibits its counterpart. The initial ends represent the unknown activator/promoter of hlh-2 transcription.

6.1.1 Models of the AC/VU Decision

As in § (4.4), chains of reactions are modeled using 1-D advection equations.

$$\begin{aligned} \frac{\partial u_i}{\partial t} + c_i \frac{\partial u_i}{\partial x} &= 0 \qquad (6.1) \\ t &\in [0, \infty) \\ x &\in [0, x^*] \end{aligned}$$

Here $u(x,t)$ is the level of signal in the chain at time t and phase point x, while c is the signal transduction speed. Subscripts denote the first born cell (i=1) and the second born cell (i=2). The rate and activators of HLH-2 production are not well-classified in the literature, hence the rate of HLH-2 production is taken to be an unknown function.

$$c_i u_i (0,t) = s_i (t) \qquad (6.2)$$

Analogous to the derivation in § (5.2), the accumulated inhibitor is collected in a new set of variables, $v_i (x,t)$.

$$\begin{aligned} c_i u_i \left(x^{0,+}, t\right) &= c_i u_i \left(x^{0,-}, t\right) - q_{i,u} v_j u_i \left(x^{0,+}, t\right) \qquad (6.3) \\ \frac{dv_i}{dt} &= c_i u_i (x^*, t) - q_{i,v} v_i u_j \left(x^{0,+}, t\right) \qquad (6.4) \end{aligned}$$

Here $q_{i,u}$ describes the rate of removal of u_i due to interactions with inhibitor v_j, $i \neq j$. The quantity $q_{i,v}$ is defined conversely. Equation (6.1) is solved by functions of the form $u_i (x,t) = f_i \left(t - \frac{x}{c_i}\right)$. Applying conditions given by Equation (6.2) and

(6.3) gives an expression for u_i.

$$u_i(x,t) = \begin{cases} \frac{1}{c_i} s_i\left(t - \frac{x}{c_i}\right) & \text{for } x \in [0, x^0) \\ \frac{s_i\left(t-\frac{x}{c_i}\right)}{c_i + q_{i,u} v_j\left(t-\frac{x-x^0}{c_i}\right)} & \text{for } x \in (x^0, x^*] \end{cases} \tag{6.5}$$

Formula (6.5) is applied to Equation (6.4), obtaining a delay differential equation for v_i and an expression for the LAG-2 production rate.

$$\frac{dv_i}{dt} = \frac{c_i\, s_i\left(t - \frac{x^*}{c_i}\right)}{c_i + q_{i,u}\, v_j\left(t - \frac{x^*-x^0}{c_i}\right)} - \frac{q_{i,v}\, v_i(t)\; s_j\left(t - \frac{x^0}{c_j}\right)}{c_j + q_{j,u}\, v_i(t)} \tag{6.6}$$

$$R_i(t) = \frac{c_i\, s_i\left(t - \frac{x^1}{c_i}\right)}{c_i + q_{i,u} v_j\left(t - \frac{x^1-x^0}{c_i}\right)} \tag{6.7}$$

Here x^1 denotes the state representing LAG-2. The goal is now to understand the behavior of this system in a biological context. The variables are made dimensionless as follows:

$$\tau = \frac{c_1}{x^*} t \quad , \tag{6.8}$$

$$S_i(\tau) = \xi_i\, s_i(t) \quad , \tag{6.9}$$

$$V_i(\tau) = \frac{c_1}{\xi_1\, x^*} v_i(t) \quad . \tag{6.10}$$

The system is now dimensionless.

$$\begin{aligned} \frac{dV_1}{d\tau} &= \frac{S_1(\tau - 1)}{1 + \frac{q_{1,u}\xi_1 x^*}{c_1^2} V_2\left(\tau - \frac{x^*-x^0}{x^*}\right)} - \frac{q_{1,v}\xi_2 x^*}{c_1^2} \frac{V_1(\tau)\; S_2\left(\tau - \frac{x^0}{x^*}\frac{c_1}{c_2}\right)}{\frac{c_2}{c_1} + \frac{q_{2,u}\xi_1 x^*}{c_1^2} V_1(\tau)} \\ \frac{dV_2}{d\tau} &= \frac{\xi_2}{\xi_1} \frac{S_2\left(\tau - \frac{c_1}{c_2}\right)}{1 + \frac{q_{2,u}\xi_1 x^*}{c_1^2} V_1\left(\tau - \frac{x^*-x^0}{x^*}\frac{c_1}{c_2}\right)} - \frac{q_{2,v}\xi_1 x^*}{c_1^2} \frac{V_2(\tau)\; S_1\left(\tau - \frac{x^0}{x^*}\right)}{1 + \frac{q_{1,u}\xi_1 x^*}{c_1^2} V_2(\tau)} \end{aligned} \tag{6.11}$$

To this point the model's derivation has been aimed towards mathematical generality. However, biological observations suggest that the two cells are equipotent, *i.e.*, equally likely and capable of adopting the VU fate. We henceforth refer to this as the *equipotency hypothesis*. We may interpret this hypothesis as the two cells being identical from a gene expression and signal transduction standpoint. This assumption implies $q_{1,u} = q_{2,u}$, $q_{1,v} = q_{2,v}$, $c_1 = c_2$, and $\xi_1 = \xi_2$. With these relations, the model simplifies.

$$\begin{aligned} \frac{dV_1}{d\tau} &= \frac{S_1(\tau-1)}{1+\beta V_2(\tau-\phi)} - \gamma \frac{V_1(\tau)\, S_2(\tau-1+\phi)}{1+\beta V_1(\tau)} \\ \frac{dV_2}{d\tau} &= \frac{S_2(\tau-1)}{1+\beta V_1(\tau-\phi)} - \gamma \frac{V_2(\tau)\, S_1(\tau-1+\phi)}{1+\beta V_2(\tau)} \end{aligned} \tag{6.12}$$

The dimensionless parameters are

$$\begin{aligned} \beta &= \frac{q_u \xi x^*}{c^2} \quad , \\ \gamma &= \frac{q_v \xi x^*}{c^2} \quad , \\ \phi &= 1 - \frac{x^0}{x^*} \quad . \end{aligned} \tag{6.13}$$

System (6.12) exhibits a symmetry with respect to interchange of index, reflecting the equipotency of the two cells. This seems to suggest that the two cells should behave identically. However, initial data has yet to be discussed. From a mathematical perspective this data is required in order that the model system be a well-posed problem. From a biological perspective, this data will describe the birth order, break the symmetry of the system, and give the model the potential to produce different

fates in different cells.

As noted above, the subscripts of variables denote the birth order. Also noted above is that it is likely that both cells behave identically, *i.e.*, the equipotency hypothesis holds. Fix $t = 0$ as the time at which the first cell is born and define $t = b$ as the time at which the second cell is born. The quantity b is the birth time separation. Equipotency suggests that the HLH-2 production rates should be identical up to this time shift, $s_2(t) = s_1(t - b)$, or in terms of dimensionless variables,

$$S_2(\tau) = S_1(\tau - \psi) \quad , \tag{6.14}$$

$$\psi = \frac{b\,c}{x^*} \quad . \tag{6.15}$$

Note that $V_1 = 0$ in the first born cell for all time up to $t = 0$ and $V_2 = 0$ in the second born cell for all time up to $t = b$. It was observed in [24] that HLH-2 transcription appears to proceed at a steady level in both cells after being turned on, presumably prior to cell birth. This suggests that we set $S(\tau) \equiv 1$, making variations among the model cells dependent only on the birth time separation. The delay ϕ is now the only one in the DDE system. Normalize by defining $W(s) = \beta V(\phi s) = \beta V(\tau)$.

$$\begin{aligned}
\frac{dW_1}{ds} &= \phi\left(\frac{\beta}{1 + W_2(s-1)} + \frac{\gamma}{1 + W_1(s)} - \gamma\right) \\
\frac{dW_2}{ds} &= \phi\left(\frac{\beta}{1 + W_1(s-1)} + \frac{\gamma}{1 + W_2(s)} - \gamma\right) \\
W_1(s) &= 0 \quad \text{for all } s \in [-1, 0] \\
W_2(s) &= 0 \quad \text{for all } s \in [-1, \delta] \\
\delta &= \frac{b\,c}{x^* - x^0} > 0
\end{aligned} \tag{6.16}$$

The flux is given by:

$$R_i = \frac{\xi}{1 + W_j \left(s - \frac{x^1 - x^0}{x^* - x^0} \right)} \quad . \tag{6.17}$$

6.2 Non-Destructive Inhibition

If we assume that "Factor-X", the down-regulator of HLH-2 accumulation, is not used up in this capacity, then $q_v = 0$ and hence $\gamma = 0$.

$$\begin{aligned} \frac{dW_1}{ds} &= \frac{\sigma}{1 + W_2 (s-1)} \\ \frac{dW_2}{ds} &= \frac{\sigma}{1 + W_1 (s-1)} \\ W_1(s) &= 0 \quad \text{for all } s \in [-1, 0] \\ W_2(s) &= 0 \quad \text{for all } s \in [-1, \delta] \\ \sigma &= \phi\beta \end{aligned} \tag{6.18}$$

Result 2 *If $\sigma > 0$, then the solutions of DDE initial value problem (6.18) are non-decreasing for $s > 0$, bounded for finite $s > 0$, and unbounded as $s \to \infty$. Moreover, $W_1 > W_2$ for all $s > 0$.*

Proof of Result 2: Because $\sigma > 0$, the right hand sides of the DDE are non-negative for $s \in [0, 1]$ and so the W_i are non-decreasing on $s \in [0, 1]$. By induction the W_i are non-decreasing for all $s > 0$.

Because the W_i are non-decreasing, $W_i \geq 0$ and so $W_i' \leq \sigma$. Hence $W_i < \sigma s$ for all $s > 0$, so that the W_i are bounded for finite s.

To prove unboundedness as $s \to \infty$, suppose that for some i, $W_i < M_i$ for all s. This implies that, for $j \neq i$, $W_j' \geq \frac{\sigma}{1+M_i}$ so that W_j is unbounded as $s \to \infty$. Thus at least one of the W_i will not have an upper bound. Suppose that W_i is bounded as $s \to \infty$ while W_j is not. The fact that $0 \leq W_i$ implies that $W_j' \leq \sigma$ so that $W_j \leq \sigma\, s$. This implies that $W_i \geq \frac{\sigma}{1+\sigma\, s}$ so that $W_i \geq \ln|1 + \sigma\, s|$, which is unbounded. This contradiction shows that both W's are unbounded.

Note that, on $s \in [0, \delta]$, $W_2 = 0$ and $W_1 = \sigma s$, so that $W_1 > W_2$ on $s \in [0, \delta]$. Because $\frac{1}{1+x}$ is a monotonic decreasing function for $x > 0$, we find that $(W_1 - W_2)' = \frac{\sigma}{1+W_2(s-1)} - \frac{\sigma}{1+W_1(s-1)} > 0$ on $\delta \in [\delta, 2\delta]$. This implies that $W_1 > W_2$ on $s \in [0, 2\delta]$. By induction $W_1 > W_2$ for all $s > \delta$. $\square$

This result proves that the LAG-2 production rate in each cell goes to 0 as time progresses. A depiction of this result is in Figures 6.3 and 6.4 where numerical solutions of this system are plotted for various values of σ and δ.

The elimination of LAG-2 production in both cells is indicative of the two anchor cell phenotype. This phenotype is observed experimentally only under the constraint of no lateral signaling. Our model accounts for lateral signaling. We conclude that this non-destructive inhibition model is a poor description of the biological phenomena.

6.3 Destructive Inhibition

In the previous section a model neglecting the destruction of inhibitor was in poor agreement with experimental observations. Instead assume that "Factor-X", the down-regulator of HLH-2 accumulation, is consumed in this capacity so that $q_v =$

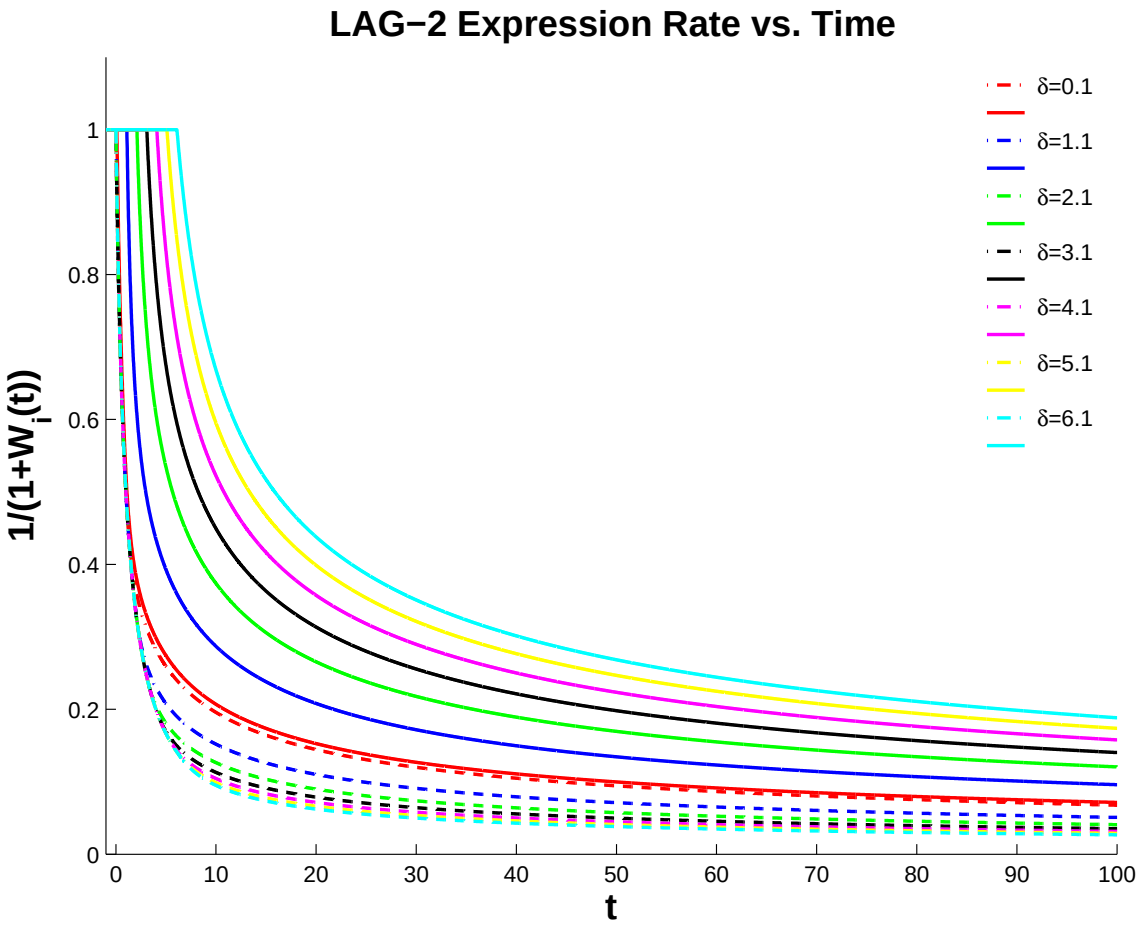

Figure 6.3: Non-Destructive Inhibition in the AC/VU Decision: Variations in δ. Plots show LAG-2 expression over time in the first born cell (dashed curves) and in the second born cell (solid curves) for values of δ in [0,7]. The diminishing of LAG-2 in both cells is indicative of the two AC phenotype, which is not observed experimentally when lateral signaling is permitted.

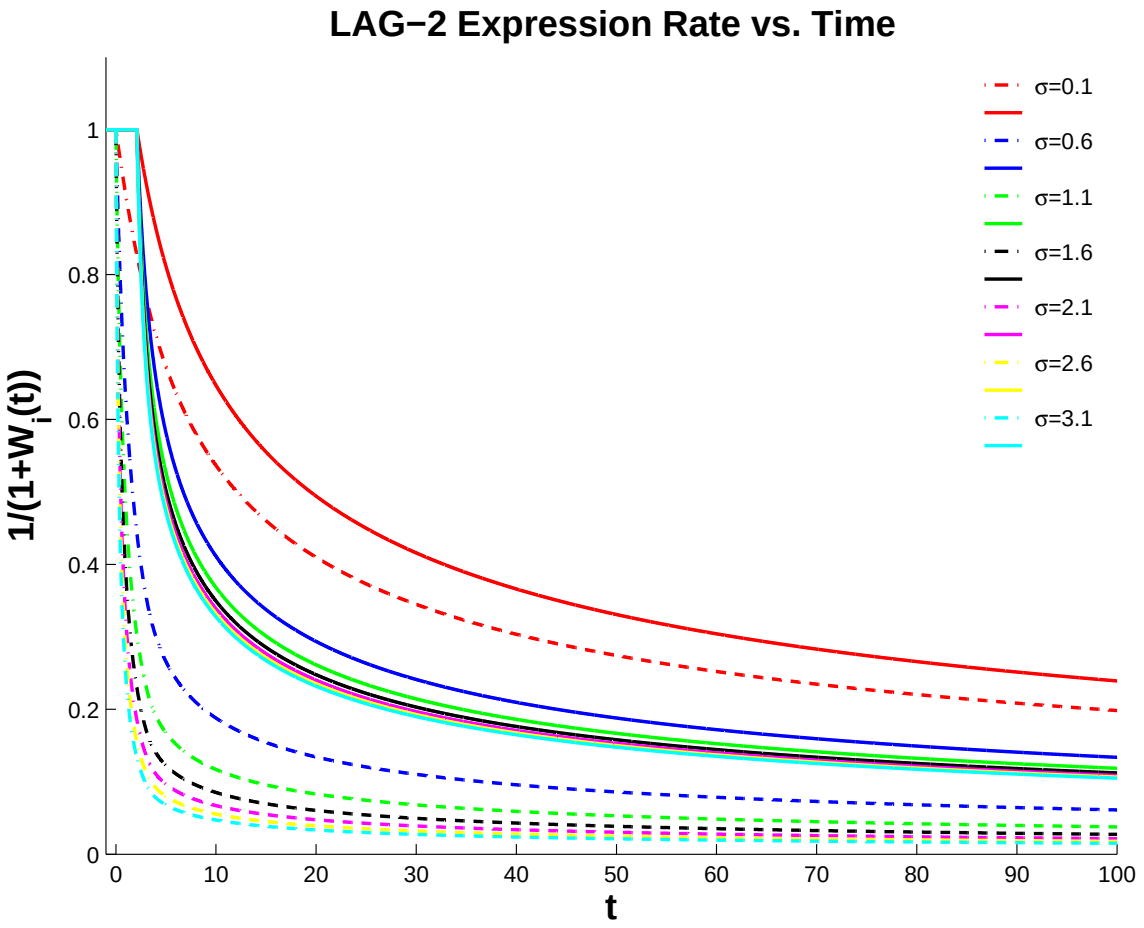

Figure 6.4: Non-Destructive Inhibition in the AC/VU Decision: Variations in σ. Plots show LAG-2 expression over time in the first born cell (dashed curves) and in the second born cell (solid curves) for values of σ in [0,4]. The diminishing of LAG-2 in both cells is indicative of the two AC phenotype, which is not observed experimentally when lateral signaling is permitted.

q_u,*i.e.*, $\gamma = \beta$. The model now takes the form of System (6.19).

$$\begin{aligned}
\frac{dW_1}{ds} &= \sigma\left(\frac{1}{1+W_2(s-1)} + \frac{1}{1+W_1(s)} - 1\right) \\
\frac{dW_2}{ds} &= \sigma\left(\frac{1}{1+W_1(s-1)} + \frac{1}{1+W_2(s)} - 1\right) \\
W_1(s) &= 0 \quad \text{for all } s \in [-1, 0] \\
W_2(s) &= 0 \quad \text{for all } s \in [-1, \delta] \\
\sigma &= \phi\beta
\end{aligned} \tag{6.19}$$

The equilibrium points of this system form the line $W_1 W_2 = 1$. Numerical investigations show that this set of equilibria appear to be stable. See Figure (6.5).

For small values of σ support can be added to this last claim using the method developed in § (A.2.1). First transform the problem into the form covered by Method 1. For $s \in [0, \delta]$ integrate System (6.19) to extend the initial data for W_1 to $[-1, \delta]$. This is easily accomplished, because on $s \in [0, \delta]$ the governing equation for W_1 is a simple ODE. The solution is given by $W_1(s) = \sqrt{2\sigma\, s + 1} - 1$. Now shift the independent variable and redefine the dependent variable using $W_1(s + \delta) = X(s)$ to get a system of the form treated by Method 1.

$$\begin{aligned}
\frac{dx_1}{ds} &= \sigma\left(\frac{1}{1+x_2(s-1)} + \frac{1}{1+x_1(s)} - 1\right) \\
\frac{dx_2}{ds} &= \sigma\left(\frac{1}{1+x_1(s-1)} + \frac{1}{1+x_2(s)} - 1\right) \\
x_1(s) &= \begin{cases} 0 & \text{for } s \in [-1, -\delta] \\ \sqrt{2\sigma(s+\delta)+1} - 1 & \text{for } s \in [-\delta, 0] \end{cases} \\
x_2(s) &= 0 \quad \text{for all } s \in [-1, 0]
\end{aligned} \tag{6.20}$$

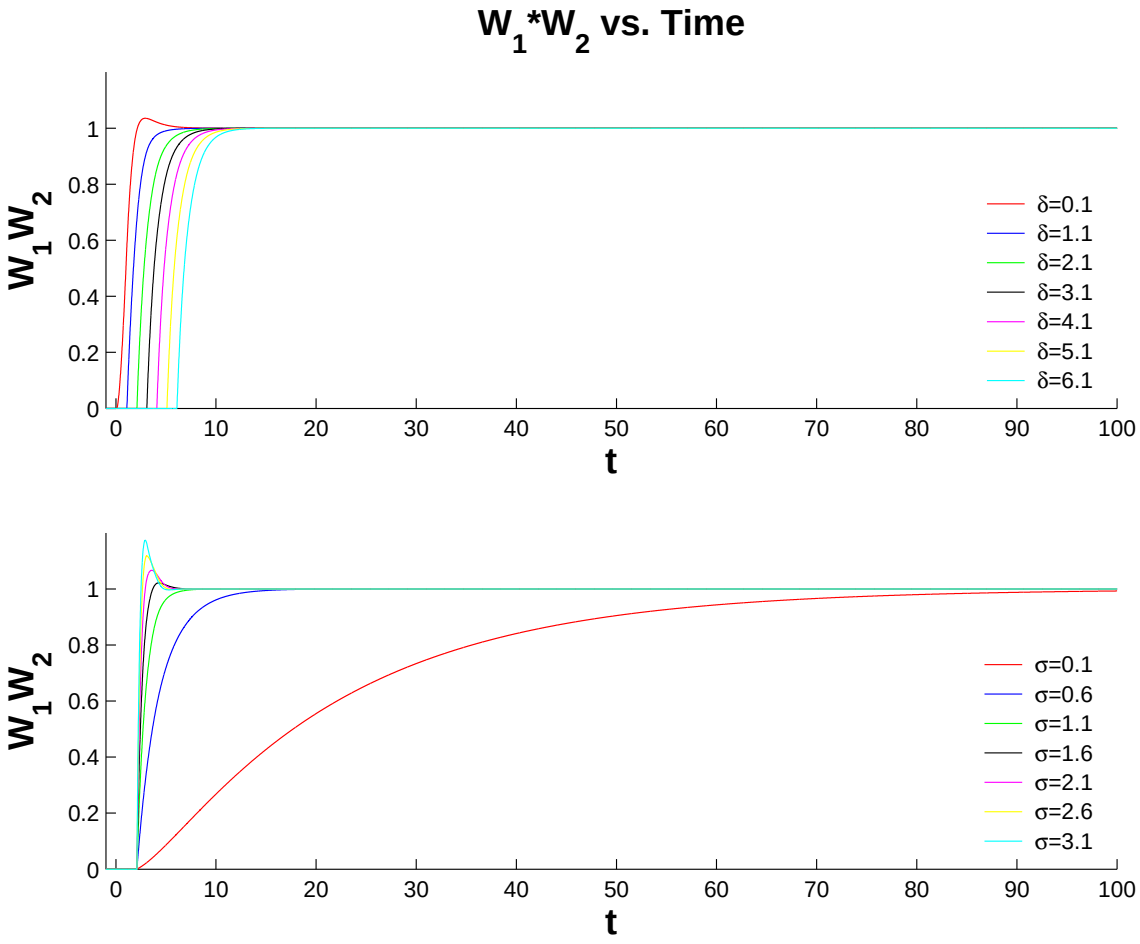

Figure 6.5: Destructive Inhibition in the AC/VU Decision: Variations in σ and δ.

As shown in Appendix A.2.3.2, the behavior of this system, to leading order in $\sigma \ll 1$, is independent of the initial data and is given by

$$x_1(s) \sim x_2(s) \sim 1 + 2\ ProductLog\left(-\frac{1}{2}e^{-(\epsilon(s-1)+1)/2}\right) \quad . \tag{6.21}$$

This suggests that, for $\sigma \ll 1$, as $s \to \infty$ the x_i go to steady state $x_i(s) \to 1$. Numerical approximations suggest that this is generally true for all σ.

Numerical computations in Figures (6.6) and (6.7) show that the steady state production of LAG-2 is lower in the first born than it is in the second born. This character is especially pronounced for large values of σ and δ. For a fixed value of δ (σ) the steady state ratio of LAG-2 production rates appears to be linear in σ (δ). See Figure (6.8). These results suggest that the ratio is approximately a biaffine form. In Figure (6.9) numerical data is fit to a biaffine surface of the form $f(\sigma, \delta) = a\delta\sigma + b\sigma + c\delta + 1$. The steady state ratio of LAG-2 production is best fit by $\sigma\delta + 1$. This implies the following result at steady state.

$$\frac{\text{Second Born LAG-2 Production Rate}}{\text{First Born LAG-2 Production at Rate}} \quad \sim \quad \sigma\,\delta + 1 = \frac{b\,q\,\xi}{c} + 1 \tag{6.22}$$

Relation (6.22) indicates that the steady state LAG-2 production rate ratio depends linearly on the birth time separation, b. This observation both supports and detracts from the validity of our model.

The observation that the model first born cell exhibits diminished LAG-2 production is in agreement with experimental observation. In [24] a lag-2 transcriptional reporter was observed to initially turn on in both cells but subsequently become

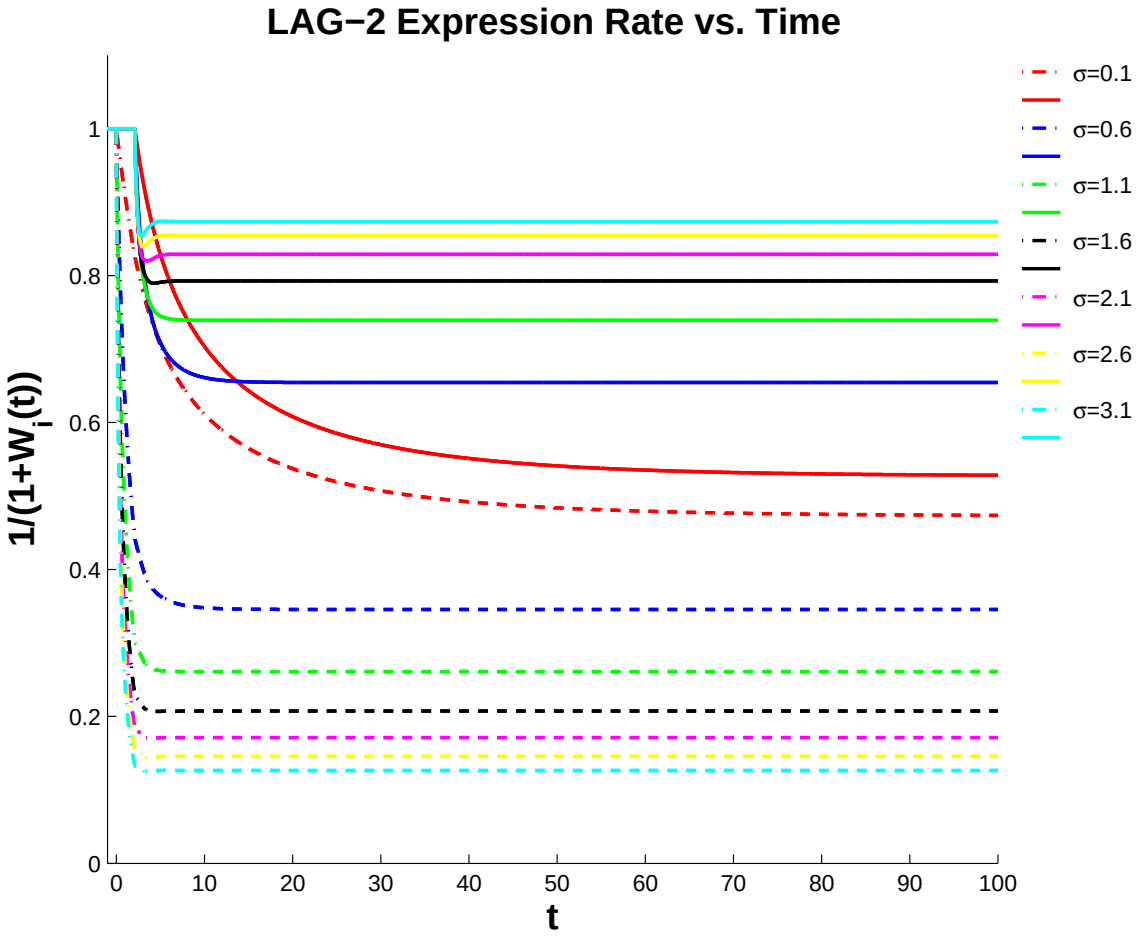

Figure 6.6: Destructive Inhibition in the AC/VU Decision: Variations in σ. LAG-2 production rates are lower in the first born cell (dashed curves) than in the second born (solid curves) for a range of σ values.

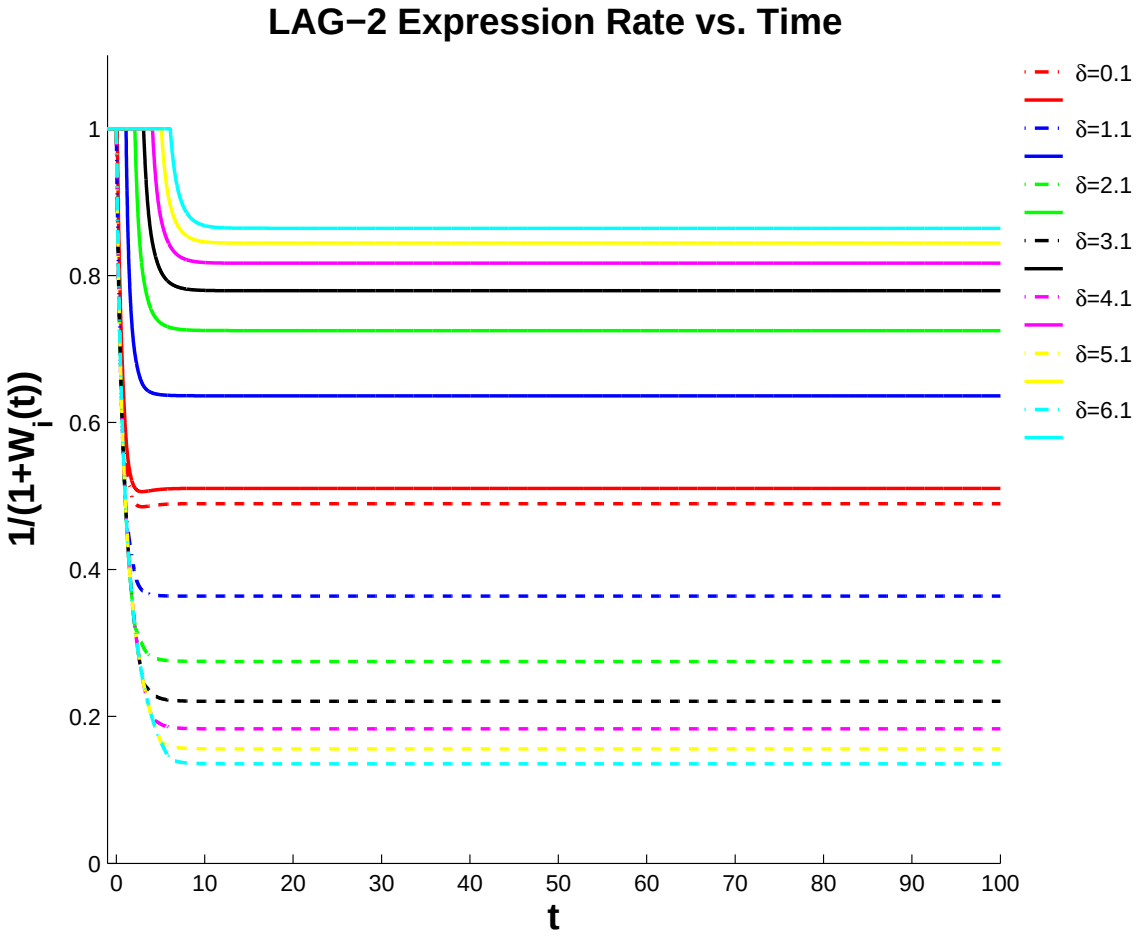

Figure 6.7: Destructive Inhibition in the AC/VU Decision: Variations in δ. LAG-2 production rates are lower in the first born cell (dashed curves) than in the second born (solid curves) for a range of δ values.

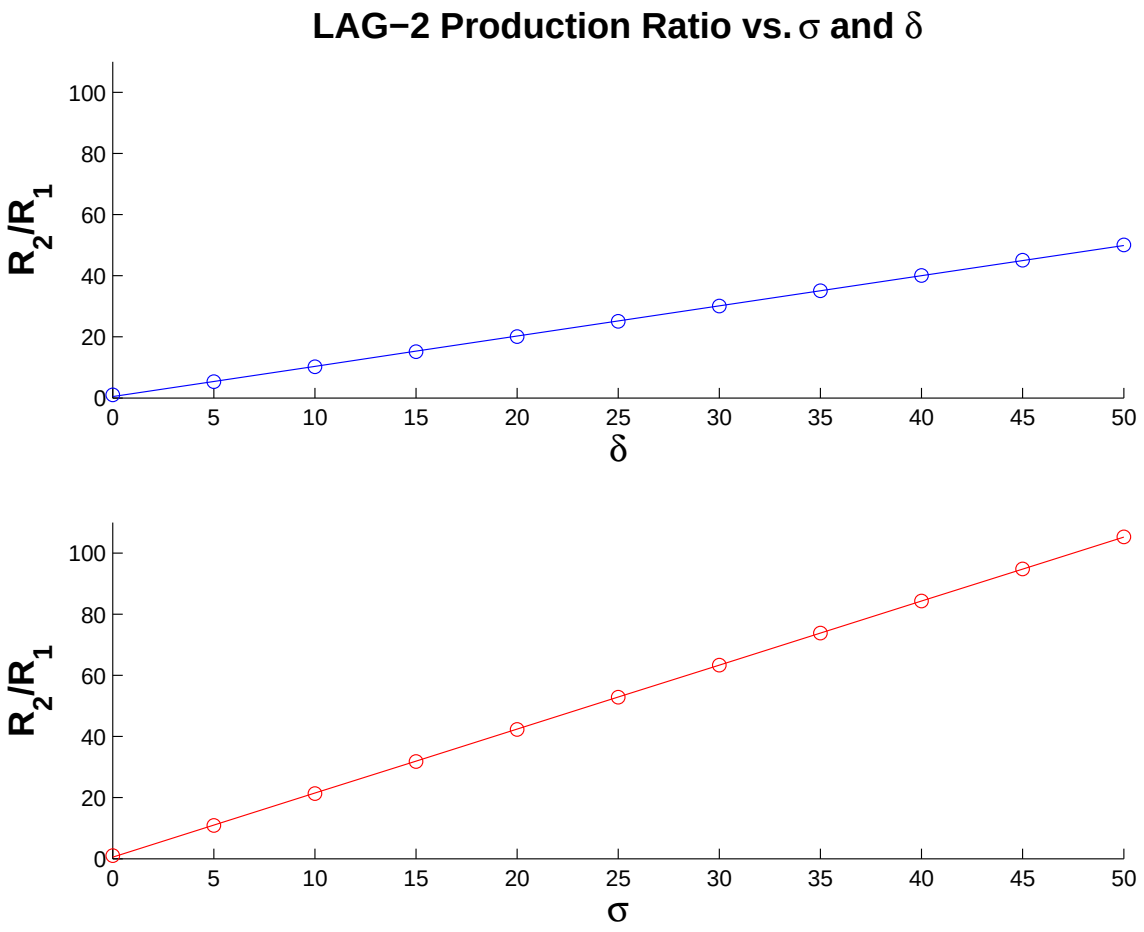

Figure 6.8: Destructive Inhibition in the AC/VU Decision: Variations in δ and σ. For a fixed value of δ (σ) the steady state ratio of LAG-2 production rates appears to be linear in σ (δ). The $\circ$ represent numerical computations of steady states with the solid lines being the least-squares linear fit to this data.

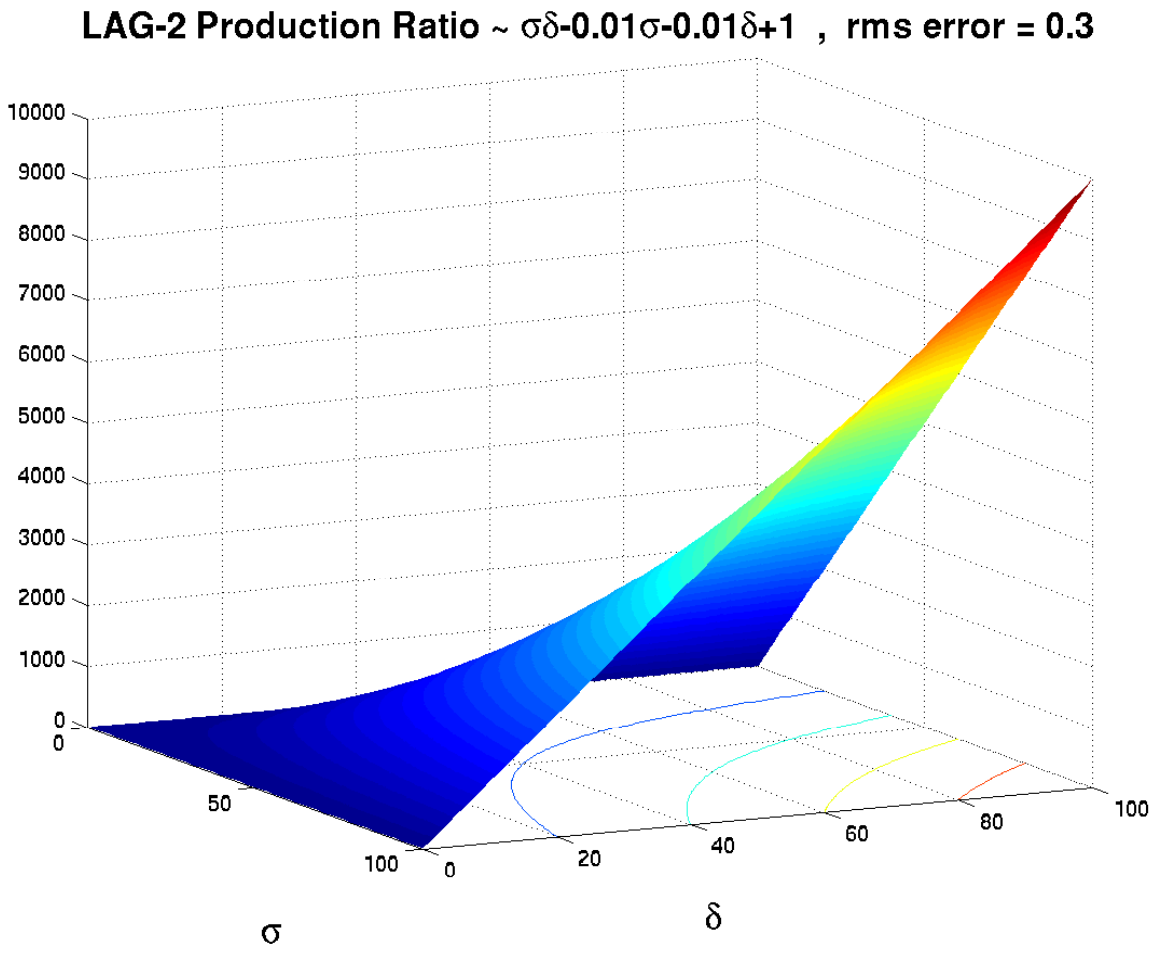

Figure 6.9: Destructive Inhibition in the AC/VU Decision: Steady State Dependence on δ and σ. The ratio of steady state LAG-2 production rates has a least-squares fit given approximately by $1.000\sigma\delta - 0.014\sigma - 0.014\delta + 1$

restricted to the presumptive AC, *i.e.*, the second born cell.

The apparent linear dependence of the LAG-2 production ratio on the birth time separation and the non-vanishing production rate of LAG-2 in the first born are two features that may detract from our model's validity.

Birth time separations as short as two minutes (see Table (3.1)) are sufficient to promote proper cell fate specifications. Intuitively we might expect sensitive behavior such as this not to be the result of a linear proportional relationship between birth time and LAG-2 production ratio, but rather a non-linear one. Also, LAG-2 production rates have been experimentally observed to diminish below detectable levels in the presumptive VU, suggesting that lag-2 transcription is rapidly shut down by the feedback loop. The current model exhibits similar behavior, but rather than vanishing in the VU, the LAG-2 production rate settles to a non-zero steady state.

These two experimental observations, while not contradictory to the model's results, point to the potential for a better model, one exhibiting a non-linear relationship between the LAG-2 production rate ratio and the birth time separation as well as allowing for the rapid shutdown of LAG-2 production.

6.4 Destructive Inhibition: An Improved Model Arising from a Novel Mechanism

6.4.1 Introduction

In § (6.3) we analyzed a model of the AC/VU decision and found that it was consistent with experiments in that the first born of the gonadal cells Z1.ppp and Z4.aaa is predicted to adopt the Ventral Uterine fate while the second born adopts the default anchor cell fate. We also noted that two important experimental observations, while consistent with our model, might find better agreement with a revised model. For clarity, we itemize our expectations below.

- Our mathematical model should exhibit a non-linear relationship between the cell birth time separation and the steady LAG-2 production ratio, if such steady values exist.

- If steady values do not exist, we ask that our model predict the rapid vanishing of LAG-2 production in the first born cell, *i.e.*, the presumptive VU.

In this section we reexamine the model we developed in § (6.1) and explore a key assumption leading to the model of § (6.3), namely that of equipotency. We demonstrate that nullification of the equipotency hypothesis in the model depicted in Figure (6.1) is capable of producing the features itemized above. We've previously discussed the strong evidence for the equipotency hypothesis, and in keeping with this assumption we show how a modified version of the Karp and Greenwald model can exhibit these

desirable traits while not contradicting the equipotency hypothesis.

6.4.2 The Effects of Varied HLH-2 Expression: A "Proof of Concept" Model

Recall the model before the equipotency hypothesis was employed, *i.e.*, System (6.11).

$$\begin{aligned}
\frac{dV_1}{d\tau} &= \frac{S_1(\tau-1)}{1+\frac{q_{1,u}\xi_1 x^*}{c_1^2}V_2\left(\tau-\frac{x^*-x^0}{x^*}\right)} - \frac{q_{1,v}\xi_2 x^*}{c_1^2}\frac{V_1(\tau)\ S_2\left(\tau-\frac{x^0}{x^*}\frac{c_1}{c_2}\right)}{\frac{c_2}{c_1}+\frac{q_{2,u}\xi_1 x^*}{c_1^2}V_1(\tau)} \\
\frac{dV_2}{d\tau} &= \frac{\xi_2}{\xi_1}\frac{S_2\left(\tau-\frac{c_1}{c_2}\right)}{1+\frac{q_{2,u}\xi_1 x^*}{c_1^2}V_1\left(\tau-\frac{x^*-x^0}{x^*}\frac{c_1}{c_2}\right)} - \frac{q_{2,v}\xi_1 x^*}{c_1^2}\frac{V_2(\tau)\ S_1\left(\tau-\frac{x^0}{x^*}\right)}{1+\frac{q_{1,u}\xi_1 x^*}{c_1^2}V_2(\tau)}
\end{aligned} \tag{6.23}$$

This is the starting point for an improved model. We begin by demonstrating that violating the equipotency hypothesis in a particular way leads to a model with desirable qualities.

Some assumptions of the equipotency hypothesis seem more valid than others. While it seems valid to assume that the genetics of the two cells are identical and that the gene transcripts are as well, it may not be true that the transcription of these genes proceeds at exactly the same rates at exactly the same times. To this end, we suppose that the interaction between two proteins is identical, regardless of the cell they reside in, but allows for the rate of production of proteins to vary between cells. Later we describe a mechanism by which these effects can be produced without violating the equipotency hypothesis. As in § (6.1), take $q_{1,u} = q_{2,u}$, $q_{1,v} = q_{2,v}$, and $c_1 = c_2$. Because we suppose that production rates of HLH-2 protein may vary, we allow for the possibility that $\xi_1 \neq \xi_2$. Further, we assume that while the absolute

levels of production, ξ_i, may differ, the functional form does not (up to a delay) and, as in § (6.1), is constant. The assumption of destructive inhibition is again necessary to get a qualitatively accurate model, $q_u = q_v$. We obtain a new model (*c.f.* Equations (6.12), (6.13), and (6.19)).

$$\begin{aligned}
\frac{dW_1}{ds} &= \sigma\left(\frac{1}{1+W_2(s-1)} + \frac{\Xi}{1+W_1(s)} - \Xi\right) \\
\frac{dW_2}{ds} &= \sigma\left(\frac{\Xi}{1+W_1(s-1)} + \frac{1}{1+W_2(s)} - 1\right) \\
W_1(s) &= 0 \quad \text{for all } s \in [-1, 0] \\
W_2(s) &= 0 \quad \text{for all } s \in [-1, \delta]
\end{aligned} \tag{6.24}$$

The dimensionless variables are given by

$$\begin{aligned}
W_i(s) &= \beta\, V(\phi\, s) \\
\sigma &= \frac{q_u \xi_1 (x^* - x^0)}{c^2} \\
\Xi &= \frac{\xi_2}{\xi_1} \neq 1 \\
\delta &= \frac{b\, c}{x^* - x^0},
\end{aligned} \tag{6.25}$$

and the dimensionless LAG-2 production rate ratio is

$$\Psi(s) = \frac{R_2}{R_1} = \Xi \frac{1 + W_1\left(s - \frac{x^1 - x^0}{x^* - x^0}\right)}{1 + W_2\left(s - \frac{x^1 - x^0}{x^* - x^0}\right)} \quad . \tag{6.26}$$

Unlike the previous model for destructive inhibition, System (6.24) admits no finite steady states for $\Xi \neq 1$. In fact, the only possible attractors are $(W_1, W_2) \in \{(0, \pm\infty), (\pm\infty, 0)\}$. This shows that $\Psi(\infty) \in \{0, \pm\infty\}$.

Assuming $\Xi > 1$, numerical investigations indicate that $\lim_{t\to\infty} \Psi(t) = \infty$ (plots not shown). As anticipated, nullifying the equipotency hypothesis leads to a system for which a small birth order time separation leads to the rapid shutdown of LAG-2 production in the first born cell. Assuming that HLH-2 production rates are lower in the first born cell leads to a model that predicts cell fate behaviors consistent with and resemblant of experimental observations. We now ask whether this same favorable behavior might be exhibited by a mechanism that respects the equipotency hypothesis but that differs from the Karp and Greenwald proposal.

6.4.3 Discussion

Newly born Z1.ppp and Z4.aaa cells may, as suggested in [24], be influenced by LAG-2 from the parent cells or by other sources of LAG-2 in the gonad, giving the first born an incremental bit of signaling before the second born enters the signaling scenario. If this were true, then the model of § (6.3) predicts that this extraneous signal would encourage the first born to lower its LAG-2 production, biasing it before the two-cell interaction begins, destining it for the VU fate. The problem with the extraneous signal explanation is that, as we have seen, birth time separations may be short and hence give rise to only a small difference in the first born's LAG-2 expression unless the extraneous signal is very strong. However, the extraneous signal can't be strong because preventing interaction between Z1.ppp and Z4.aaa leads to a two AC phenotype. The extraneous signal, if there is one, isn't strong enough to determine fates, only to introduce a bias into the first born. Our model of § (6.3) predicts that a

small bias will have a small effect, detracting from the extraneous signal hypothesis as it pertains to that model. There is another related possibility, which we now describe together with the extraneous signal hypothesis.

- *Extraneous Signal Hypothesis:* A source of LAG-2 ligand exists in the surrounding gonadal environment. It is sufficient to introduce a slight bias in HLH-2 accumulation in the first born cell while not being sufficient to specify the VU fate entirely.

- *Inherent Receptor Level Bias:* LIN-12 receptor accumulates from birth, giving the first born cell enhanced ability to bind LAG-2.

The receptor bias hypothesis, when applied to the model of § (6.3), suffers from the same impotency as the extraneous signal hypothesis– that if the receptor bias is small then during short birth time separation intervals only a small advantage could be afforded to the first born, resulting in only a small steady state LAG-2 production level difference. If the receptor bias were significant enough to give the first born full advantage in becoming VU then it would likely allow for a two VU phenotype when signaling between Z1.ppp and Z4.aaa is blocked. As mentioned several times previously, this experimental scenario bears a two AC phenotype instead.

These two hypotheses are capable of slightly enhancing the results obtained from the model of § (6.3) but are not capable of producing the rapid shutdown of LAG-2 production expected from the first born cell. However, we now make a case that an analogous DELTA/NOTCH system in *Drosophila*, when used to modify the mechanism of Figure (6.1), gives rise to a model akin to that of § (6.4), *i.e.*, one that makes

the expected predictions of LAG-2 shutdown in the first born. The advantage of this new model is that it obtains the more desirable result without violating the equipotency hypothesis. In addition, the extraneous signal and receptor bias hypothesis serve only to reinforce this result.

6.4.4 A Novel Mechanism of the ACVU Fate Descision

Lessons From *Drosophila* The lateral signaling event that coordinates AC/VU fate specification among the Z1.ppp and Z4.aaa cells parallels a critical event during the development of two cells found in the fruitfly, *Drosophila melanogaster*. During the development of proneural clusters in *D. melanogaster*, cells coordinate fates in much the same way that Z1.ppp and Z4.aaa do in *C. elegans*. Specifically, a DELTA/NOTCH lateral signaling feedback loop coordinates the specification of the Sensory Mother Cell (SMC) fate via the hlh-2 ortholog Daughterless ([7],[19]). Daughterless, together with the aschaete scute complex (AS-C) operates in a self-stimulatory mode to promote further transcription of AS-C. A detailed diagram appears in Figure (6.10) taken directly from [7] (Figure 7).

Figure (6.11) shows an abstraction of this mechanism put into the context of our AC/VU models. Observe the DELTA/NOTCH feedback loop with the incorporation of a self-stimulatory loop that augments the DELTA transcription promoter. Based on this mechanism, we propose in Figure (6.12) an analogous self-stimulatory mechanism for HLH-2. As of this writing such a component has not been identified biologically, although the authors of [24] posit its existence.

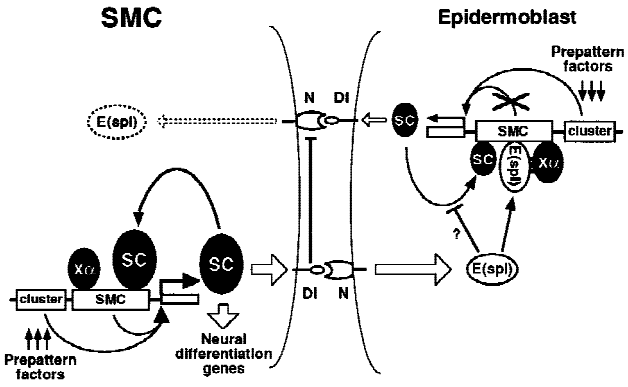

Figure 6.10: SMC Development in *D. melanogaster* 1. The specification of the SMC fate in the *D. melanogaster* proneural cluster proceeds in analogy with VU specification in *C. elegans*. A DELTA/NOTCH interaction between neighboring cells activates the enhancer of split complex, E(spl), which plays the role of the proposed Factor-X in *elegans* by inhibiting the accumulation of DELTA transcription factors. These transcription factors, SC, are activated by prepattern factors while simultaneously operating in a self-stimulatory loop mediated by a complex of proteins. This is Figure 7 in reference [7]

The self-stimulatory loop promoting AS-C in *Drosophila* appears to be an enzyme coordinated interaction, as such we propose that a Michaelis-Mentin type term be used to describe the mechanism. That is, we replace Equation (6.3) with the following:

$$c_i u_i\left(x^{0,+},t\right) \;=\; c_i u_i\left(x^{0,-},t\right) - q_{i,u} v_j u_i\left(x^{0,+},t\right) + \frac{k_{i,1}\, u_i\left(x^{0,+},t\right)}{1 + k_{i,2}\, u_i\left(x^{0,+},t\right)} \quad . \quad (6.27)$$

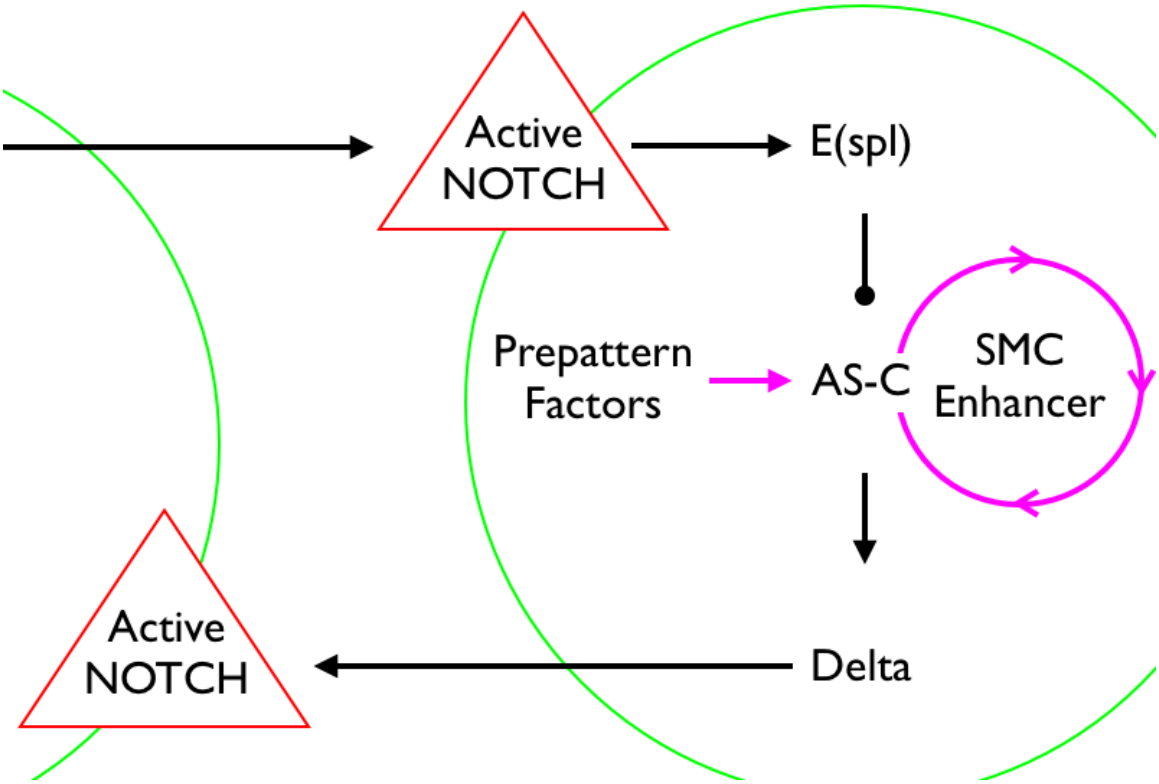

Figure 6.11: SMC Development in *D. melanogaster* 2. An abstraction of Figure (6.10) showing the essential character of the positive and negative feedback loops at work during SMC fate specification in *D. melanogaster* proneural cluster cells.

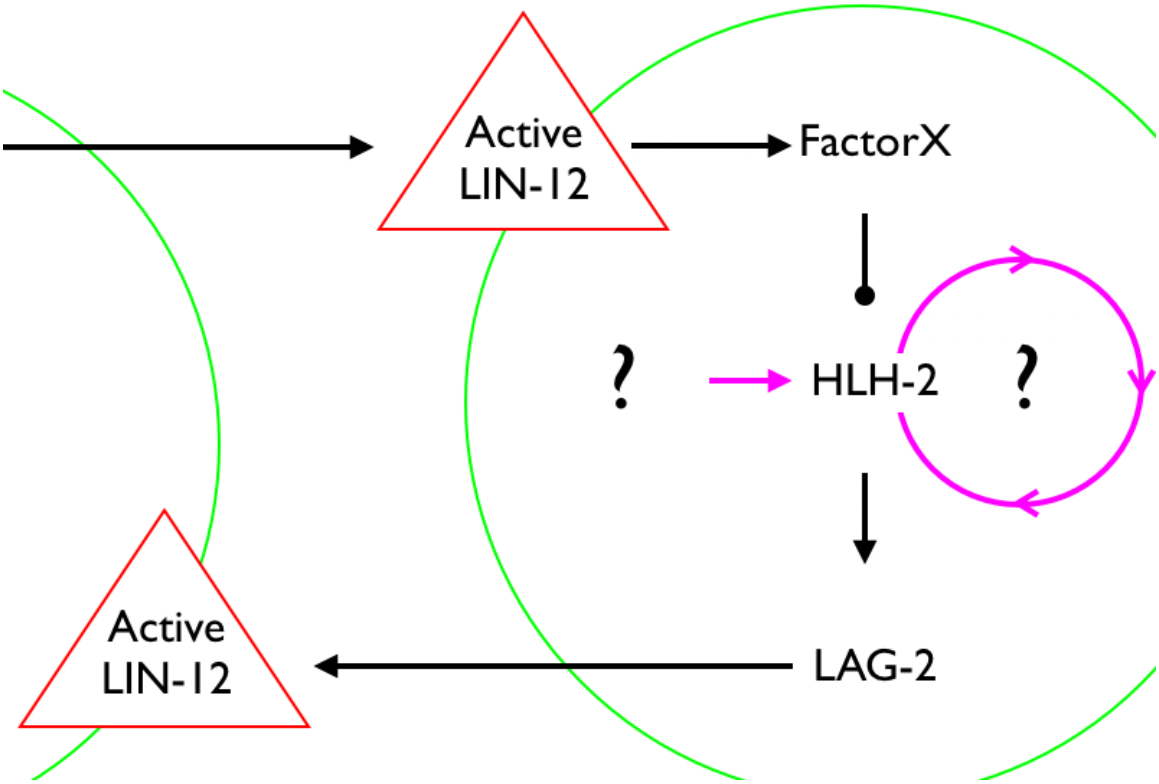

Figure 6.12: A Novel Mechanism for the AC/VU Decision Suggested by *Drosophila* SMC Development, *c.f.* Figure (6.11)

As with previous derivations we solve this to find $u_i(x,t)$, *c.f.* Equation (6.5).

$$u_i(x,t) = \begin{cases} \frac{1}{c_i} s_i\left(t - \frac{x}{c_i}\right) & \text{for } x \in [0, x^0) \\ \frac{a_{i,1}+a_{i,2}-1+\sqrt{(a_{i,1}+a_{i,2}-1)^2+4\,a_{i,1}}}{2\,k_{i,2}} & \text{for } x \in (x^0, x^*] \end{cases} \tag{6.28}$$

$$a_{i,1}(t) \equiv \frac{k_{i,2}\, s_i\left(t - \frac{x}{c_i}\right)}{c_i + q_{i,u} v_j\left(t - \frac{x-x^0}{c_i}\right)} \tag{6.29}$$

$$a_{i,2}(t) \equiv \frac{k_{i,1}}{c_i + q_{i,u} v_j\left(t - \frac{x-x^0}{c_i}\right)} \tag{6.30}$$

With $k_{i,1} = 0$, the self-stimulatory loop is removed and this expression reduces to Equation (6.5). Note that s_i represents the production of HLH-2 due to prefactors. The derivation is completed by appealing to Equation (6.4), repeating the process of non-dimensionalization and enforcing the equipotency hypothesis. This leads to the following revised model for the AC/VU decision:

$$\frac{dW_i}{ds} = \frac{\sigma}{\mu}\left(U_i(s,x^*) - W_i(s)\, U_j\left(s,x^0\right)\right) \quad , \tag{6.31}$$

$$U_i(s,x) \equiv A_{i,1}(x) + A_{i,2}(x) + \sqrt{(A_{i,1}(x) + A_{i,2}(x))^2 + 2A_{i,1}(x)} \quad , \tag{6.32}$$

$$A_{i,1}(x) \equiv \frac{1}{2}\left(\frac{\mu\, S_i\left(s - \frac{x}{x^*-x^0}\right)}{1 + W_j\left(s - \frac{x^*-x}{x^*-x^0}\right)}\right) \quad , \tag{6.33}$$

$$A_{i,2}(x) \equiv \frac{1}{2}\left(\frac{\nu}{1 + W_j\left(s - \frac{x^*-x}{x^*-x^0}\right)} - 1\right) \quad , \tag{6.34}$$

$$\nu \equiv k_1/c \quad , \tag{6.35}$$

$$\mu \equiv k_2\xi/c \quad . \tag{6.36}$$

If the positive feedback loop is neglected, then $\nu = 0$ and the previous model emerges. It is only dependent on σ and δ. With the feedback loop in place, there

is additional dependence on ϕ, μ, and ν, making the dynamics of the model more challenging to analyze. A thorough analysis of model behavior over parameter space is not given here. Instead we wish only to demonstrate that, as claimed in § (6.4.3), the incorporation of the feedback loop produces similar results as System (6.24), only without neglecting the equipotency hypothesis to achieve this end.

Figures (6.13) and (6.14) show numerical computations for $\phi = \mu = \nu = 1$ over a range of δ and σ. Observe that LAG-2 production shuts down in the first born cell, leading it to the VU fate. This behavior was previously found only by violating the equipotency hypothesis, but here no such violation occurs. The desirable behavior demonstrated by this model is due solely to the combination of positive and negative feedback loops.

Above we discussed the observation of the $(\infty, 0)$ steady state being approached. However, when the birth time separation is small, the positive feedback loop isn't sufficient to quickly specify the VU fate and the $(1, 1)$ state is approached. See Figure (6.15). However, this state appears to be a saddle point, so trajectories may approach it temporarily, but given long enough time the positive feedback loop causes them to depart and go to $(\infty, 0)$.

Due to the complexity of the model, our treatment here has not been mathematically rigorous, but instead of a more experimental nature. The presence of self-reinforcing positive feedback in the AC/VU decision has never been observed in an experimental biological context. Intuition has led some biologists to suspect that such a mechanism exists [24]. Our modeling serves as a mathematical experiment. An ex-

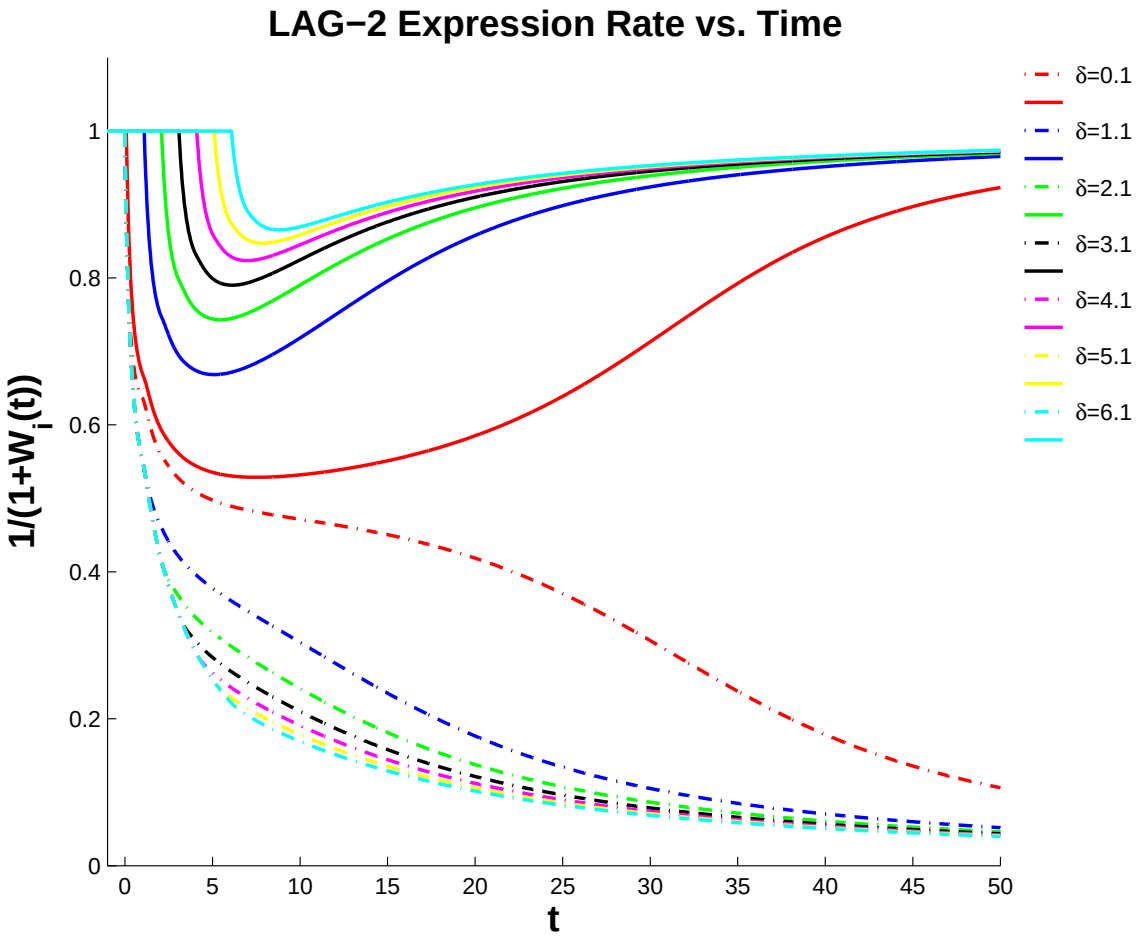

Figure 6.13: *D. melanogaster* Inspired AC/VU: δ. First born (dashed lines) second born (solid lines) $\nu = 5$, $\mu = 1$. Any non-zero birth order separation, described by δ, appears to be sufficient to give the first born a "head start" in initiating non-linear self-stimulation of HLH-2. This advantage allows for the shutdown of LAG-2 production in the first born, committing it to the VU fate.

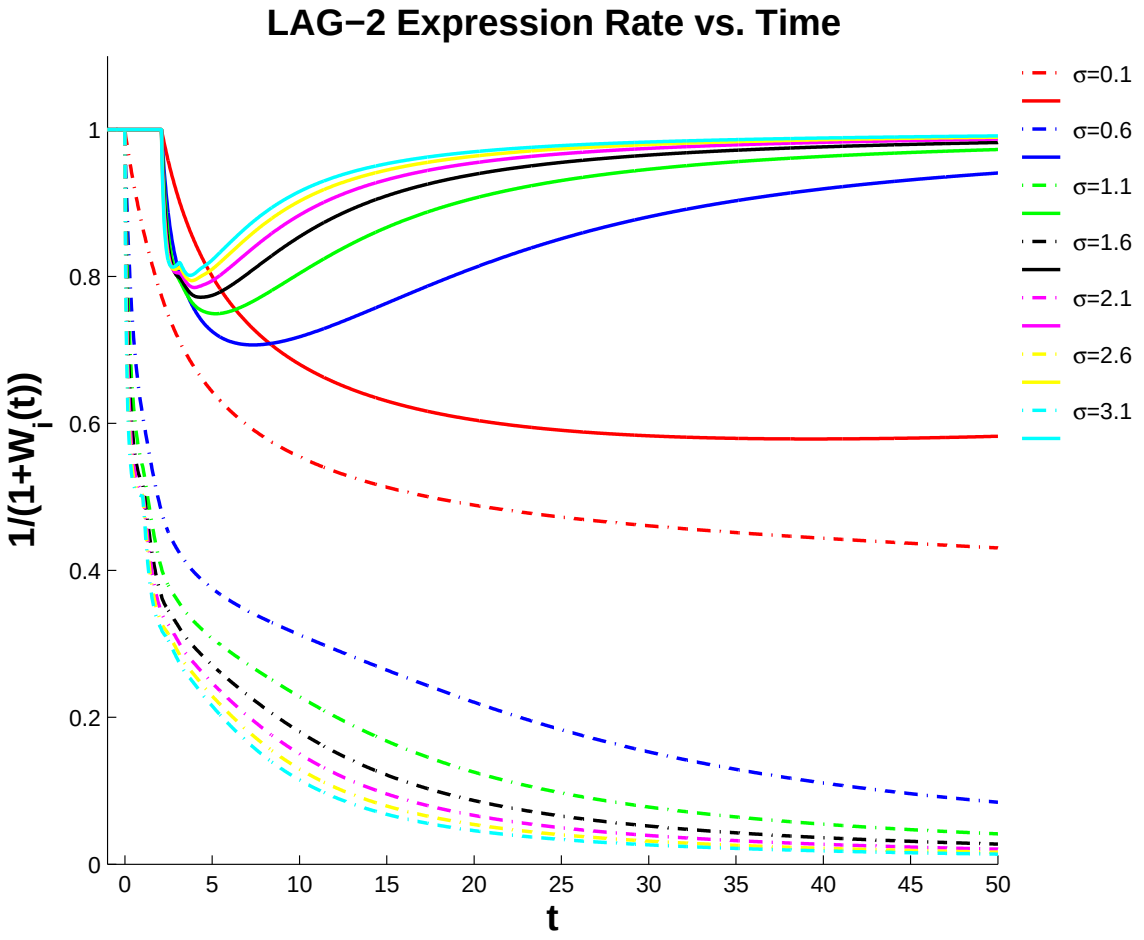

Figure 6.14: *D. melanogaster* Inspired AC/VU: σ. First born (dashed lines) second born (solid lines) $\nu = 5$, $\mu = 1$. Any value of σ appears to be sufficient to give the first born an advantage in committing to the VU fate.

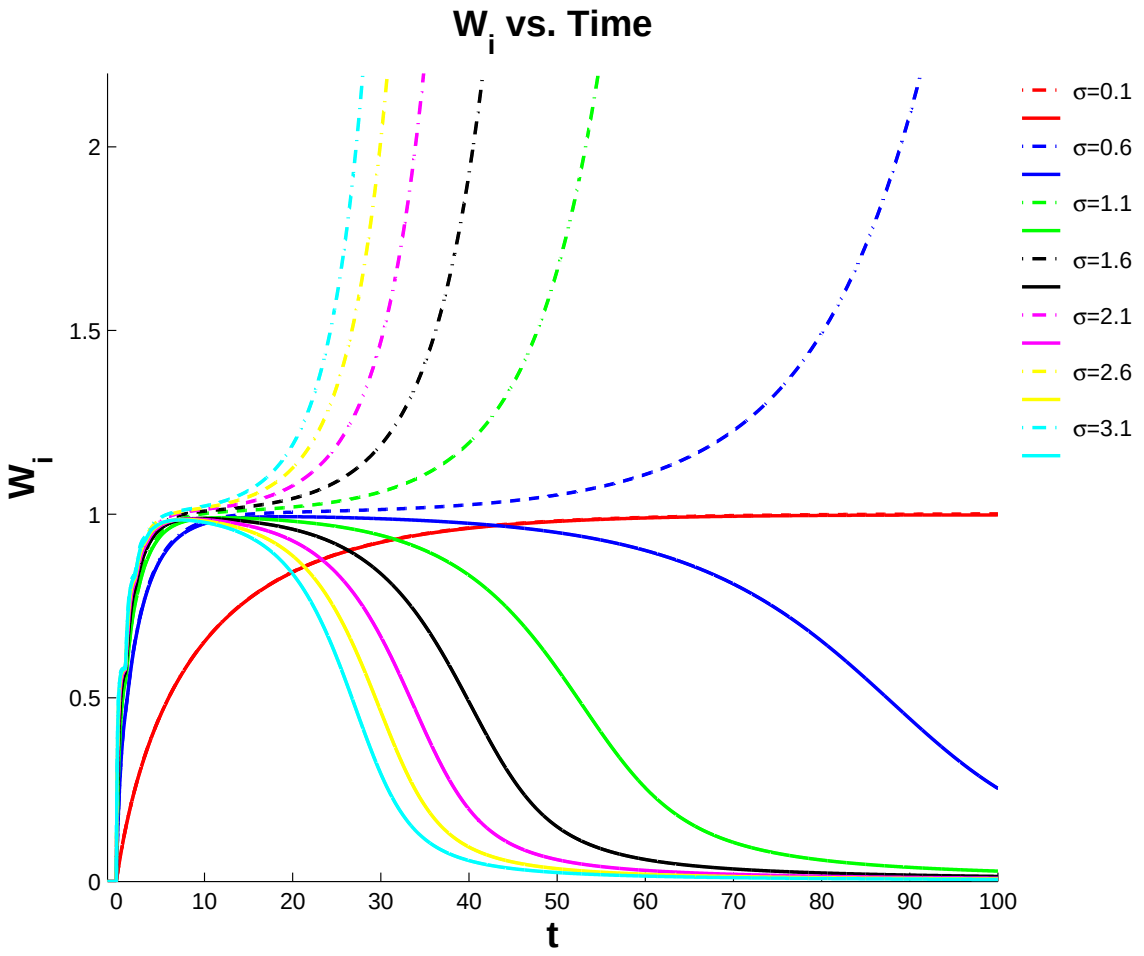

Figure 6.15: *D. melanogaster* Inspired AC/VU: $\delta \ll 1$. First born (dashed lines) second born (solid lines) $\nu = 5$, $\mu = 1$, $\delta = 0.005$.

periment that confirms biological intuition, suggests that even the shortest birth time separations are capable of clearly specifying cell fates, and proposes a definite mechanism by which this feat may be achieved. This result mechanism begs experimental confirmation by laboratory biologists.

Appendix A

Mathematical Appendix

A.1 Theory of Delay Differential Equations

Delay differential equations (DDE) are elements of a general class known as functional differential equations [9, 18]. The general form of a quasilinear first order DDE with n delays is $y'(t) = f(t, y(t), y(t-d_1), y(t-d_2), \ldots, y(t-d_n))$ with $0 < d_1 < \ldots < d_n$. In most circumstances, initial data is not sufficient to determine the solutions of DDE for all $t > 0$. There are however exceptional cases. See [36] for a theorem of limited applicability and a counter example. Generally, we specify the dependent variable over the interval $t \in [-d_n, 0]$, and consider the following initial value problem:

$$\begin{aligned} \frac{dy(t)}{dt} &= f\left(t, y\left(t\right), y\left(t-d_1\right), y\left(t-d_2\right), \ldots, y\left(t-d_n\right)\right) \qquad \text{(A.1)} \\ y(0) &= y_0 \\ y(t) &= g(t) \quad for\ t \in [-d_n, 0) \quad . \end{aligned}$$

The proofs of local and global existence of solutions to these DDE initial value problems are similar to those for ODE [18]. Because the functions $y(t-d_j)$ are known

for $t \in [0, d_1]$ the existence of a solution for $t \in [0, d_1]$ is found exactly as in the ODE case. If the solution exists up to time $t = d_1$, then the functions $y(t - d_j)$ are known for $t \in [0, 2d_1]$ and the same ODE existence proofs are applicable in the interval $t \in [d_1, 2d_1]$. The process is bootstrapped in this way until the local existence proofs for ODE fail for some $t = t^*$. We then have the existence of a solution to IVP (A.1) for $t \in [0, t^*)$.

Convergent numerical methods of Euler and Runge-Kutta type have been formulated for DDE IVPs [36]. Once again the proofs of convergence of such methods follow similarly to their ODE counterparts.

A.2 Asymptotics for Delay Differential Equations

A.2.1 Derivation

Suppose that $x(t)$ is a vector-valued function of the scalar variable t. Consider the delay differential equation initial value problem described by equations (A.2), (A.3), and (A.4).

$$\frac{dx}{dt} = \epsilon F\left(x\left(t\right), x\left(t-1\right)\right) \tag{A.2}$$

$$x\left(0\right) = A\left(\epsilon\right) \tag{A.3}$$

$$x\left(t\right) = B\left(t, \epsilon\right) \quad \text{for } t \in [-1, 0) \tag{A.4}$$

Here ϵ is an $o\left(1\right)$ parameter while $A\left(\epsilon\right)$ $B\left(t, \epsilon\right)$, and $F(\cdot, \cdot)$ are vector-valued functions. In what follows, we assume that A and B are differentiable in ϵ near $\epsilon = 0$, *i.e.*, that

equations (A.5) and (A.6) hold.

$$A(\epsilon) = A_0 + \epsilon A_1 + O\left(\epsilon^2\right) \tag{A.5}$$

$$B(t,\epsilon) = B_0(t) + \epsilon B_1(t) + O\left(\epsilon^2\right) \tag{A.6}$$

Look for a regular perturbation expansion about $\epsilon = 0$ in the form of equation (A.7).

$$X(t) = X_0(t) + \epsilon X_1(t) + O\left(\epsilon^2\right) \tag{A.7}$$

Inserting the expression (A.7) into Equations (A.2), (A.3), and (A.4) gives a sequence of ordinary differential equation initial value problems that are easily solved by quadrature. To order ϵ the solution is given by (A.8).

$$\begin{cases} B_0(t) + \epsilon B_1(t) & t \in [-1, 0) \\ A_0 + \epsilon\left(A_1 + \int_0^t F\left(A_0, B_0(s-1)\right) ds\right) & t \in [0, 1) \\ A_0 + \epsilon\left(A_1 + \int_0^1 F\left(A_0, B_0(s-1)\right) ds + (t-1) F\left(A_0, A_0\right)\right) & t \in [1, \infty) \end{cases} \tag{A.8}$$

Note that, depending on the form of F, the solution may exhibit secular terms for $t \gg 1$. We attempt to find an asymptotic approximation to order ϵ for all $t \geq 1$. Introduce a new time scale, τ.

$$\tau = \epsilon(t-1) \tag{A.9}$$

Using this new scale, define a new dependent variable, Y.

$$x(t) \equiv Y(t, \tau) \tag{A.10}$$

In the coordinate system described by these new variables, Y is the solution to a partial differential delay equation.

$$\frac{\partial Y}{\partial t} + \epsilon \frac{\partial Y}{\partial \tau} = \epsilon F\left(Y\left(t,\tau\right), Y\left(t-1, \tau-\epsilon\right)\right) \tag{A.11}$$

Look for a singular perturbation expansion in the form of Equation (A.12).

$$Y\left(t,\tau\right) = Y_0\left(t,\tau\right) + \epsilon Y_1\left(t,\tau\right) + \epsilon^2 Y_1\left(t,\tau\right) + \ldots \tag{A.12}$$

Inserting (A.12) into (A.11) and collecting common powers of ϵ gives a sequence of problems.

$$\frac{\partial Y_0}{\partial t} = 0 \tag{A.13}$$

This shows that Y_0 is independent of t.

$$\frac{\partial Y_1}{\partial t} = F\left(Y_0\left(\tau\right), Y_0\left(\tau\right)\right) - \frac{dY_0}{d\tau} \tag{A.14}$$

The general solution is easily found by quadrature.

$$Y_1\left(t,\tau\right) = \left(t-1\right)\left(F\left(Y_0, Y_0\right) - \frac{dY_0}{d\tau}\right) + C(\tau) \tag{A.15}$$

The removal of secular terms from the expansion requires

$$\frac{dY_0}{d\tau} = F\left(Y_0, Y_0\right) \quad . \tag{A.16}$$

The next problem gives the first order correction term.

$$\frac{\partial Y_2}{\partial t} = \nabla_1 F\left(Y_0, Y_0\right) \cdot Y_1 + \nabla_2 F\left(Y_0, Y_0\right) \cdot \left(Y_1 - \frac{dY_0}{d\tau}\right) - \frac{dY_1}{d\tau} \tag{A.17}$$

Here, and throughout this thesis, ∇_i denotes the gradient with respect to the i^{th} argument. This is solved by quadrature and with the condition that secular terms be removed from our expansion.

$$Y_1\left(\tau\right) = \Phi\left(\tau\right)\left(\alpha - \int_1^t \Phi^{-1}\left(s\right)\beta\left(s\right) ds\right) \tag{A.18}$$

$$\beta\left(\tau\right) = \nabla_2 F\left(Y_0, Y_0\right) \cdot F\left(Y_0, Y_0\right) \tag{A.19}$$

Here Φ is the fundamental matrix solution to a linear ODE.

$$\frac{d\Phi}{d\tau} = \left(\nabla_1 F\left(Y_0, Y_0\right) + \nabla_2 F\left(Y_0, Y_0\right)\right) \cdot \Phi \tag{A.20}$$

$$\Phi\left(0\right) = I \tag{A.21}$$

The constant vector α is yet to be determined. I is the identity matrix.

The singular perturbation expansion, Y, is now matched to the regular perturbation expansion, X, in a region about $t = 1$. Introduce an intermediate scale, ξ , such that $\epsilon \ll \xi \ll 1$. Introduce a new scaled variable, $\eta = \xi\left(t - 1\right) = \frac{\xi}{\epsilon}\tau$. Solutions X and Y near $t = 1$ may now be expanded in terms of these intermediate variables.

$$X = A_0 + \epsilon\left(A_1 + \int_0^1 F\left(A_0, B_0\left(s - 1\right)\right) ds\right) + \frac{\epsilon}{\xi}\eta\ F\left(A_0, A_0\right) + \ldots \tag{A.22}$$

$$Y = Y_0\left(0\right) + \epsilon\alpha + \frac{\epsilon}{\xi}\eta\ F\left(Y_0\left(0\right), Y_0\left(0\right)\right) + \ldots \tag{A.23}$$

In order for these expressions to agree, (A.24) and (A.25) must hold.

$$Y_0(0) = A_0 \tag{A.24}$$

$$\alpha = A_1 + \int_0^1 F(A_0, B_0(s-1))\, ds \tag{A.25}$$

For $t > 1$ the asymptotic approximation is given by Equations (A.12), (A.16), (A.18), (A.19), (A.20), (A.21), (A.24), and (A.25). For clarity, these results are now summarized.

Method 1 *Let $F(x, y)$ be a vector-valued function. Then, for $t > 1$, the solution to the DDE system*

$$\frac{dx}{dt} = \epsilon F(x(t), x(t-1)) \tag{A.26}$$

$$x(0) = A(\epsilon) \tag{A.27}$$

$$x(t) = B(t, \epsilon) \quad \textit{for } t \in [-1, 0) \tag{A.28}$$

with

$$A(\epsilon) = A_0 + \epsilon A_1 + O\left(\epsilon^2\right) \tag{A.29}$$

$$B(t, \epsilon) = B_0(t) + \epsilon B_1(t) + O\left(\epsilon^2\right) \tag{A.30}$$

is asymptotically approximated to leading order by

$$x(t) \sim Y_0(\tau) + \epsilon\, Y_1(t, \tau) \tag{A.31}$$

$$\tau = \epsilon(t-1) \tag{A.32}$$

where

$$\frac{dY_0}{d\tau} = F\left(Y_0, Y_0\right) \tag{A.33}$$

$$Y_0\left(0\right) = A_0 \tag{A.34}$$

and

$$Y_1\left(t,\tau\right) = \Phi\left(\tau\right)\left(\alpha - \int_0^\tau \Phi^{-1}\left(s\right)\beta\left(s\right)ds\right) \tag{A.35}$$

$$\alpha = A_1 + \int_0^1 F\left(A_0, B_0\left(s-1\right)\right)ds \tag{A.36}$$

$$\beta\left(\tau\right) = \nabla_2 F\left(Y_0, Y_0\right)\cdot F\left(Y_0, Y_0\right) \tag{A.37}$$

where Φ *is the fundamental matrix solution to*

$$\frac{d\Phi}{d\tau} = \left(\nabla_1 F\left(Y_0, Y_0\right) + \nabla_2 F\left(Y_0, Y_0\right)\right)\cdot\Phi \tag{A.38}$$

$$\Phi\left(0\right) = I \quad . \tag{A.39}$$

The approximation will contain no secular terms of the form $\epsilon\tau$ provided that the following requirement is satisfied for fixed $\epsilon\tau$:

$$\epsilon\ \Phi\left(\tau\right)\left(\alpha - \int_0^\tau \Phi^{-1}\left(s\right)\beta\left(s\right)ds\right) \ll Y_0\left(\tau\right) \quad . \tag{A.40}$$

A.2.2 Examples

Secular Terms Consider the DDE initial value problem:

$$\begin{aligned} \frac{du}{dt} &= \epsilon\, u(t-1) \\ u(0) &= A \\ u(t) &= B(t) \quad \text{for} -1 \leq t < 0 \quad . \end{aligned} \tag{A.41}$$

By the method derived in § (A.2.1) we find an asymptotic approximation.

$$u \sim Ae^{\tau} + \epsilon \left(\int_0^1 B(s-1)ds - A\tau \right) e^{\tau} \tag{A.42}$$

$$\tau = \epsilon(t-1) \tag{A.43}$$

This will contain no secular terms if

$$\epsilon \left(\int_0^1 B(s-1)ds - A\tau \right) e^{\tau} = o(Ae^{\tau}). \tag{A.44}$$

This requirement is equivalent to requiring $\epsilon\tau = o(1)$, *i.e.*, $t \ll \epsilon^{-2}$. Hence approximation (A.42) is valid for $1 \leq t \ll \epsilon^{-2}$. This result can be improved upon by instead defining $\tau = (\epsilon + a\epsilon^2)(t-1)$ and repeating our derivation choosing the value of a so as to eliminate $O(\epsilon\tau)$ terms. We find

$$u \sim \left(A + \epsilon \int_0^1 B(s-1)ds \right) e^{\tau} \tag{A.45}$$

$$\tau = (\epsilon - \epsilon^2)(t-1). \tag{A.46}$$

Higher Order Approximations The asymptotic method currently under study has one peculiar requirement. Its specific implementation requires an *a priori* decision as to the desired order of accuracy. Unlike other asymptotic methods for ODE, PDE, and integrals, one cannot simply iterate a generic process to produce more terms in the expansion should one desire a higher order approximation. Indeed, in the example and derivation above, we required a first order asymptotic approximation and so integrated the DDE to extend the initial data to $[-1, 1]$ before matching in an intermediate region about $t = 1$. If we desire a second order approximation, the integration procedure must be carried out twice to extend the data to $[-1, 2]$ before matching in a region about $t = 2$. To make this explicit, consider again the example system (A.41). By the method of § (A.2.1) we integrate to find a short time first order approximation for $t > 2$.

$$\begin{aligned} X(t) \quad &= A + \epsilon \left(A(t-1) + \int_{-1}^{0} B(s)\, ds \right) + \\ &\epsilon^2 \left(\frac{1}{2} A (t-2)^2 + (t-2) \int_{-1}^{0} B(s)\, ds + \int_{1}^{2} \int_{-1}^{z-2} B(s)\, ds dz \right) \end{aligned} \tag{A.47}$$

Using Equation (A.47) we repeat the procedure of § (A.2.1) with the slow scale $\tau = (\epsilon + a\,\epsilon^2 + b\epsilon^3 + \ldots)(t-2)$, where a and b will be chosen to remove secular terms. We now have an approximation.

$$Y(\tau) = (\alpha + \epsilon\delta + \gamma\epsilon^2) e^{\tau} \tag{A.48}$$

$$\tau = \left(\epsilon - \epsilon^2 + \frac{3}{2}\epsilon^3 + \ldots \right)(t-2) \tag{A.49}$$

The matching procedure requires that the following conditions hold.

$$\alpha = A \tag{A.50}$$

$$\delta = A + \int_{-1}^{0} B(s)\, ds \tag{A.51}$$

$$\gamma = \int_{1}^{2} \int_{-1}^{z-1} \beta(s)\, ds\, dz \tag{A.52}$$

Hence the long time higher order approximation is given by (A.53) and (A.54).

$$x \sim \left(A + \epsilon \left(A + \int_{-1}^{0} \beta(s)\, ds \right) + \epsilon^2 \int_{1}^{2} \int_{-1}^{z-1} \beta(s)\, ds\, dz \right) e^{\tau} \tag{A.53}$$

$$\tau = \left(\epsilon - \epsilon^2 + \frac{3}{2}\epsilon^3 + \ldots \right) (t-2) \tag{A.54}$$

A.2.3 Autocrine Signals from Isolated Vulval Precursor Cells

A.2.3.1 Non-Destructive Inhibition

Consider the problem posed by System (5.37).

$$\begin{aligned} \frac{dW(z)}{dz} &= \frac{\delta}{1 + \beta\, W(z-1)} \\ W(z) &= \gamma \quad \text{for } z \in [-1, 0] \end{aligned} \tag{A.55}$$

Previously we had intuited that the asymptotic behavior of this system for large z is $\sqrt{\frac{2\delta z}{\beta}}$. This also appears to be the small β approximation. We now formally derive this result using the asymptotic method of § (A.2.1). First set $W = x/\beta$. This puts

our DDE into the form of the system treated by method (1).

$$\begin{aligned} \frac{dx(z)}{dz} &= \beta \, \frac{\delta}{1 + x(z-1)} \\ x(z) &= \beta \, \gamma \quad \text{for } z \in [-1, 0] \end{aligned} \tag{A.56}$$

Following the method we find

$$x(z) \sim \sqrt{2\delta\tau + 1} - 1 + \beta \left(\delta + \frac{\gamma - \delta}{\sqrt{2\delta\tau + 1}} \right) \tag{A.57}$$

Hence, for $z > 1$ we have

$$\begin{aligned} W(z) &\sim \frac{\sqrt{2\delta\tau + 1} - 1}{\beta} + \delta + \frac{\gamma - \delta}{\sqrt{2\delta\tau + 1}} \\ \tau &= \beta \, (t - 1) \end{aligned} \tag{A.58}$$

Alternatively, for $z \gg 1$, the method of dominant balances can be used to find an asymptotic solution.

$$\begin{aligned} x(z) \sim \sqrt{2\beta\delta z} - 1 + \frac{\sqrt{2\beta\delta z}}{4} \Bigg(& \frac{\ln z}{z} \\ & + \frac{1}{z^2} \left(-\frac{1}{8} (\ln z)^2 + \frac{1}{2} \ln z - \frac{3}{4} \right) \\ & + \frac{1}{z^3} \left(\frac{1}{32} (\ln z)^3 - \frac{1}{4} (\ln z)^2 + \frac{13}{16} \ln z - 1 \right) \\ \Bigg) & \end{aligned} \tag{A.59}$$

We support these approximations by giving an upper and lower bound on the solution to System A.56.

Result 3 *The solution to initial value problem A.56, x(z) satisfies the following inequality for all* $z > 1$.

$$\sqrt{2\beta\delta z + (1+\beta\gamma)^2} - 1 < x(z) < \sqrt{2\beta\delta(z-1) + (1+\beta\gamma)^2} + \frac{\beta\,\delta}{1+\beta\,\gamma} - 1 \tag{A.60}$$

Proof of Result (3). By Result 1, $x(z)$ is monotonically increasing. From this we deduce that $x(z) > x(z-1)$ so that $\frac{dx}{dz} < \frac{\beta\,\delta}{1+x(z)}$ for $z > 0$. Integrate this expression to find the lower bound $x(z) > \sqrt{2\beta\delta z + (1+\beta\gamma)^2} - 1$ for $z > 0$. Adapting this into a lower bound for $x(z-1)$, applying this bound to System A.56, and integrating once more gives an upper bound $x(z) < \sqrt{2\beta\delta(z-1) + (1+\beta\gamma)^2} + \frac{\beta\,\delta}{1+\beta\,\gamma} - 1$ for $z > 1$. □

The bounds given by Result (3), valid for all parameter values, are in agreement with our asymptotic estimate and confirm the intuited growth rate of $x(z)$. See Figure (A.1).

A.2.3.2 Destructive Inhibition

Consider now the problem posed by System (5.38). Setting $V = x/\beta$ we have

$$\begin{aligned} \frac{dx}{dt} &= \beta\left(\frac{H(t-1)}{1+x(t-(1-\phi))} - \frac{x(t)\,H(t-\phi)}{1+x(t)}\right) \quad , \\ x(t) &= \beta\gamma \quad \text{for } \tau \in [-1,0] \quad . \end{aligned} \tag{A.61}$$

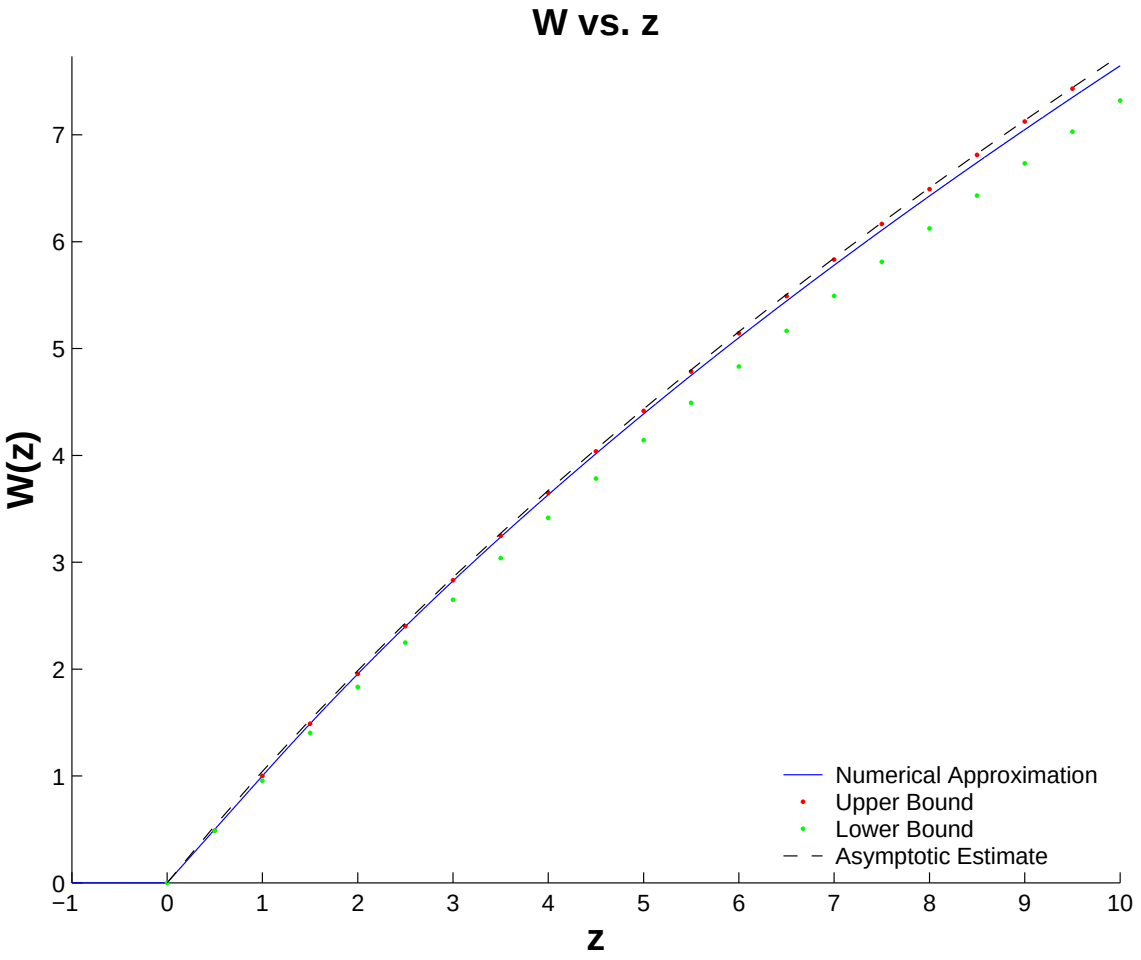

Figure A.1: Asymptotic Estimate and Bounds for Non-Destructive Inhibition during Autocrine Signaling. $\gamma = 0 \quad \delta = 1 \quad \beta = 0.1$. Figure shows the numerically calculated solution (blue solid curve), the asymptotic estimate of Equation (A.58)(black dashed curve), and the upper and lower bounds of Result (3) (red and green dots, respectively).

We study this system for the two extreme values $\phi = 0$ and $\phi = 1$. First consider the case $\phi = 0$.

$$\begin{aligned} \frac{dx}{dt} &= \beta\left(\frac{H\left(t-1\right)}{1+x\left(t-1\right)} - \frac{x\left(t\right)}{1+x\left(t\right)}\right) \\ x(t) &= \beta\gamma \quad \text{for } \tau \in [-1,0] \end{aligned} \tag{A.62}$$

Despite the fact that the Heaviside unit step function [1] appearing on the right hand side of Equation (A.62) depends explicitly on t, method 1 is still applicable because, F is still essentially autonomous but defined piecewise.

$$F\left(x\left(t\right), x\left(t-1\right)\right) = \begin{cases} -\frac{x(t)}{1+x(t)} & \text{if } 0 \leq t < 1 \\ \frac{1}{1+x(t-1)} - \frac{x(t)}{1+x(t)} & \text{if } 1 \leq t \end{cases} \tag{A.63}$$

The leading order term in our asymptotic approximation is given by

$$\begin{aligned} \frac{dY_0}{d\tau} &= \frac{1-Y_0}{1+Y_0} \\ Y_0\left(0\right) &= 0 \quad . \end{aligned} \tag{A.64}$$

Implicitly the solution is

$$Y_0 + 2\log\left(1-Y_0\right) = -\tau \tag{A.65}$$

This can be made explicit in terms of the ProductLog function, also known as the Lambert W-function [45]. The ProductLog is the functional inverse of $f\left(x\right) = x\,e^x$, valid for $x > -e^{-1}$. See Figure (A.2).

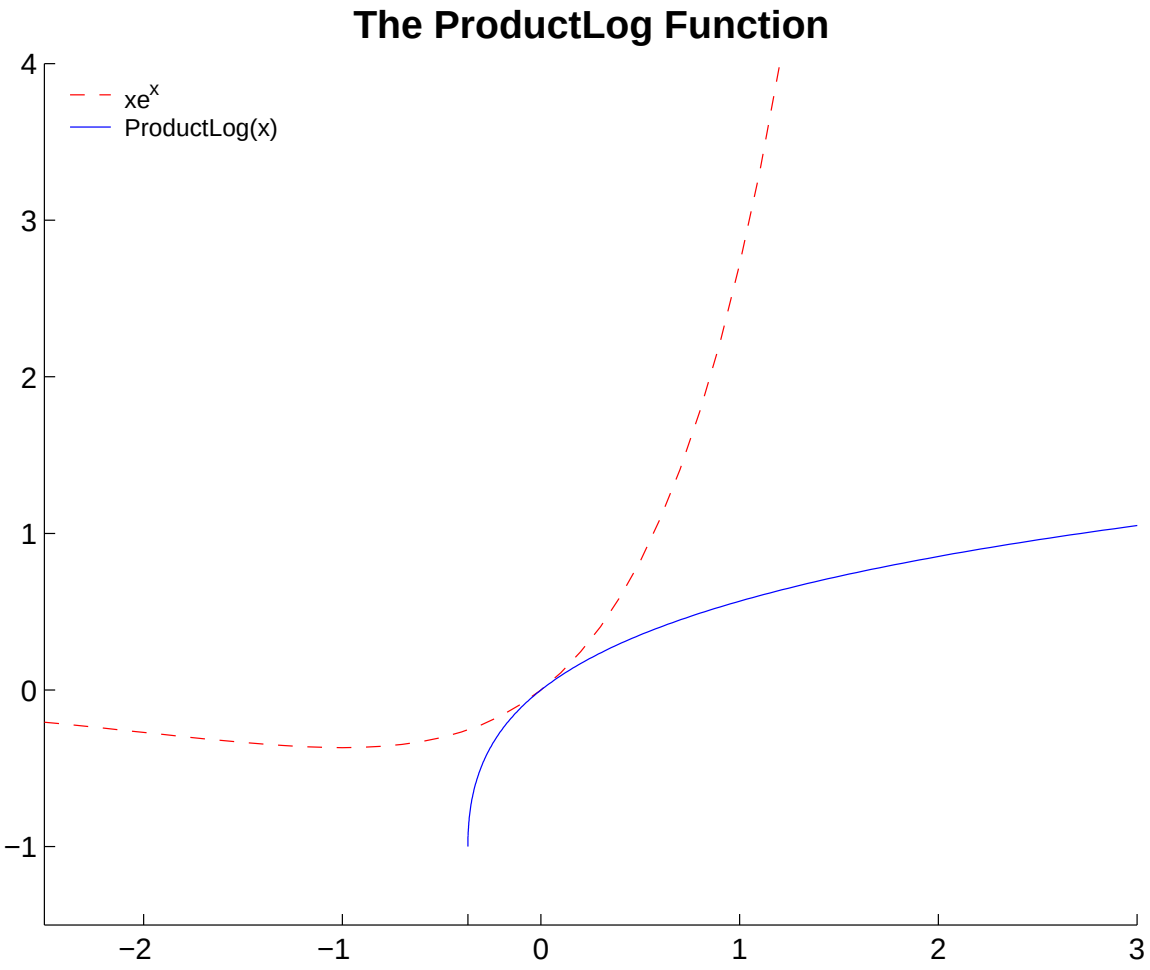

Figure A.2: The ProductLog Function. $ProductLog(x) = f^{-1}(x)$ where $f(x) = x\,e^x$. Its domain is $[-e^{-1}, \infty)$. Its range is $[-1, \infty)$.

$$Y_0(\tau) = 1 + 2\ ProductLog\left(-\frac{1}{2}e^{-(\tau+1)/2}\right) \tag{A.66}$$

For $\phi = 1$ our DDE reduces to an ODE

$$\begin{aligned} \frac{dx}{dt} &= \beta\ H(t-1)\frac{1-x(t)}{1+x(t)} \\ x(t) &= \beta\ \gamma \quad \text{for } t \in [-1, 0] \end{aligned} \tag{A.67}$$

The exact solution of this is again given in terms of the ProductLog function.

$$x(t) = 1 + 2\ ProductLog\left(-\frac{1}{2}(1-\beta\ \gamma)\, e^{-(\beta t - \beta\gamma + 1)/2}\right) \tag{A.68}$$

Lateral Signals between Z1.ppp and Z4.aaa in the AC/VU Decision Consider the problem posed by System (6.20). Using Method 1 the behavior of the system is described asymptotically by the following system:

$$\frac{dY_0^1}{d\tau} = \frac{1}{1+Y_0^2(\tau)} + \frac{1}{1+Y_0^1(\tau)} - 1 \quad , \tag{A.69}$$

$$\frac{dY_0^2}{d\tau} = \frac{1}{1+Y_0^2(\tau)} + \frac{1}{1+Y_0^1(\tau)} - 1 \quad , \tag{A.70}$$

$$Y_0^1(0) = 0 \quad , \tag{A.71}$$

$$Y_0^2(0) = 0 \quad . \tag{A.72}$$

By the uniqueness of solutions to ODE initial value problems, $Y_0^2 = Y_0^1$, so that the system reduces to a single ODE.

$$\frac{dY_0^1}{d\tau} = \frac{1 - Y_0^1}{1 + Y_0^1} \tag{A.73}$$

$$Y_0^1(0) = 0 \tag{A.74}$$

This is identical to System (A.64) hence the solution is given by formula (A.66).

A.3 Phase Plane Analysis of Delay Differential Equations

In studying the stability of equilibria of a system of ODE, linear stability analysis is often used to determine local behavior. Specifically, suppose that the vector-valued function $F(x)$ has the root $x = x^*$, then this equilibrium of the autonomous ODE system $x' = F(x)$ can be studied by considering the eigenvalues of the matrix $\nabla F(x^*)$. If the equation under consideration contains a delay, this approach must be modified.

Suppose that the vector-valued function $F(x, y)$ has the property that $F(x^*, x^*) = 0$ for some vector x^*. Then the linear stability of the system $x' = F(x(t), x(t-1))$ about the point x^* can be ascertained by perturbing about this steady state and solving the resulting system via Laplace transform [4]. To make this explicit, consider

perturbing the initial data by some small amount described by ϵ.

$$x(0) = x^* + \epsilon X_1 \tag{A.75}$$

$$x(t) = x^* + \epsilon X_2(t) \quad \text{for } t \in [-1, 0) \tag{A.76}$$

Seek a solution as a regular perturbation about $x = x^*$.

$$x(t) = x^* + \epsilon X(t) + O\left(\epsilon^2\right) \tag{A.77}$$

Collecting terms of common order gives a linear DDE system for $X(t)$.

$$\frac{dX}{dt} = \nabla_1 F(x^*, x^*) \cdot X(t) + \nabla_2 F(x^*, x^*) \cdot X(t-1) \tag{A.78}$$

$$X(0) = X_1 \tag{A.79}$$

$$X(t) = X_2(t) \quad \text{for } t \in [-1, 0) \tag{A.80}$$

Laplace transforming this system gives an algebraic equation.

$$sY - X_1 = \nabla_1 F(x^*, x^*) \cdot Y + e^{-s} \nabla_2 F(x^*, x^*) \cdot \left(\int_{-1}^{0} X_2(t)\, dt + Y \right) \tag{A.81}$$

Here s is the Laplace transform variable and $Y(s)$ is the Laplace transform of $X(t)$. This system is easily solved.

$$Y = M^{-1} \cdot \left(X_0 + e^{-s} \nabla_2 F(x^*, x^*) \cdot \int_{-1}^{0} X_2(t)\, dt \right) \tag{A.82}$$

$$M = sI - \nabla_1 F(x^*, x^*) - e^{-s} \nabla_2 F(x^*, x^*) \tag{A.83}$$

Here I is the identity matrix. Inversion of the Laplace transform involves a study of the invertibility of the matrix M. Indeed, setting the determinant of M equal to zero gives a transcendental expression known as the characteristic equation. Moreover, let $\Sigma = \{s \in \mathbb{C} : \det(M(s)) = 0\}$. If Σ is a subset of the complement of the right half-plane, $\Sigma \subseteq \{s : Re(s) \leq 0\}$, then the equilibrium point x^* is linearly stable. If Σ lies strictly in the left half of the complex s-plane, $\Sigma \subseteq \{s : Re(s) < 0\}$, the equilibrium point x^* is linearly asymptotically stable.

Consider an autonomous nonlinear system of ODE with an equilibrium point, x^*. If this system is linearized about x^* and the resulting system only has eigenvalues with negative real parts, then the stable manifold theorem (see for example Theorem 1.3.2 in [17]) guarantees that the nonlinear system is also locally asymptotically stable at x^*. This result has been generalized to DDE. See for example Theorem 6.8 in [8]. This theorem states that if the roots of the characteristic equation of a linearized autonomous system of DDE all have negative real parts, then the corresponding nonlinear system of DDE is also locally asymptotically stable. Thus, analysis of local asymptotic stability of a nonlinear DDE system is reduced to the analysis of the characteristic equation when this equation has all of its roots in the left half of the complex plane.

A.3.1 Autocrine Signals from Isolated Vulval Precursor Cells

A.3.1.1 Destructive Inhibition

Consider System (5.38). Its equilibrium is the point $V = 1/\beta$. Linearizing about this point gives a linear DDE, $X'(t) = -\frac{\beta}{4}\left(X\left(t-(1-\phi)\right)+X(t)\right)$, and, by remarks above, leads to the study of the complex roots of Equation (A.84).

$$s = -\frac{\beta}{4}\left(e^{-s(1-\phi)}+1\right) \tag{A.84}$$

Result 4 *For $0 \leq \phi \leq 1$ and $\beta > 0$, solutions of A.84 lie in the left half of the complex plane,* i.e., *System (5.38) has the locally asymptotically stable equilibrium $1/\beta$.*

Proof of Result 4. The proof is simple and follows by drawing a contradiction. Let the complex variable s be given by $s = x + \imath y$ where x and y are real. This gives the following system:

$$x = -\frac{\beta}{4}\left(1+e^{-x(1-\phi)}\cos y\,(1-\phi)\right) \quad , \tag{A.85}$$

$$y = \frac{\beta}{4}e^{-x(1-\phi)}\sin y\,(1-\phi) \quad . \tag{A.86}$$

Suppose that $x > 0$ so that $0 < e^{-x(1-\phi)} \leq 1$. Because $0 \leq |\cos y\,(1-\phi)| \leq 1$ we necessarily have $0 \leq 1 + e^{-x(1-\phi)}\cos y\,(1-\phi) \leq 2$. This shows that the right-hand side of Equation (A.85) is non-positive while the left-hand side is positive, a contradiction. Hence x is non-positive. To complete the proof, suppose that $x = 0$. Equation (A.85) implies that $y = \frac{(2n+1)\pi}{1-\phi}$ for some integer n. This, together with

Equation (A.86), implies that $2n + 1 = 0$, a contradiction. We conclude that $x < 0$.

□

Equations (A.85) and (A.86) can actually be solved to find x and y in terms of β and ϕ. First set $X = (1 - \phi)\, x$, $Y = (1 - \phi)\, y$, and $\alpha = (1 - \phi)\, \frac{\beta}{4}$. Our system becomes the following:

$$X + \alpha = -\alpha\, e^{-X} \cos Y \quad , \tag{A.87}$$

$$Y = \alpha\, e^{-X} \sin Y \quad . \tag{A.88}$$

If $Y = 0$ then Equation (A.88) is satisfied and Equation (A.87) gives $X\,(\alpha)$ implicitly. See the red dashed curve in Figure (A.3).

Result 5 *If $Y = 0$, then $\frac{d\alpha}{dx} = 0$ at the point*

$$(\alpha, x) = (ProductLog(e^{-1}), -ProductLog(e^{-1}) - 1) \approx (0.28, -1.28) \quad . \tag{A.89}$$

Proof of Result 5. If $Y = 0$, then Equation (A.87) gives α as a function of x.

$$\alpha = -\frac{x}{1 + e^{-x}} \tag{A.90}$$

$$\frac{d\alpha}{dx} = -e^{x} \frac{1 + x + e^{x}}{(1 + e^{x})^{2}} \tag{A.91}$$

Setting the numerator of (A.91) to zero and rearranging gives $-(1 + x)e^{-(1+x)} = e^{-1}$. Applying the ProductLog function to this equation gives $x = -ProductLog(-1) - 1$. Inserting this critical value of x into (A.90) and simplifying gives $\alpha = ProductLog(-1)$.

□

The value of α determined by this result, which we call α^*, is important because, at this point, there is a bifurcation from non-oscillatory solutions to slowly decaying oscillatory solutions. See Figure (A.3).

When $Y \neq 0$, forming the ratio of these equations allows X to be solved for, $X = -\alpha - Y \cot Y$. Inserting this into Equation (A.88) gives an expression involving Y and α, which can be solved for α using the ProductLog function. The expressions for X and α as functions of the parameter Y may now be written:

$$\begin{aligned} \alpha &= ProductLog\left(Y\, e^{-Y\cot Y}\csc Y\right) \quad , \\ X &= -ProductLog\left(Y\, e^{-Y\cot Y}\csc Y\right) - Y\cot Y \quad . \end{aligned} \tag{A.92}$$

X is plotted versus α in Figure (A.3) for $-50\pi < Y < 50\pi$.

For $\alpha > \alpha^*$ there exist slowly decaying low frequency oscillations but below this threshold oscillations are more rapid and decay more quickly. Moreover, Corollary 1 in [10] applies to this problem and ensures that the linearized DDE will exhibit oscillations for $\alpha < \alpha^*$ only for initial data from a nowhere dense subset of $C^0\,[-1, 0]$. We thus expect to see a more oscillatory approach to equilibrium when $(1-\phi)\,\beta > 4 * \alpha^* \approx 1.113$. Figure (A.4) shows numerical approximations for the non-linear DDE with $\phi = 0$. Note the onset of oscillations for $\beta > 1$.

For $\alpha \gg 1$ the most slowly decaying solutions have a period of approximately two ($P = 2\pi/Y$). Asymptotically the decay rate and period are given by the following

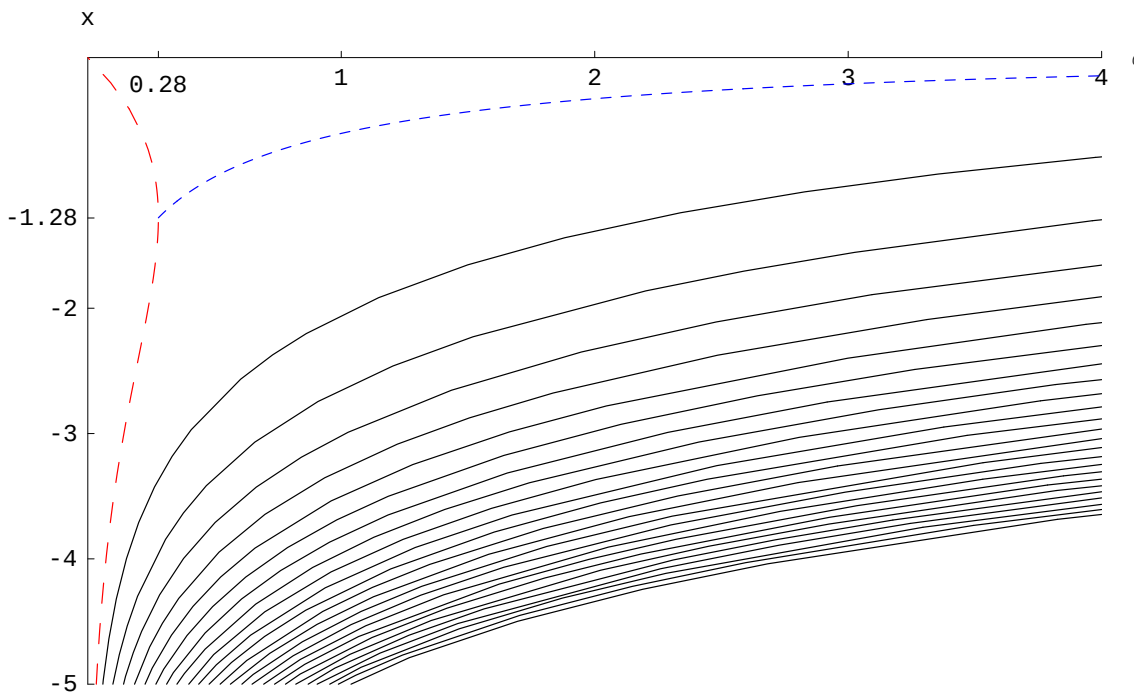

Figure A.3: The Decay Rate of Oscillatory Solutions in Destructive Autocrine Signaling. A parametric plot of System (A.92) for $-50\pi < Y < 50\pi$. Observe that for $\alpha > \alpha^* \approx 0.278$ there is a branch of oscillatory solutions that decays at a slower rate (blue dotted curve). Values of X on this upper branch correspond to slowly oscillating slowly decaying solutions ($Y \in [0, \pi]$, $X > -\alpha^* - 1 \approx -1.278$). For α below this threshold, oscillations are of higher frequency and rapidly decaying ($|Y| \gtrsim 7.46$, $X \lesssim -3.38$, black solid curves), or have no oscillatory component at all (red dashed curve). For $\alpha < \alpha^*$ we expect the equilibration of our non-linear system to exhibit negligible oscillatory character.

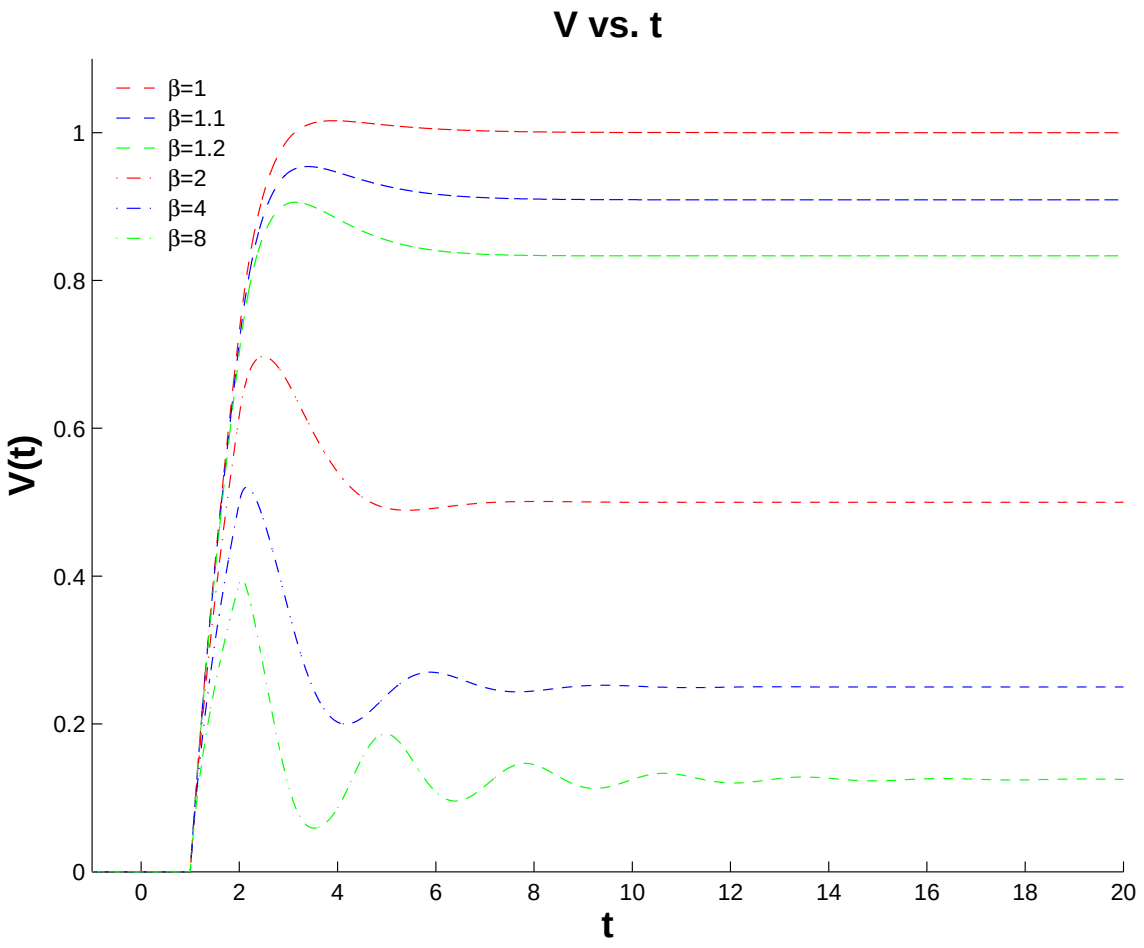

Figure A.4: Oscillatory Decay to Equilibrium in Destructive Autocrine Signaling. $\phi = 0 \quad \gamma = 0$. As β increases beyond the critical value $1.113\ldots$ solutions approach the equilibrium $1/\beta$ in a more oscillatory fashion.

relations:

$$X \sim -\frac{\pi^2}{2\,\alpha^2} + \frac{3\,\pi^2}{2\,\alpha^3} \quad , \tag{A.93}$$

$$P \sim 2\left(1 + \frac{1}{\alpha} - \frac{\pi^2}{3\,\alpha^3}\right) \quad . \tag{A.94}$$

These limiting period-two solutions may be extracted directly from the non-linear System (5.38) by using a method developed in [14]. First set $V = x/\beta$ to obtain System (A.61). For $\beta \gg 1$ the "outer" solution is given by equating the right hand side of this to zero.

$$\frac{1}{1 + x(t - (1 - \phi))} - \frac{x(t)}{1 + x(t)} = 0 \tag{A.95}$$

This can be thought of as a difference equation by equating $x(t)$ on the interval $(1 - \phi)\, n \leq t < (1 - \phi)\,(n + 1)$ with the discrete sequence of functions $y_n\,(t)$. In this way we obtain the following recursive relation:

$$\frac{1}{1 + y_{n-1}} - \frac{y_n}{1 + y_n} = 0 \quad . \tag{A.96}$$

This is easily solved to find $y_n\,(t) = 1/y_{n-1}\,(t)$, a piecewise continuous period-two function of t.

Index

Bibliography

[1] C. M. Bender and S. A. Orszag, *Advanced Mathematical Methods for Scientists and Engineers*, International Series in Pure and Applied Mathematics, McGraw-Hill, Inc., 1978.

[2] M. Bier, B. M. Bakker, and H. V. Westerhoff, *How yeast cells synchronize their glycolytic oscillations: a perturbation analytic treatment*, Biophysical Journal, 78 (2000), pp. 1087–1093.

[3] R. C. Buck, *Advanced Calculus*, International Series in Pure and Applied Mathematics, McGraw-Hill Higher Education, 3rd ed., January 1978.

[4] G. F. Carrier, M. Krook, and C. E. Pearson, *Functions of a Complex Variable: Theory and Technique*, Hod Books, Ithaca, New York, 1983.

[5] N. Chen and I. Greenwald, *The lateral signal for lin-12/notch in c. elegans vulval development comprises redundant secreted and transmembrane dsl proteins*, Dev Cell, 6 (2004), pp. 183–92.

[6] F. S. Crawford Jr., *Waves: Berkeley Physics Course*, vol. 3, McGraw-Hill College, June 1968.

[7] J. Culí and J. Modolell, *Proneural gene self-stimulation in neural precursors: an essential mechanism for sense organ development that is regulated by notch signaling*, Genes Dev, 12 (1998), pp. 2036–47.

[8] O. Diekmann, S. A. van Gils, S. M. V. Lunel, and H.-O. Walther, *Delay Equations*, vol. 110 of Applied Mathematical Sciences, Springer-Verlag New York, Incorporated, 1995.

[9] R. D. Driver, *Ordinary and Delay Differential Equations*, vol. 20 of Applied Mathematical Sciences Ser., Springer-Verlag New York, Incorporated, February 1977.

[10] R. D. Driver, D. W. Sasser, and M. L. Slater, *The equation* $x'(t) = ax(t) + bx(t-\tau)$ *with "small" delay*, The American Mathematical Monthly, 80 (1973), pp. 990–995.

[11] A. Einstein, *Investigations on the Theory of the Brownian Movement*, Dover Publications, March 1985.

[12] I. R. Epstein, *Differential delay equations in chemical kinetics: Some simple linear model systems*, Journal of Chemical Physics, 92 (1990), pp. 1702–1712.

[13] I. R. Epstein and J. A. Pojman, *An Introduction to Nonlinear Chemical Dynamics: Oscillations, Waves, Patterns, and Chaos*, Topics in Physical Chemistry, Oxford University Press, October 1998.

[14] T. Erneux, *Asymptotic methods for delay differential equations.* Unpublished notes from lectures given at the Universite Joseph Fourier, Grenoble, April 2003.

[15] W. J. Gehring, *Historical perspective on the development and evolution of eyes and photoreceptors*, International Journal of Developmental Biology, 48 (2004), pp. 707–717.

[16] I. S. Greenwald, P. W. Sternberg, and H. R. Horvitz, *The lin-12 locus specifies cell fates in caenorhabditis elegans*, Cell, 34 (1983), pp. 435–44.

[17] J. Guckenheimer and P. Holmes, *Nonlinear Oscillations, Dynamical Systems, and Bifurcations of Vector Fields*, vol. 42 of Applied Mathematical Sciences, Springer-Verlag New York, Incorporated, 1983.

[18] J. K. Hale, *Theory of Functional Differential Equations*, vol. 3 of Applied Mathematical Sciences Ser., Springer-Verlag New York, Incorporated, 1977.

[19] P. Heitzler, M. Bourouis, L. Ruel, C. Carteret, and P. Simpson, *Genes of the enhancer of split and achaete-scute complexes are required for a regulatory loop between notch and delta during lateral signalling in drosophila*, Development, 122 (1996), pp. 161–71.

[20] R. J. Hill and P. W. Sternberg, *The gene lin-3 encodes an inductive signal for vulval development in c. elegans*, Nature, 358 (1992), pp. 470–6.

[21] ——, *Cell fate patterning during c. elegans vulval development*, Dev Suppl, (1993), pp. 9–18.

[22] N. A. Hopper, J. Lee, and P. W. Sternberg, *Ark-1 inhibits egfr signaling in c. elegans*, Mol Cell, 6 (2000), pp. 65–75.

[23] H. R. Horvitz and P. W. Sternberg, *Multiple intercellular signalling systems control the development of the caenorhabditis elegans vulva*, Nature, 351 (1991), pp. 535–41.

[24] X. Karp and I. Greenwald, *Post-transcriptional regulation of the e/daughterless ortholog hlh-2, negative feedback, and birth order bias during the ac/vu decision in c. elegans*, Genes Dev, 17 (2003), pp. 3100–11.

[25] W. S. Katz, R. J. Hill, T. R. Clandinin, and P. W. Sternberg, *Different levels of the c. elegans growth factor lin-3 promote distinct vulval precursor fates*, Cell, 82 (1995), pp. 297–307.

[26] J. Keener and J. Sneyd, *Mathematical Physiology*, vol. 8 of Interdisciplinary Applied Mathematics Ser., Springer, October 1998.

[27] J. Kevorkian and J. D. Cole, *Multiple Scale and Singular Perturbation Methods*, vol. 114 of Applied Mathematical Sciences Ser., Springer, May 1996.

[28] J. Kimble, *Alterations in cell lineage following laser ablation of cells in the somatic gonad of caenorhabditis elegans.*, Dev Biol, 87 (1981), pp. 286–300.

[29] G. Lahav, *The strength of indecisiveness: oscillatory behavior for better cell fate determination.*, Sci STKE, 2004 (2004), p. pe55.

[30] B. Lee, *Tao of Jeet Kun Do*, Ohara Publications, Inc., 1975.

[31] R. J. LeVeque, *Finite Volume Methods for Hyperbolic Problems*, Cambridge Texts in Applied Mathematics Ser., Cambridge University Press, August 2002.

[32] C. C. Lin and L. A. Segal, *Mathematics Applied to Deterministic Problems in the Natural Sciences*, Classics in Applied Mathematics, Society for Industrial and Applied Mathematics, Philadelphia, PA, 1988.

[33] N. Moghal and P. W. Sternberg, *The epidermal growth factor system in caenorhabditis elegans*, Exp Cell Res, 284 (2003), pp. 150–9.

[34] A. Ogura, K. Ikeo, and T. Gojobori, *Comparative analysis of gene expression for convergent evolution of camera eye between octopus and human*, Genome Research, 14 (2004), pp. 1555–1561.

[35] D. L. Riddle, T. Blumenthal, B. J. Meyer, and J. R. Priess, eds., *C. Elegans II*, vol. 33 of Monographs, Cold Spring Harbor Laboratory Press, 1997.

[36] K. Schmitt, ed., *Delay and Functional Differential Equations and Their Applications*, Elsevier Science & Technology Books, 1972.

[37] L. A. Segel and A. S. Perelson, *Exploiting the diversity of time scales in the immune system: A b-cell antibody model*, Journal of Statistical Physics, 63 (1991), pp. 1113–1131.

[38] D. D. Shaye and I. Greenwald, *Endocytosis-mediated downregulation of lin-12/notch upon ras activation in caenorhabditis elegans*, Nature, 420 (2002), pp. 686–90.

[39] J. S. Simske, S. M. Kaech, S. A. Harp, and S. K. Kim, *Let-23 receptor localization by the cell junction protein lin-7 during c. elegans vulval induction.*, Cell, 85 (1996), pp. 195–204.

[40] P. W. Sternberg, *Lateral inhibition during vulval induction in caenorhabditis elegans*, Nature, 335 (1988), pp. 551–4.

[41] P. W. Sternberg and H. R. Horvitz, *The combined action of two intercellular signaling pathways specifies three cell fates during vulval induction in c. elegans*, Cell, 58 (1989), pp. 679–93.

[42] J. J. Tyson, K. C. Chen, and B. Novak, *Sniffers, buzzers, toggles and blinkers: dynamics of regulatory and signaling pathways in the cell*, Current Opinion in Cell Biology, 15 (2003), pp. 221–231.

[43] M. Wang and P. W. Sternberg, *Competence and commitment of caenorhabditis elegans vulval precursor cells*, Dev Biol, 212 (1999), pp. 12–24.

[44] H. A. Wilkinson and I. Greenwald, *Spatial and temporal patterns of lin-12 expression during c. elegans hermaphrodite development*, Genetics, 141 (1995), pp. 513–26.

[45] Wolfram Research, *Lambert w-function*. http://mathworld.wolfram.com/LambertW-Function.html.

[46] ——, *The numerical method of lines*. http://documents.wolfram.com/mathematica/Built-inFunctions/AdvancedDocumentation/DifferentialEquations/NDSolve/PartialDifferentialEquations/TheNumericalMethodOfLines/index.en.html.

[47] A. S. Yoo, C. Bais, and I. Greenwald, *Crosstalk between the egfr and lin-12/notch pathways in c. elegans vulval development*, Science, 303 (2004), pp. 663–6.